Experiments that illustrate anomalous and non-local transport

A Thesis

SUBMITTED TO THE FACULTY OF THE

UNIVERSITY OF MINNESOTA

BY

Natasha Brynaert Filipovitch

IN PARTIAL FULFILLMENT OF THE REQUIREMENTS

FOR THE DEGREE OF

MASTER OF SCIENCE

Vaughan Voller, Kimberly Hill

June 2017

Abstract

In this work our focus is the related phenomena of anomalous diffusion and non-local transport. The former refers to physical systems in which the spreading of a solute does not exhibit the classic square root of time behavior; the later describes cases where the flux of a solute at a point is controlled by features at locations removed from that point. Two experimental systems that produce clear signals of anomalous diffusion and non-local transport are presented. The first measures the infiltration of fluid into an obstacle filled cavity. We show that when the obstacles are laid out in a fractal pattern the infiltration measure exhibits an anomalous diffusion behavior. The second experiment studies the steady state by-pass profile of a two-dimensional rice pile. We show that the pile's profile has a concave down curvature that, through modeling we argue, is a consequence of non-local transport.

Contents

List of Tables

List of Figures

Chapter 1

Introduction

1.1 Overview

The work we present here explores two sets of experiments completed with the goal of improving our understanding of two concepts: anomalous diffusion and non-local transport. With anomalous diffusion we want to specifically explore the conditions that produce anomalous diffusion. With non-local transport we want to specifically recognize direct signals of the presence and weighting direction of non-locality.

1.2 Anomalous Diffusion

To understand anomalous diffusion we must first discuss normal diffusion. The classic model for normal diffusion is that of Brownian motion [*Weeks et al.*, 1996]. Brownian motion refers to the random motion of a particle suspended in a fluid that results due to the collisions of that particle with the molecules or atoms of the fluid [*Philibert*, 2005]. It is with this motion that particles diffuse from areas of higher concentration to areas of lower concentration. At first glance this motion may appear to be random, but with further study scalings emerge. *Einstein* [1905] showed that the average displacement of a brownian

particle, from its starting position, is proportional to the square root of elapsed time,

$$\overline{x^2} = 2Dt \tag{1.1}$$

$$x \sim t^{\frac{1}{2}} \tag{1.2}$$

This time exponent of $\frac{1}{2}$ is the defining characteristic of normal diffusion.

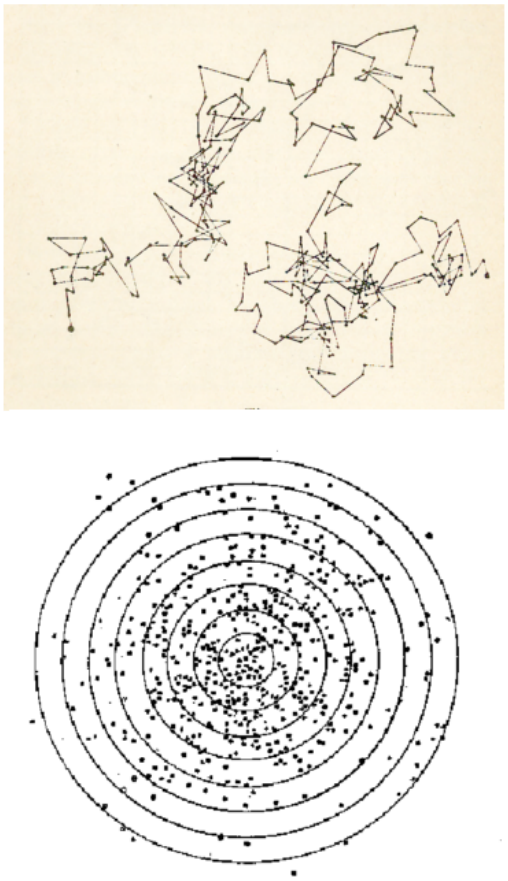

Figure 1.1: Brownian motion: (above) an example of a trajectory of a single particle and (below) statistical distribution of displacements (the circles correspond to fractions and multiples of the square root of the mean square displacement) [*Philibert*, 2005]

Anomalous diffusion, therefore, describes a system in which the time exponent does not equal $\frac{1}{2}$ [*Korabel and Barkai*, 2011]. The introduction of traps (hold ups), which impede the motion of certain particles [*Metzler and Klafter*, 2004], or increased slopes (fast paths),

which accelerate the motion of some of the particles [*Foufoula-Georgiou et al.*, 2010], may result in such a time exponent. When the time exponent is less than $\frac{1}{2}$ this is called sub-diffusion; when the time exponent is greater than $\frac{1}{2}$ this is called super diffusion. Therefore anomalous diffusion may be induced by introducing hold ups, which leads to sub-diffusion, or fast paths, which leads to super-diffusion.

One way to model anomalous transport is through non-local definitions of the fluxes in the system [*Schumer et al.*, 2009]. To describe this approach we will discuss an example of moisture infiltration into a porous tube, (Figure 1.2). In this example, fluid flow is governed by Darcy's Law,

$$q = -K\frac{dh}{dx} \tag{1.3}$$

where q is the moisture flux [$\frac{m^3}{m^2 s}$], K is the hydraulic conductivity, and $\frac{dh}{dx}$ is the driving head gradient. The fluid infiltrates a porous tube driven by a fixed head, h_0, at $x = 0$. At time $t = 0$ the moisture infiltration front is at $x = 0$, at time $t > 0$ the front is at $x = s(t)$. At $x = 0$, $h = h_0$, and at $x = s$, $h = 0$. Between $x = 0$ and $x = s$, at any point in time, the head gradient is fixed, meaning that $\frac{dh}{dx} = -\frac{h_0}{s}$ [*Bear*, 1988]. Since the moisture front is directly proportional to this gradient (i.e. Darcy's Law) we can present the following differential equation for the position of the infiltration front, $s(t)$.

$$\frac{ds}{dt} = -K\frac{dh}{dx}\bigg|_s = K\frac{h_0}{s}, \quad s(0) = 0 \tag{1.4}$$

When we solve for s in terms of t the resulting time exponent is $\frac{1}{2}$, i.e.

$$s = \left[\sqrt{2Kh_0}\right] t^{\frac{1}{2}} \tag{1.5}$$

indicating that this moisture infiltration has the signal of a normal diffusion process.

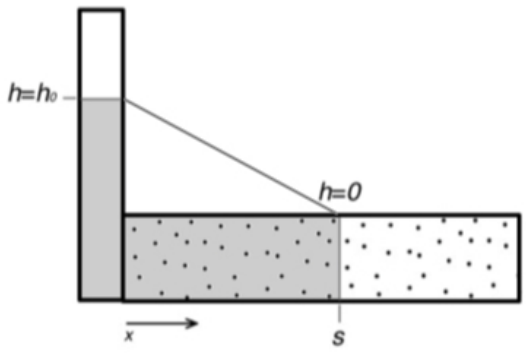

Figure 1.2: Porous tube example. Fluid from tank with a fixed head (h) infiltrates a tube filled with porous media along the x direction. Speckled area represents porous medium, grey area represents fluid filled regions.

Darcy's Law (Eq 1.3) describes a local definition of flux since it depends on a constant coefficient (hydraulic conductivity K) and the *local* gradient of the head (i.e. the value of the head gradient is at the point where we are calculating the flux). We can, however, also define a non-local flux, (with a new hydraulic conductivity, K^*) where the discharge at any given point is determined not only by conditions at that point but also by conditions either up or down stream from that point. This can be easily achieved through a weighted sum (W) where the effect on a point decreases with increasing distance from that point. In this way, for example, a non-local flux can be defined as the weighted sum of the gradient at points upstream of the point of interest,

$$q^{NL} = -K^* \sum W \frac{dh}{dx} \tag{1.6}$$

With a particular, (but still fairly general), choice of weights and letting the sum extend over every upstream point back to the origin $x = 0$, we can write this flux as a fractional derivative [*Podlubny*, 1999],

$$q^{NL,up} = -K^* \frac{d^\alpha h}{dx^\alpha}, \quad \alpha \leq 1 \tag{1.7}$$

defined, in the Caputo sense [*Caputo*, 1967], as the convolution integral [*Li et al.*, 2011]

$$q^{NL,up} = -K^* \left[\frac{1}{\Gamma(1-\alpha)} \int_0^x (x-\xi)^{-\alpha} \frac{dh(\xi)}{d\xi} d\xi \right] \tag{1.8}$$

In Figure 1.8 we compare the solution of the tube infiltration problem using the normal derivative with that using the fractional gradient in Eq 1.7. Here we see that the replacement of the local flux, Eq 1.3, with the non-local flux, Eq 1.7 in our porous tube filling, shows how the non-local flux modifies the nature of the movement of the moisture front. In particular when $\alpha < 1$ we see that the time exponent in the expression for the front movement exhibits super-diffusion, i.e. the exponenton time $n = \frac{1}{\alpha+1} > \frac{1}{2}$. Thus, a fractional definition of the head gradient in the porous tube leads to super-diffusive (fast path) behavior. For completeness, we note that an alternative to introducing a fractional gradient would be to define the time derivative of the problem as a fractional derivative. Analysis with this setting [*Voller*, 2015] leads to sub-diffusive movement for the moisture front; in this case the time exponent is less than $\frac{1}{2}$. The introduction of a fractional time derivative represents "memory" and hold up, thus the observed sub-diffusion is to be expected.

Normal Diffusion

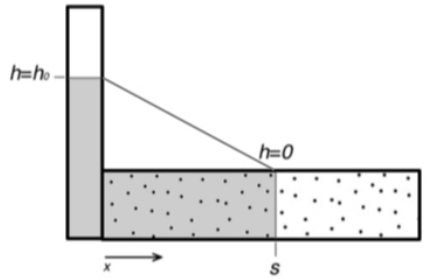

$\frac{\partial}{\partial x}(q) = 0 \quad \text{in } x < s$

$q = -K\frac{\partial h}{\partial x} = \text{constant}$

$h = \left(\frac{s-x}{s}\right)h_0$

$\frac{ds}{dt} = q = \frac{Kh_0}{s}$

$s \sim t^{\frac{1}{2}}$

Anomalous Diffusion

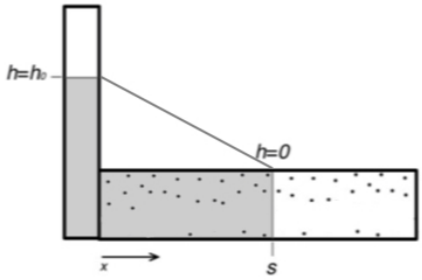

$\frac{\partial}{\partial x}(q) = 0$

$q = -K^*\frac{\partial^\alpha h}{\partial x^\alpha} = \text{constant}, \quad 0 < \alpha \leq 1$

$h \sim \frac{x^\alpha}{s^\alpha}$

$\frac{ds}{dt} = q \sim \frac{1}{s^\alpha}$

$s \sim t^{\frac{1}{\alpha+1}}$

Figure 1.3: A comparison of normal and anomalous porous tube equations. Note c and b are constants and $0 < \alpha \leq 1$ is a parameter that controls the weights and determines the level of non-locality in the flux definition; a value of $\alpha = 1$ recovers our local definition in Eq 1.3.

1.3 Non-local Fluxes

Non-local definitions may also affect the spatial distribution of a system. *Falcini et al.* [2013] discuss that the steady state longitudinal profile in sediment transport may show evidence of non-locality. To demonstrate this let us consider a simple by-pass one dimensional sedimentary fan in the absence of tectonics. In a unit length domain a standard model for this, based on the Exner equation [*Paola and Voller*, 2005], is as follows

$$\frac{\partial}{\partial x}(-q) = 0 \qquad 0 < x < 1 \tag{1.9}$$

with the boundary conditions $q_{x=0} = \text{constant}, \quad \eta(1) = 0$

In a simple approach, which neglects the critical shear stress, we can model the sediment

unit flux, q, as a diffusion like term, i.e. η, the elevation of the sediment deposit, takes on a similar role to the pressure head h in our previous example.

$$q \sim -K\frac{\partial \eta}{\partial x} \tag{1.10}$$

where K is a "conductivity". When this flux definition is used in Eq 1.9 we get a linear profile for the sediment deposit, i.e. $\eta \sim (1-x)$.

Moving away from the flux model in Eq 1.10 we can also use a particular non-local model which treats the flux as a weighted sum of upstream slopes i.e. we define our flux using Eqs 1.7 & 1.8 (we replace h with η, the height of the sediment deposit). In this case as indicated in Figure 1.4 we get a concave up profile $\eta \sim 1-x^{\alpha}$. *Falcini et al.* [2013] also point out that one could use a non-local definition as a weighted sum of downstream slopes, in this case the flux is given by the fractional derivative

$$q^{NL,down} = -K\frac{d^{\alpha}\eta}{d(-x)^{\alpha}} \tag{1.11}$$

In a unit domain, using the Caputo definition, this can be written as

$$q^{NL,down} = -K\left[\frac{-1}{\Gamma(1-\alpha)}\int_{x}^{1}(\xi-x)^{-\alpha}\frac{d\eta(\xi)}{d\xi}d\xi\right] \equiv \frac{\partial^{\alpha}\eta}{\partial(1-x)^{\alpha}} \tag{1.12}$$

Now as indicated in Figure 1.4 we will get a concave down profile $\eta \sim (1-x)^{\alpha}$. Thus in sediment and granular transport systems the long profile shape of a steady state deposit may indicate the presence of non-local (anomalous) transport.

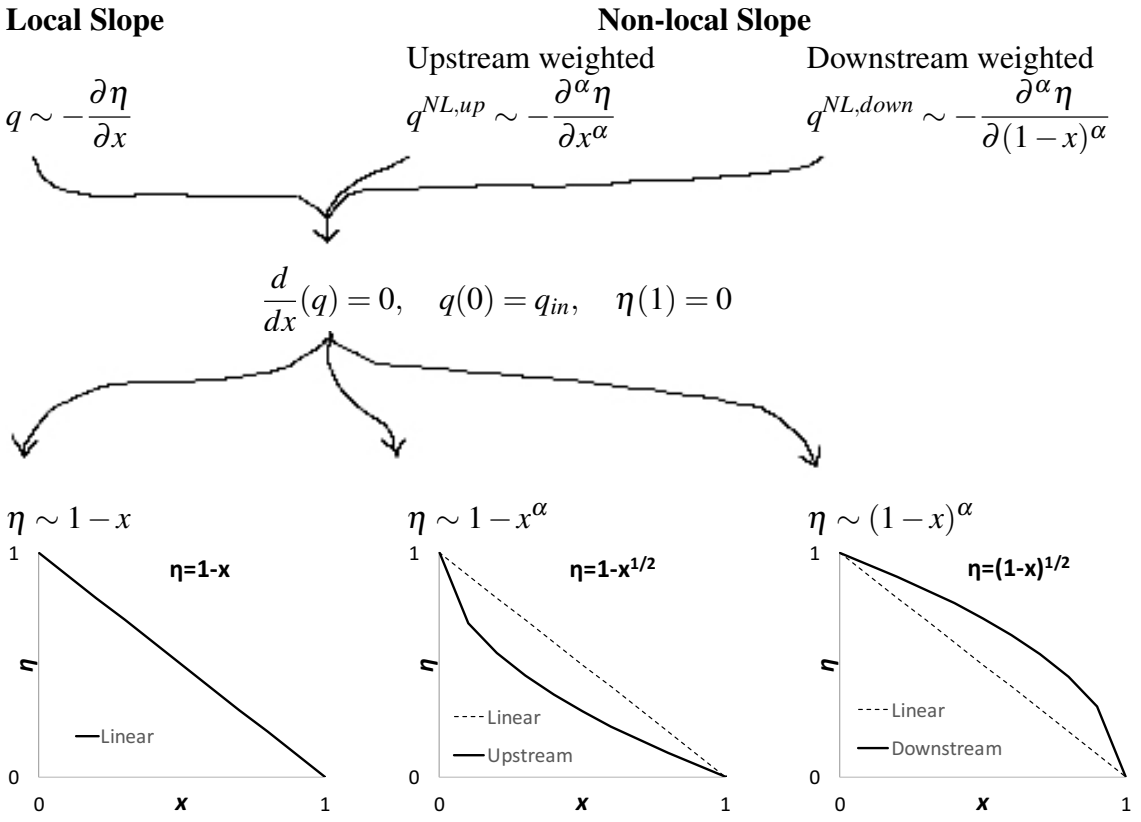

Figure 1.4: An example of how the spatial relations of a system can be controlled by the presence of non-locality in the fluxes. Here we show that when a non-local model is used for flux the curvature of the slope provides information about the level and direction of non-locality in the system. Note that $0 \leq \alpha \leq 1$ in all cases and $\alpha = \frac{1}{2}$ for purposes of building these sample graphs.

1.4 Previous Observations

Very much related to our porous tube and non-local modeling examples, one physical system where anomalous transport has been observed and measured is moisture infiltration into porous brick [*Gerolymatou et al.*, 2006, *Küntz and Lavallée*, 2001]. *Küntz and Lavallée* [2001] reanalyzed NMR (nuclear magnetic resonance) data from a number of experiments involving infiltration into clay fired brick and limestone brick [*Carpenter et al.*, 1993, *Pel et al.*, 1995, 1996, 1998]. They found that the infiltration results did not match

with expectations that include a time exponent of $\frac{1}{2}$. By using a theoretical model based on a non-Fickian (anomalous) diffusion process, where the time exponent is not $\frac{1}{2}$, they found they could fit the observed NMR data well. Figure 1.5 shows how the data from the clay fired brick experiments aligns with the anomalous (non-Fickian) diffusion model, whose time exponent is 0.58, rather than the Fick's diffusion model, whose time exponent is 0.50. *Gerolymatou et al.* [2006] noted a number of papers reporting anomalous diffusion behavior during infiltration of building materials [*El Abd and Milczarek*, 2004, *Küntz and Lavallée*, 2001, *Taylor et al.*, 1999] and attempted to explain this anomalous infiltration through the use of fractional calculus. They started with the classical Richards equation (used to describe air-water flow through unsaturated zone in soils) and generalized this equation by introducing fractional time derivatives. In their investigation of the resulting fractional Richards equation they note that data from the experiments performed by *Taylor et al.* [1999] (on white silicious brick) fit much more closely with the fractional Richards equation, whose time exponent is 0.43, than they do with the classical Richards equation, whose time exponent is 0.5, as seen in Figure 1.6. They do note that while the data seem more consistent with the fractional approach the uncertainty in the data is too large to conclusively determine a time exponent.

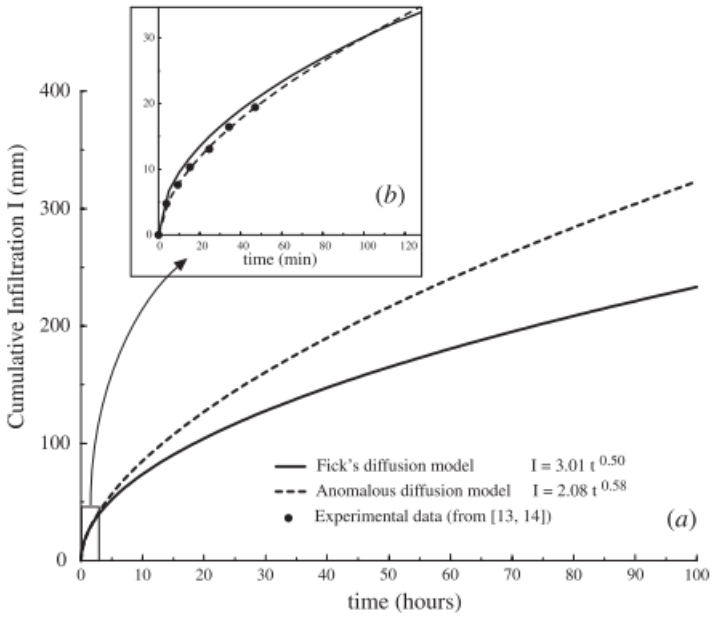

Figure 1.5: *Küntz and Lavallée* [2001] show the experimental data (from *Pel et al.* [1995, 1996]) aligns much more closely with the non-Fickian anomalous diffusion model they proposed (time exponent 0.58) than it does with Fick's classic diffusion model (time exponent 0.50).

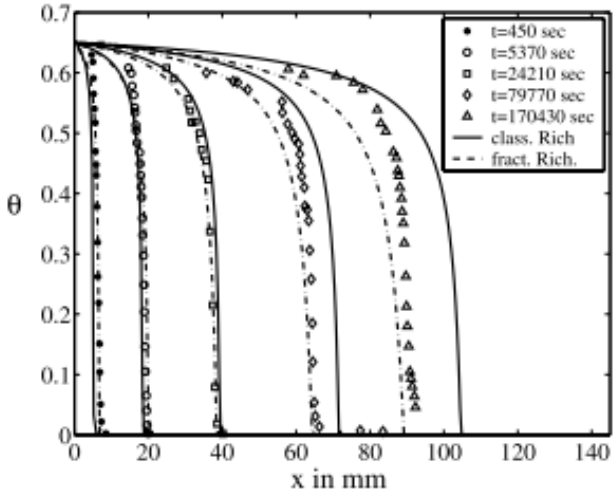

Figure 1.6: *Gerolymatou et al.* [2006] present data from infiltration experiments with white silicious bricks [*El Abd and Milczarek*, 2004]. This data is presented as isochrones of θ, volumetric moisture content, and aligns more closely with the fractional Richards equation they developed (time exponent 0.43) than it does with the classical Richards equation (time exponent 0.5), this is particularly evident for the data collected in the later times of the experiment.

1.5 Intentions

Following on, and extending, the infiltration observations in *Küntz and Lavallée* [2001] and *Gerolymatou et al.* [2006] and non-local sediment transport theory presented by *Falcini et al.* [2013], in this thesis we will present two systems where non-local and anomalous transport can occur. Moving beyond observation and exponent fitting, however, our intention will be to understand what physical features in a given system induce and control the observed anomalous behavior. Our first experiment is infiltration into a analogue porous medium constructed by placing a fractal object pattern in a Hele-Shaw cell. This is an experimental arrangement that allows us to understand how heterogeneity controls observed anomalous time exponents. The second experiment considers a rice pile as an analogue for a sediment transport system. This experiment shows how the assumption of the appropriate non-local flux (in terms of fractional derivative constructs) is needed to match observed surface curvatures in the rice pile experiments.

Chapter 2

Infiltration

Our first set of experiments studies the relationship between the heterogeneity of a porous medium and the resulting anomalous diffusion during infiltration. These experiments were performed in the Multiphase Flow Laboratory in the CEGE Department at the University of Minnesota. We use a Hele-Shaw cell as a analogue for this system. A Hele-Shaw cell involves fluid flowing between closely spaced parallel plates (see Figure 2.1). The plates are parallel to the *xy* plane and flow moves in the positive *x* direction. Our Hele-Shaw cells are all square in plan view as seen in Figure 2.2. A Hele-Shaw cell may contain obstacles between the plates and the size and arrangement of these obstacles may effect the flow of the fluid. A Hele-Shaw system results in potential flow under the condition that the viscous length scale (ℓ_v) is significantly smaller than the plan view length of the largest obstacle (ℓ_{min}) [*Batchelor*, 1967].

$$\ell_v = \frac{g d^4 |\nabla h|}{\nu^2} << \ell_{min} \tag{2.1}$$

Where g is the gravitational acceleration, d is the distance between plates, ν is the kinematic viscosity of the fluid (in our case glycerin), and ∇h is the gradient of the pressure head that drives the flow; note when there are no obstacles $\ell_{min} = \ell$ the cell plan view dimension.

Figure 2.1: A simple diagram of a Hele-Shaw cell. The two plates are parallel to the xy plane and the distance between them is d, the fluid moves perpendicular to the z axis.

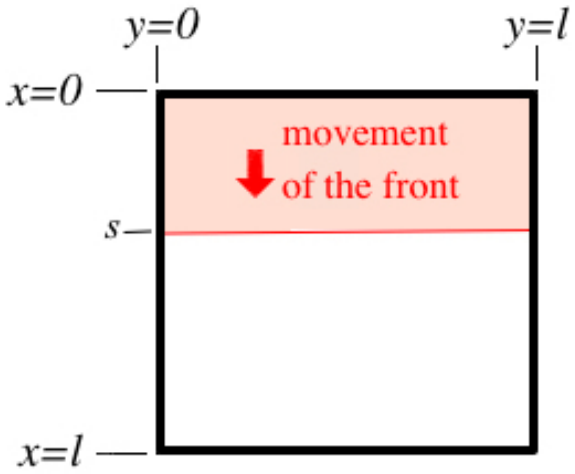

Figure 2.2: A simple diagram of a Hele-Shaw cell looking down the z axis. The fluid is driven into the cavity by a fixed head h_0, applied along the side $x = 0$, and moves in the x direction. Note at the front of the infiltration fluid the pressure head is $h = 0$. In this example the cell is a square with x and y dimensions of ℓ by ℓ.

Here we will consider a Hele-Shaw system in which the flow is driven into the cell by a fixed head along the side $x = 0$, see Figure 2.2. With the assumption that the flow is potential flow in form, the governing equation for the average fluid front in Hele-Shaw flow is identical to the governing equation for flow in a porous medium presented in the introduction. In particular, for the uni-directional flow case shown in Figure 2.2 the fluid flux($\frac{m}{s}$) in the x direction is given by

$$q_x = -K\frac{dh}{dx} \tag{2.2}$$

c.f. Eq 1.3. The parameter, K, in Eq 2.3 is a fluidic conductivity which, by the Hele-Shaw theory [*Batchelor*, 1967], is given by

$$K = \frac{1}{12}\frac{d^2 g}{\nu} \tag{2.3}$$

As with our porous tube the head gradient in the filled portion of the cavity ($0 \leq x \leq s(t)$) is a constant thus

$$\frac{ds}{st} = -K\frac{dh}{ds} = K\frac{h_0}{s}, \quad \big(0 \leq x \leq s(t)\big) \tag{2.4}$$

c.f. Eq 1.4 and

$$s = \left[\sqrt{2Kh_0}\right] t^{\frac{1}{2}} \tag{2.5}$$

c.f. Eq 1.5. The time dependence here has the exponent = $\frac{1}{2}$ which, as we discussed earlier, is the hallmark of normal diffusion. This means that when the cell is obstacle free normal diffusion can be expected and allows us to observe any changes in diffusive behavior as heterogeneity (obstacles) is introduced. Note that in making those observations it is not appropriate, due to interference of the obstacles, to track the flow as $s(t)$, see Figure 2.3. As an alternative we consider the infiltration $F(t)$ defined as (for a rectangle or square cell),

$$F(t) = \frac{\text{Area Filled}}{\ell} \tag{2.6}$$

i.e. the equivalent length of the fluid infiltration in the absence of obstacles. So with no obstacles $F(t) = s(t)$.

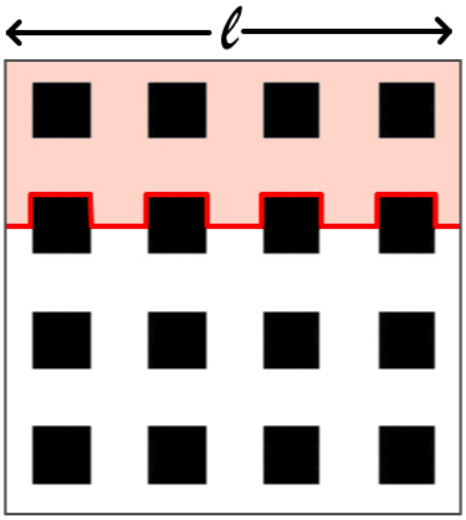

Figure 2.3: Schematic of infiltration with obstacles diagramming the non-planar location for the fluid front.

2.1 Experimental Design

The apparatus used for these experiments includes a tank, gate and chamber (see Figure 2.4). The chamber is constructed of a base piece, or cell, (Figure 2.5) and a 6.35mm ($\frac{1}{4}$") piece of transparent plastic bolted to the base piece that extends from the tank. The Hele-Shaw cells were 3D printed using ABS filament. They were printed in white to provide for maximum contrast. The fluid filled region of the cell is square, with a maximum area of 96mm x 96mm x 2mm. Any obstacles printed have a height (in the z direction) of 2mm. Parallel to the x direction there is an additional 12mm on each side with holes to allow for positioning of bolts to attach a 6.35mm ($\frac{1}{4}$") piece of transparent plastic to the top and attach the whole cell to the apparatus. The only difference between printed cells was the pattern of obstacles (or lack thereof) printed within.

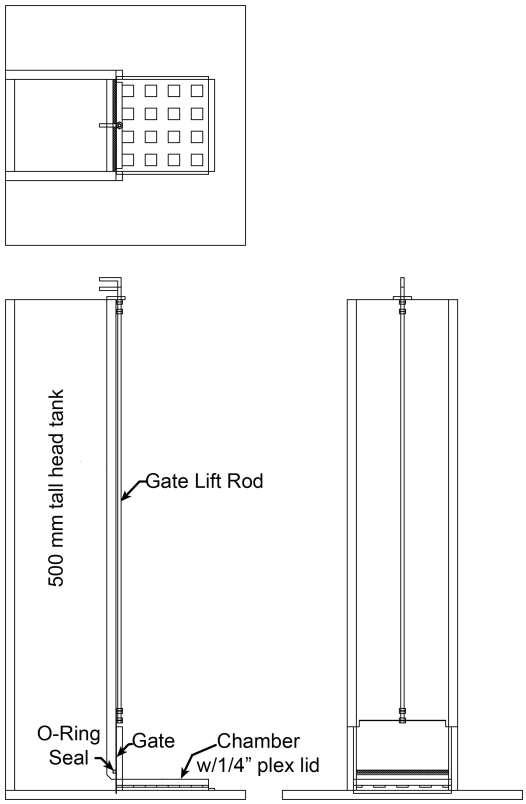

Figure 2.4: Design for the apparatus for Hele-Shaw experiments. The half meter tall tank was built from transparent plastic. The gate was manually operated using the lift rod with a lever (not shown) to improve speed of gate opening. Insert shows view looking down the z axis but does not include the 12mm sections on either side of the cell for bolt attachment.

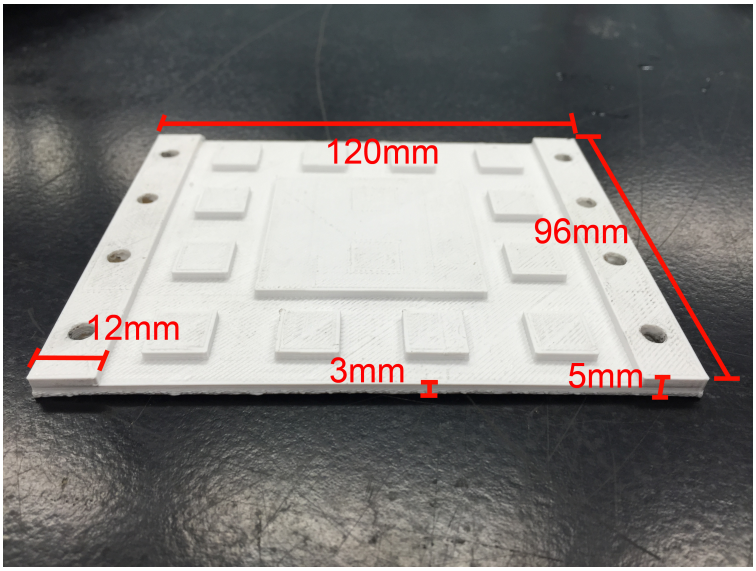

Figure 2.5: Example of a printed Hele-Shaw cell. Fluid filled region in 96mm x 96mm square. 12mm on each side with holes for bolts to affix transparent plastic above cell and cell to apparatus. Fluid filled region and obstacles are 2mm in the z direction. The only difference between printed cells is the obstacle arrangement within.

The half meter tall tank is made from clear transparent plastic, allowing for easy head measurements before each experiment. Measured h_0 values for each of the ten experiments are shown in table 2.2. The fluid in the tank was glycerin with a small amount of food coloring added to increase contrast between the fluid and the cell, we assume the value of the kinematic viscosity of glycerin at 20° is $\nu = 0.00112\ \frac{\mathrm{m}^2}{\mathrm{s}}$ [*Anonymous*, 1963]. We positioned a video camera (COHU 4910 series CCD) directly above the cell in front of the tank. During each experiment lamps were positioned at varying angles to decrease shadowing and increase contrast between fluid and cell in the videos. A gate lift rod manually opens the gate to begin the experiment.

We started the filming before each experiment began and the video was taken at a rate of 10 frames/second. Each experiment was considered complete when the fluid first exited the cell at $x = 96$mm. Depending on the obstacle distribution and the applied tank head h_0 the glycerin traversed the cell in $t_{exp} = 38 - 120$s. It was determined that the volume of fluid required to fill an obstacle free cell ($\sim 2 \times 10^4$ mm^3) was significantly smaller than the

initial volume ($\sim 4 \times 10^5$ mm^3) in the tank thus a constant head was assumed throughout each experiment.

By dividing the $F(t)$ in Eq 2.6 by the x dimension of the cell we can discuss a non-dimensionalized $\%F(t)$ representing the percentage of area infiltrated,

$$\%F(t) = \frac{A_F}{A} \tag{2.7}$$

We used a threshold and binarized the images from the video of each experiment. We quantitatively measured the filled area of a cell at each time step, raw data collected for each time step included area filled (A)[square pixels] and area filled fraction ($\%F$) [percent of total area] .

In practice we found that a small portion ($\sim$2%) of the plan-view area of the cell was obscured by the gate and we adjusted all calculations accordingly. In addition, to avoid possible bias from the initial entry into the cavity we neglected measurements taken at times less than $t = 1$s.

Heterogeneity was introduced in the form of different obstacle patterns (table 2.1) with the printed cells. We printed a blank cell, one with a repeating pattern, and five with different Sierpinski carpet fractal patterns [*Guo et al.*, 2006]. The fractal patterns are produced by first looking at the whole plan-view area as one square. This square is then divided N (pattern) number of times in the x and y directions, all but the outer row of (new smaller) squares is filled as an obstacle, this is then a fractal of m (order) = 1. To build a fractal of order 2 this process is repeated within each of the new smaller squares that were created in the first process. As the fractal order increases the obstacle size decreases. The examples in table 2.1 with a fractal order of 0 have such an indicator due to their patterns not being fractal in nature.

N (Pattern)	m (Order)	Example	N (Pattern)	m (Order)	Example
4	0	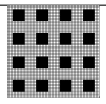	0	0	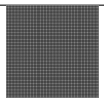
4	1	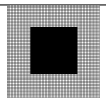	3	2	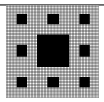
4	2	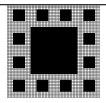	5	2	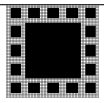
4	3	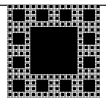			

Table 2.1: Obstacle arrangements of Sierpinski carpet design used for experiments. Pattern refers to the number of obstacles in a row or column, Order refers to the fractal order, and the example pictures are not necessarily to scale.

Exp #	N	m	h_0[m]
1	0	0	0.040
2	3	2	0.040
3	5	2	0.039
4	4	0	0.041
5	4	0	0.040
6	4	1	0.039
7	4	2	0.041
8	4	2	0.039
9	4	3	0.037
10	4	3	0.039

Table 2.2: Measured h_0 values for each experiment.

2.2 Results

2.2.1 Visual images

Figure 2.6 shows images from the experiment in the obstacle free cell at 1.8, 7, and 24 seconds. We can see the influence of an edge effect where the fluid along the side edges is moving more slowly than the fluid slightly further inside the cell. We also see a

slight slowing in the middle of the cell which may be due to irregularities in the printing process. Despite these effects we see a fluid front that can be fairly well approximated by a horizontal line, $s(t)$. Figure 2.7 shows images from an experiment in a fractal cell where N=4 and m=2 at 1.8, 7, and 24 seconds. Here the edge effect is observed not only along the outside edges but also along the edges of the obstacles but they appear to be the same order as the non-obstacle case.

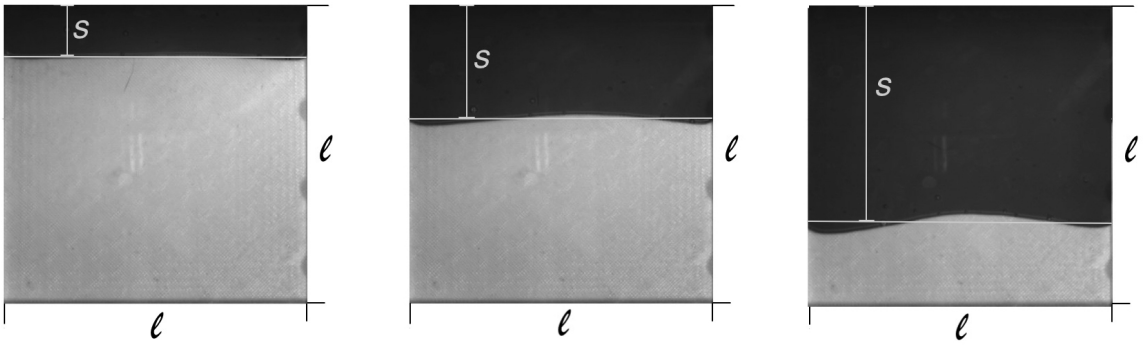

Figure 2.6: Video stills from an experiment using an obstacle free cell (1.8,7, and 24 seconds into the experiment). ℓ = 96mm and s = the progress in the x direction of the average front.

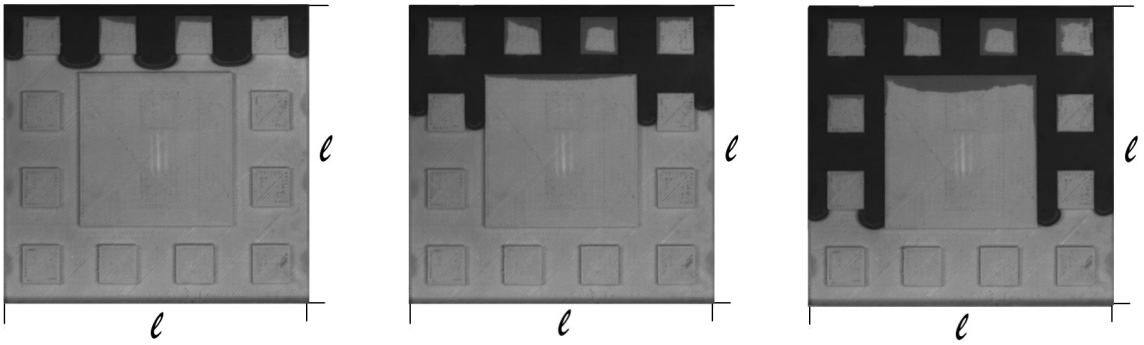

Figure 2.7: Video stills from an experiment using an fractal obstacle cell where N=4 and m=2 (1.8,7, and 24 seconds into the experiment). ℓ = 96mm

2.2.2 Comparison with theory

As noted above, when we have no obstacles the infiltration will go as

$$\%F(t) = \frac{s \times \ell}{\ell^2} = \left[\frac{\sqrt{2Kh_0}}{\ell}\right] t^{\frac{1}{2}} \tag{2.8}$$

It has also been suggested [*Filipovitch et al.*, 2016] that when we have a pattern (non-fractal)

$$\%F(t) = \left[\frac{\mu\sqrt{2h_0\mu K}}{\ell}\right] t^{\frac{1}{2}} \tag{2.9}$$

where μ is the pattern porosity, which is defined as the plan view area fraction of the cell free of obstacles. We use the following values in these equations to determine what results are expected by this theory; $K = 0.0029\frac{\text{m}}{\text{s}}$ by Eq 2.3 (using $\nu = 0.00112\frac{\text{m}^2}{\text{s}}$, $d = 0.002$m, and $g = 9.8\frac{\text{m}}{\text{s}^2}$), $\ell = 0.096$m, and h_0 values found in table 2.2. We plotted these lines alongside the infiltration data for the the empty cell ($N = 0, m = 0$) and repeating pattern ($N = 4, m = 0$) experiments (Figure 2.8) in log log space where the time exponent (n) could be easily determined by looking at the best fit line for each data set. Here we see the theory and experimental data aligning very well which can be seen visually as well as through the time exponent (n) values associated with a best fit for each experiment. The n values for both the empty cell and repeating pattern experiments are very close to $\frac{1}{2}$ which is a clear sign of normal diffusion. What this comparison shows us is that these experiments are behaving as they should, meaning that this experimental design is producing normal diffusion when theory expects normal diffusion.

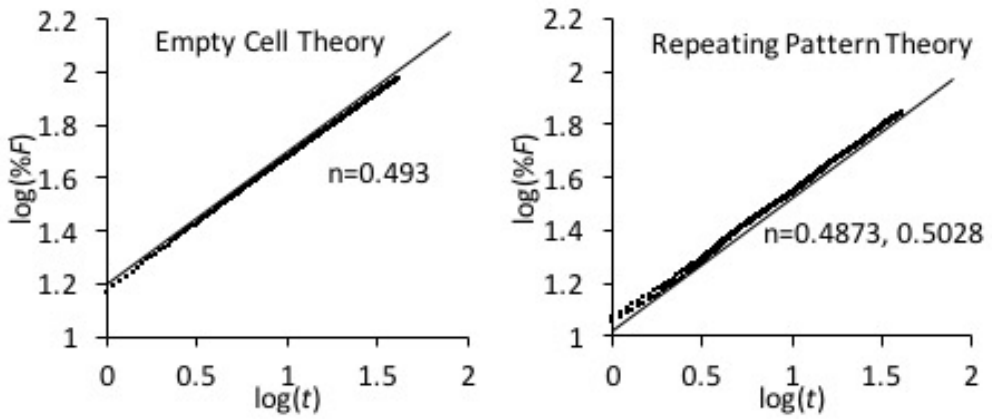

(i) (ii)

Figure 2.8: The dotted lines are measured data points and the solid line is the theory line determined by Eqs 2.8 and 2.9 respectively. The n values shown on each graph are gathered from the best fit for each set of experimental data. Infiltration results for both the empty cell and the cell with a repeating pattern show a good match with theory. This is evidenced visually by the close approximation the line gives for the data points as well as by the time exponent (n) values all being approximately $\frac{1}{2}$.

2.2.3 Anomalous results

Now that we know this experimental design produces normal diffusion as expected we look at the results from the experiments with cells containing fractal patterns. We plotted the infiltration data for the fractal experiments in log log space where the time exponent (n) could be easily determined by looking at the best fit line for each data set. In each of the fractal experiments anomalous diffusion was observed (Figure 2.9). Time exponents range from $n = 0.3328$ to $n = 0.423$ indicating sub-diffusive behavior for each of our Sierpinski carpet patterns. These results indicate that the presence of system scale heterogeneity, (i.e. the case where the obstacle size approaches the domain size and no repeating pattern can be identified), will induce anomalous diffusion behavior; particularly that the presence of heterogeneous obstacles will induce sub-diffusion.

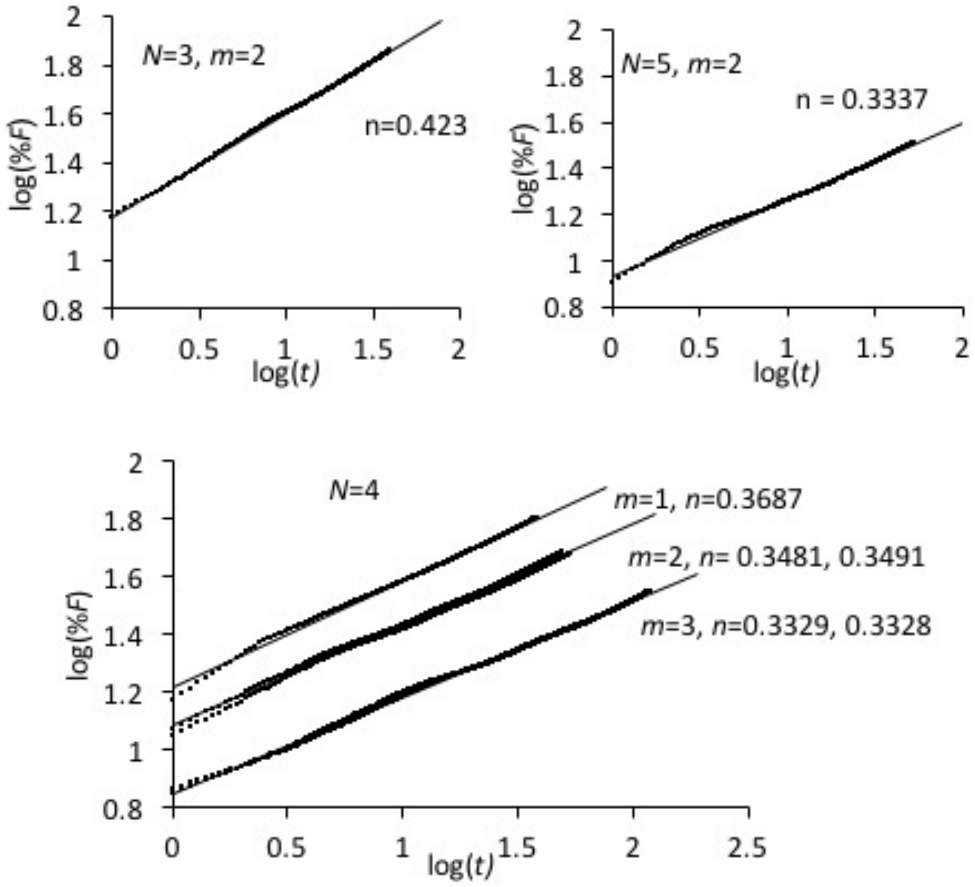

Figure 2.9: The dotted lines are measured data points and the solid line is the best fit line with the indicated time exponent (n). Infiltration results for all cells containing a fractal pattern of obstacles show anomalous diffusive behavior. This is evidenced by the time exponent (n) values all significantly less than $\frac{1}{2}$.

2.3 Discussion

While these results show that system scale heterogeneity leads to anomalous diffusion behavior, we note that each obstacle arrangement, i.e. value of N (3,4,5), appears to have a separate exponent and endeavor to quantify this relationship. We have already discussed the mathematical significance of the time exponent (n). To quantify the heterogeneous

nature of each pattern we look to the Hausdorff fractal dimension [*Guo et al.*, 2006].

$$H = \frac{\log(4N-4)}{\log(N)} \tag{2.10}$$

This dimension is determined by the ratio of the log of two quantities. The quantity on the bottom represents the number of sections any one side of the square is divided into. The quantity on the top represents the number of new smaller squares created around the previous large square in a single iteration. Note that this quantity is determined by the pattern number of a fractal and is not dependent on the order number.

To investigate the connection between the nature of the heterogeneity of the system and the resulting anomalous diffusion we plotted the H and n values of the experimental data (Figure 2.10). The data was well fit by the quadratic

$$n = 1.29H^2 - 4.17H + 3.69 \tag{2.11}$$

While this data set is not extensive enough to determine the ideal fit for this purpose it is an improvement over the simple geometric model

$$n = \frac{H-1}{2} \tag{2.12}$$

suggested by *Voller* [2015]. The fact that we see such a pattern indicates that the nature of the heterogeneity of a porous medium is directly connected to the extent of the resulting anomalous transport behavior.

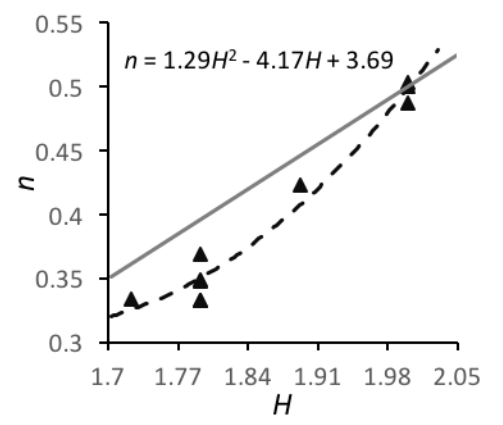

Figure 2.10: Graph of Housdorff fractal dimension (H) vs time exponent (n) from experimental data. The black dashed line is the best fit quadratic whose equation is displayed, the solid grey line shows Eq 2.12

2.4 Infiltration Summary

The infiltration experiments demonstrated that anomalous transport behavior is calculably connected to the nature of heterogeneity of the system.

- Our experimental design produces normal diffusion when the Hele-Shaw cell is empty or has a repeating pattern of obstacles which supports our conclusion that the nature of the heterogeneity in the system is what leads to the anomalous transport behavior.

- When system scale heterogeneity is introduced into the system anomalous transport is seen. In this case we observe not only the the time exponents (n) are sub-diffusive but that they vary based on the pattern (N) number of the fractal within the Hele-Shaw cell.

- The connection between the Hausdorff fractal dimension (H) and the resulting diffusive time exponent clearly indicates that anomalous diffusion can be induced by the nature of the heterogeneity in the system.

Chapter 3

Rice Pile Profile

Our second experimental study is directed at identifying and modeling non-local transport in granular piles. We can expect that the behavior of the rice pile may be related to non-local behavior due to the heterogeneity of granular piles. Granular materials are known to have high levels of heterogeneity relating to the development of discrete chains or clusters of particles within the system [*Drescher and de Josselin de Jong*, 1972, *Jaeger et al.*, 1996]. This contributes to an understanding that forces in granular materials may be effectively long-range as they are transmitted via these "force chains" to different parts of the system. [e.g. *Drescher and de Josselin de Jong*, 1972, *Jaeger et al.*, 1996]. In this way, if one particle is disturbed in such a force chain, it could result in some response of all particles in that chain [e.g. *Nichol et al.*, 2010]. Previous studies have reported evidence of non-local behaviors in sediment transport systems [*Falcini et al.*, 2013, *Foufoula-Georgiou et al.*, 2010, *Gabet and Mendoza*, 2012, *Martin et al.*, 2012, *Nikora*, 2002, *Schumer et al.*, 2009, *Voller and Paola*, 2010, *Voller et al.*, 2012]. In particular, evidence for non-local behaviors have been reported in details related to what is often called the long profile in a fluvial landscape. This is the height profile of the region that extends from the upland headwaters through the river system to the deltaic outlet in the ocean basin (see Figure 3.1). To quantify this it is helpful to consider a very simple steady state treatment where, to first

order, we assume that unit sediment flux (Area/Time) is proportional to (and decreasing with) the land surface slope, i.e.,

$$q_s = -\frac{\partial \eta}{\partial x} \tag{3.1}$$

here $\eta(x)$ is the land surface elevation above a datum at downstream position x. In this way the Exner sediment transport equation for the long profile, see Eq 1.9 in the introduction, can be written as

$$\frac{\partial}{\partial x}\left(\frac{\partial \eta}{\partial x}\right) = \sigma \tag{3.2}$$

where we have used σ to represent an uplift rate (a negative value would be used for subsidence). Broadly speaking there are three regions to consider, demarcated by the value of σ. In the upland collection headwaters (region A in Figure 3.1) we would expect an uplift ($\sigma > 0$). In order to remove the sediment provided by the uplift, satisfying the condition of $\sigma > 0$ with the model in Eq 3.2 will require that the slope increases with distance downstream, i.e., the second derivative of η is greater than zero. Thus, in the upland we would expect the fluvial sureface, $\eta(x)$, to have a concave down profile. By contrast as the system approaches the ocean region (region C in Figure 3.1) we would expect subsidence ($\sigma < 0$). Here, in order to retain the sediment removed by the subsidence, satisfying the condition of $\sigma < 0$ with the model in Eq 3.2 the slope decreases with distance downstream, i.e., the second derivative of η is less than zero. This means that in the deltaic region we would expect a concave up land surface profile. In the region connecting these two profile end regions (region B in Figure 3.1) we would not expect tectonic activity (ie., $\sigma \sim 0$), here there is no need to remove or deposit sediment so we would expect the surface, $\eta(x)$, to have a linear slope.

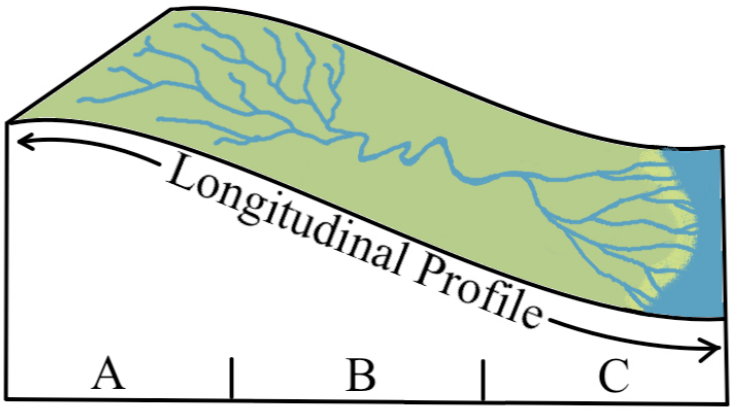

Figure 3.1: Schematic of a sample longitudinal profile. Section A shows the approximate location of the uplands where uplift would be occurring producing a concave down profile ($\sigma > 0$). Section B shows the approximate location of the region with no tectonic activity and a linear profile shape ($\sigma \sim 0$). Section C shows the approximate location of the deltaic region where subsidence would be occurring producing a concave up profile ($\sigma < 0$).

The exact modeling of the profiles in the uplands and deltaic regions have been areas of intense study [*Foufoula-Georgiou et al.*, 2010, *Schumer et al.*, 2009, *Voller and Paola*, 2010, *Voller et al.*, 2012]. This has included models that have used the concept of non-local transport fluxes as defined in Eqs 1.6-1.12. In particular *Foufoula-Georgiou et al.* [2010] have shown that an upstream weighted non-local treatment, where the sediment flux is modeled by an upstream fractional derivative, (i.e. $q \sim \frac{\partial^\alpha \eta}{\partial x^\alpha}$, $\alpha < 1$), provides a better fit to observation of upland (hill slope) land surface profiles. In contrast, *Voller and Paola* [2010] show that a downstream weight, (i.e. $q \sim \frac{\partial^\alpha \eta}{\partial (-x)^\alpha}$, $\alpha < 1$), provides a better fit to experimental observation of delta deposition systems. Further *Voller et al.* [2012] show that the assumed direction of the non-locality has a binary behavior. With the non-local flux models introduced in chapter 1 physically realistic predictions in a depositional environment can only be reproduced if the non-locality is directed downstream, i.e. downstream features in the system control the transport. In contrast realistic profiles in erosional (hill slope) regions can only be predicted if the non-locality is directed upstream.

To date, not too much attention has been applied to the by-pass case [*Postma et al.*,

2008] but in a general study of non-local transport *Falcini et al.* [2013] used this system to further investigate the consequences of the direction used in the non-local transport definition. Presented first in Figure 1.4 and summarized in Figure 3.2, this study suggested that, in the absence of tectonics ($\sigma = 0$) an upstream non-local model would produce a profile with the height (η), x relationship

$$\eta \sim 1 - x^{\alpha} \tag{3.3}$$

where $0 \leq \alpha \leq 1$. Profile shapes produced here are concave up where $\alpha < 1$. When $\alpha = 1$ the profile becomes linear. A downstream non-local model in this same tectonically neutral environment would produce a profile with the η, x relationship

$$\eta \sim (1 - x)^{\alpha} \tag{3.4}$$

where $0 \leq \alpha \leq 1$. Profile shapes produced here are concave down where $\alpha < 1$, with $\alpha = 1$ once again producing a linear profile. This simple by-pass system with no uplift or subsidence offers an opportunity to investigate the possible appearance of non-local behavior in a particulate system. *Falcini et al.* [2013] investigate a number of physical situations which might lead to profile curvature, e.g. non-linear transport coefficients; the conclusion was that in a by-pass regime only this non-locality correctly curves the profile. Therefore, any curvature seen in the profile of a by-pass system is an indication of non-locality. Further, if non-locality is established the curvature of said profile will also determine the direction in which that non-locality is weighted.

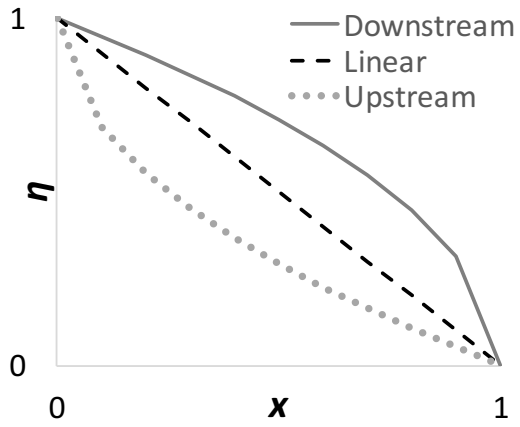

Figure 3.2: This figure shows predicted profile curvatures for a by-pass system as introduced in Figure 1.4. The profile produced by downstream weighted non-locality is shown as a solid line, the profile produced by upstream weighted non-locality is shown as a dotted line, and a linear profile is shown as a dashed line for reference. It is clear that an observed curvature in a by-pass system indicates a non-local influence and further that the nature of that curvature indicates the direction of the non-local influence.

In a preliminary treatment, *Falcini et al.* [2013] used the steady state by-pass experiments of *Postma et al.* [2008] to suggest that in a by-pass system (built through a deposition) the concave down profile suggests the presence of downstream directed non-locality, i.e. experimental profiles show a concave down shape. Here we investigate this point further but rather than using a sediment transport system we use an analogue system based around the dynamics of a granular pile. Admittedly, one system is gravity driven and one is fluid driven but both have grains that affect the surface profile so we feel comfortable considering that insight gained in these experiments will translate to the field of fluvial sediment transport. The most commonly studied granular pile is a sand pile. A sand pile is often initiated by releasing grains from a single point of grain entry into an empty system. These grains begin to build a pile whose grains periodically avalanche down the side of the pile, extending the base and growing the pile. The behavior of sand piles has been studied in both infinite and finite domains and in both three (e.g. [*Juanico et al.*, 2008]) and two dimensions (e.g. [*Alonso and Herrmann*, 1996]). In an infinite domain there is no outlet and the grains do not leave the system, the sand pile continues to build endlessly. Since there is

no outlet for the grains they must remain a part of the system. A finite domain is one that includes some sort of edge or drop off where the grains can (and do) leave the system. There is a depositional stage before the grains reach the edge while the pile is building. Once the grains begin to leave the system a by-pass stage begins when, on average, the same amount of grains are entering and exiting the system. A three dimensional sand pile is built up in the vertical direction (z direction in Figure 3.3 and out in the horizontal direction (as in the xy plane in Figure 3.3. This produces a cone shape that is commonly associated with the word "pile".

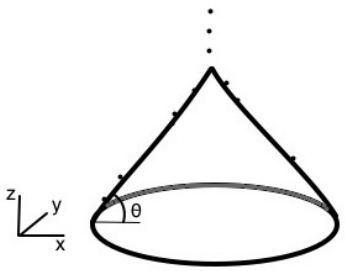

Figure 3.3: A sketch of a three dimensional granular pile with x, y, and z directions as well as the angle of repose (θ) indicated.

Two dimensional sand piles are built up in the vertical direction (the y direction in Figure 3.4) and out in the horizontal direction (the x direction in Figure 3.4) while the transverse direction (the z direction in Figure 3.4) is kept sufficiently small so that the variance across this dimension is negligible. In this study we will consider two dimensional finite piles.

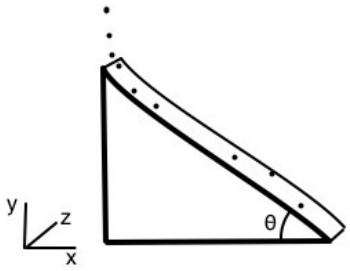

Figure 3.4: A sketch of a two dimensional granular pile with *x*, *y*, and *z* directions as well as the angle of repose (θ) indicated

A critical measure of a granular pile is the so called angle of repose. The angle of repose (e.g. θ in Figure 3.4) is the average angle at which the grains in the pile are at the threshold of movement. As the grains attempt to build the pile beyond this angle avalanching begins, bringing the pile back down to or below the angle of repose. Due to this process, there is a range of angles that a granular pile displays in the steady state. Of particular interest are the maximum angle of repose, which is the largest θ measured in a particular experiment (and sometimes is referred to as the critical angle) [*Denisov et al.*, 2012], and the average angle of repose, which is an average of all of the measured θ for a particular experiment [*Frette et al.*, 1996]. The anisotropy of the grains affects the angle of repose and its range; *Denisov et al.* [2012] report that "spherical grains have a lower angle of repose than nonspherical grains and that for nonspherical grains the angle of repose fluctuates much stronger". Angles of repose have been reported in the range of 30 degrees (spherical 65μm diameter magnetite beads [*Quintanilla et al.*, 2004]) to 51.1 degrees (polished rice with a 3.6 aspect ratio [*Frette et al.*, 1996]) with a variety of values in between [e.g. *Alonso and Herrmann*, 1996, *Denisov et al.*, 2012, *Juanico et al.*, 2008]. These reported angles have been measured using a variety of granular media including rice, sand, lentils, mung beans, polenta, and more.

All of these approaches have in common the presentation of one single angle stated as the angle of repose for that system, this implies that the angle of repose is constant for all

x. If a system has such a constant angle of repose the surface of the pile must be linear. Our hypothesis is that if there is non-locality involved in the building and maintaining of a granular pile we may expect to see curvature in the pile and an angle of repose that is not constant, $\theta(x)$. If the non-locality is upstream weighted, producing a concave up profile as previously described, we expect to see θ decrease with increasing x and if the non-locality is downstream weighted, producing a concave down profile as previously described, we expect to see θ increase with increasing x. Our core idea is to see whether this rice pile will reveal a non-linear profile shape, which would suggest non-local transport behavior, if this is the case we further would like to use the observed shape of the profile to indicate the direction of the non-locality.

3.1 Experimental Design

We used a rice pile experimental set up based on *Frette et al.* [1996] (Figure 3.5) built by Douglas Jerolmack [*Jerolmack and Paola*, 2010]. The rice was brown, long grain rice that has an average length of 7.20 $\pm$ 0.48 mm, an average width of 2.15 $\pm$ 0.34 mm and an average weight of .02 g per grain. The rice pile box is made up of two vertical parallel transparent plastic panels of height (η) = 36.50 cm spaced 2.54 cm apart making a long thin box with two closed and two open sides secured at all four corners. A styrofoam block is used at $L = 0$ giving the set up the ability to change L if desired; we ran all experiments with length (L) = 20.50 cm (exceptions described in Chapter 4).

Rice Pile Box Dimensions		**Rice Grain Characteristics**	
Height	36.50 cm	Length	7.20 $\pm$ 0.48 mm
Length	20.50 cm	Width	2.15 $\pm$ 0.34 mm
Width	2.54 cm	Average weight	.02 g

Table 3.1: Rice box (shown in Figure 3.5) and grain measurements

Each experiment begins with an empty rice box (exceptions described in Chapter 4) and it takes about 14 hours to reach the by-pass state. A toothed wheel picks up rice at an average of one grain per tooth and drops the grain into a paper funnel secured within the box. The paper funnel decreases the velocity of the grains as they are added to the pile as well as increases the precision of the grain entrance location onto the pile. For these experiments the speed at which the wheel turns was set such that the grains entered the system at a rate of approximately one grain per second. A camera with 6 megapixel resolution took time lapse photographs of the $\eta - L$ plane of the box every 5 minutes. We used these photographs to analyze the profile shape. There is a scale below the box at $x = 1$ that collects data at 1 Hz. Initially the set up included a blower connected to a timer to periodically blow rice off of the scale and into a large bin as had been used in previous studies to manage the scale's 400 g capacity [*Monbouquette*, 2008]. Due to the need to discount the data during the time the blower was running it was eventually determined unnecessary for these experiments and was not active for all experiments. The data from the scale was used for avalanche analysis discussed in Section 3.4.1.

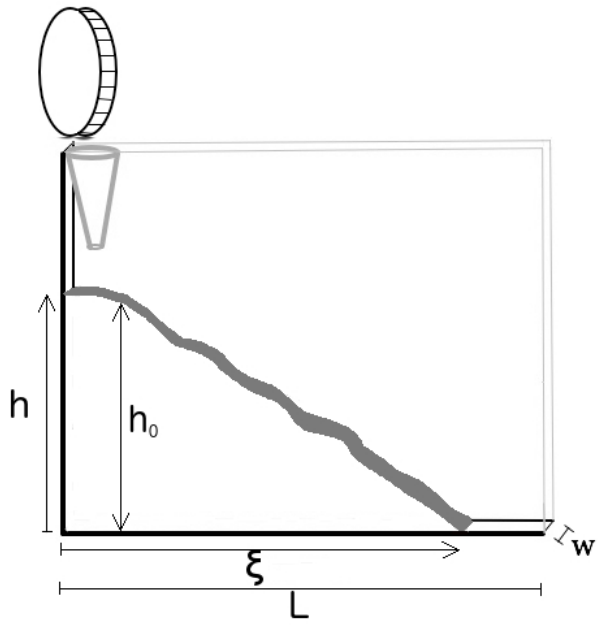

Figure 3.5: Sketch of rice pile box. The box consists of two large transparent plastic plates a distance *w* apart, with transparent plastic between the plates on the bottom and styrofoam between the plates on the left side. The edges of the box drawn in black are closed and the edges drawn in grey are open. There is also a transparent plastic peg of length *w* at the open corner. There is a wheel above the box with teeth that pick up an average of one grain of rice as each tooth passes the supply and rotates at a programmable speed to introduce rice into the system at whatever rate an experiment requires. From the wheel the rice enters into a paper funnel to ensure a more precise entry point. The height of the rice pile is shown as h and the length is shown as L.

When the rice first begins to enter the empty system a large majority of the rice stays in the system and builds a pile. Because, on average, more rice is entering the system than exiting this phase is referred to as a depositional environment. In the photographs of the build up stage we see a concave up profile as is expected in a depositional environment (Figure 3.6). This build up occurs through alternating periods of deposition and avalanching. We define deposition as the entrance of a grain that does not dislodge other grains as it comes to a rest inside the system. We define avalanching as the entrance of a grain whose addition causes some portion of the pile to exceed its critical state resulting in the movement of grains previously at rest. Avalanching is what causes the pile's width to increase and

grains to exit as the pile nears the edge of the system. As the width of the pile increases more and more grains leave the system. When, on average, the number of grains entering the system equals the number of grains leaving, the system is in a by-pass (or steady state) environment.

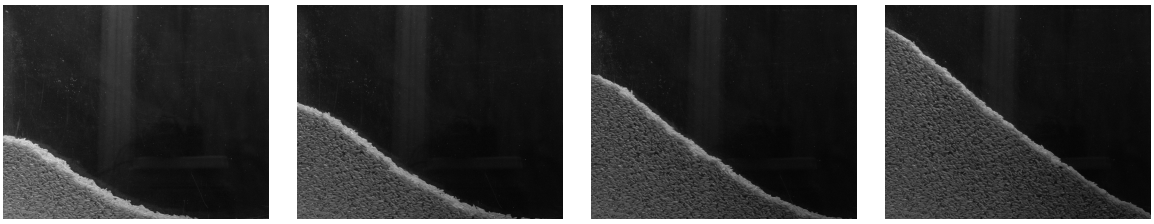

(i) (ii) (iii) (iv)

Figure 3.6: Build up process

Using the photographs from the by-pass stage, we analyzed the shape of the experimental profile. In our analysis, we consider each surface profile over the downstream 90% of the rice pile. We discount the first 10%, influenced by inertial effects from the impacts of the grains as they drop into the box. We use ξ to denote the horizontal dimension of the experiments; $0 \leq \xi \leq L$ and the top surface of the pile is $\mathrm{h}(\xi)$ (Figure 3.5). We normalize these variables according to the remaining length of the box and $\mathrm{h}_0 = \mathrm{h}(\xi = 0.1L)$: $x = (\xi - 0.1L)/0.9L$ and $\eta(x) = \mathrm{h}(x)/\mathrm{h}_0$ (Figure 3.7).

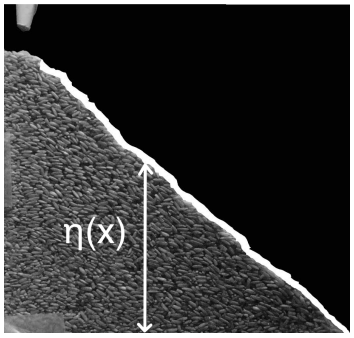

Figure 3.7: Snapshot of a ricepile in by-pass state. The thick white line indicates the approximate surface profile.

This system is consistent with similar systems in literature shown by the power law nature of the avalanches (Section 3.4.1) and the thickness of the active layer (Chapter 4).

3.2 Experimental Results

If the system dynamics are local we would expect a constant angle of repose, i.e. $\eta \sim (1-x)$ and that the profiles, when plotted on a log-log plot of η vs $(1-x)$, would appear as approximately linear and scattered about the line of slope =1. To analyze the shape of the observed profiles we plotted the normalized profiles on such a log-log plot (Figure 3.8). We then fit each profile with the power-law $\eta = (1-x)^{\alpha}$ using a linearized least squares fit. On this plot we see the profiles do appear as approximately linear but are not around the line $\alpha = 1$. The range of experimental α values is $0.8 < \alpha < 1$. The mean α value is 0.90 ± 0.02 using the standard deviation about the mean for uncertainty. The fact that none of the data shows an $\alpha = 1$ indicates a persistent curved profile surface. This curvature signals the presence of non-locality. Further we see that the curvature of this profile is a concave down curvature which indicates that if non-locality is present it is weighted in the downstream direction. Therefore our average profile can be described by

$$\eta = (1-x)^{0.9} \tag{3.5}$$

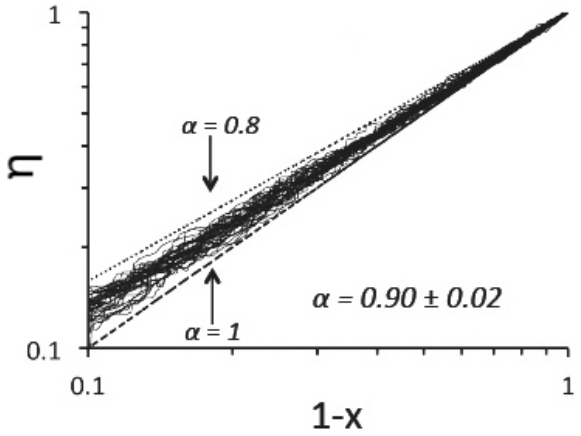

Figure 3.8: Normalized experimental profiles. Nonlinear least squares fitting indicates the results are well-fit by $\eta = (1-x)^{\alpha}$, $\alpha = 0.90 \pm 0.02$. For reference, lines representing $\alpha = 1$ (linear) and $\alpha = 0.8$ are shown.

3.3 Numerical Model Design and Results

To further investigate these results and ensure they were not merely a result of the the way we truncated the profiles, my research group, led by Anthony Longjas, developed a model of a dynamic rice pile that explores the effect of using local or non-local treatment.

The starting point of the model follows classic rice pile model of *Frette* [1993]. This models the rice pile as a set of columns (usually $\sim$100) each with a number of "grains" modeled as blocks. Each column is labeled by j, i.e. $j = 1,2,3,...,L$ and an integer height value $\eta(j)$ is assigned to each column. There is a solid wall at $x = 0$ and the drop off is at $L+1$. Starting from a stable pile, in a time step, we add a grain at $j = 1$, i.e. $\eta(1) \rightarrow \eta(1)+1$, and then iteratively track how this grain, and those it interacts with, move down the pile until a new stable state is reached. Essentially at each iteration in a time step, we progressively (from top to bottom) testing the stability of each column in turn. Stability in the classic rice pile model is defined by the difference in height between neighboring columns, S_L. The *Frette* [1993] model begins by using a constant critical slope, $S_c = 1$ (block) but also allows for the addition of randomization, or noise, by allowing the critical slope S_c to take on a value of either 1 or 2, they do so with equally probability. For the constant critical slope model if $S_L \leq S_c = 1$ (block) (a difference in height between columns of one block or less) this portion of the pile would be stable (Figure 3.10 i) and if $S_L > S_c = 1$ (a difference in height between columns greater than one) this portion of the pile would not be stable and failure would occur. In the model failure occurs by moving the top block from column j to the top of column $j+1$, as shown in Figure 3.10 ii. The net result of this model is, after appropriate normalization, a pile with an average profile of $\eta = (1-x)$. Interestingly the avalanches (i.e. the total grains leaving the system in a time step) in the system are in a power-law distribution as will be discussed further in Chapter 3.4.1.

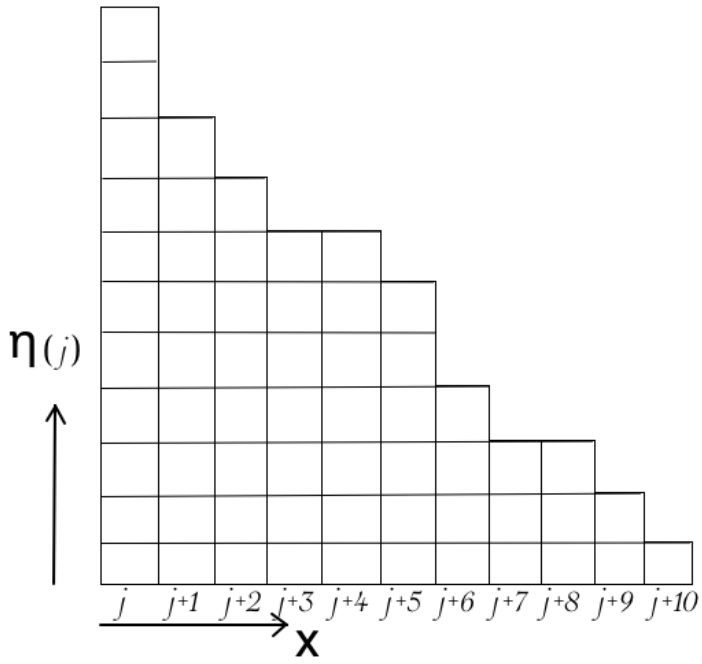

Figure 3.9: Schematic of a possible stable rice pile configuration of the model where noise is included.

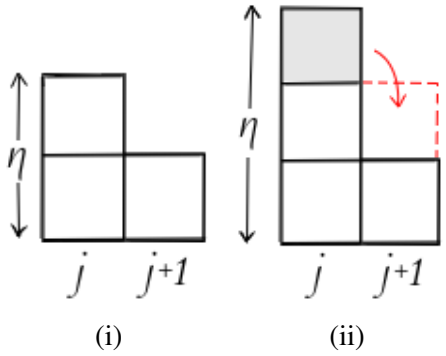

Figure 3.10: Schematic of rice pile model stability criteria. i) a stable configuration where $S_L \leq 1$. ii) an unstable configuration where $S_L > 1$ and thus failure occurs in the form of the top block in the jth column moving to the $(j+1)$th column.

The extension by Anthony Longjas to this model was to use a non-local behavior to determine the stability of a column. As before if the measured slope (S_{NL}) exceeds the critical slope, i.e. $S_{NL} > S_c = 1$, failure occurs. Where the local slope was determined

only by the difference in η between the jth and the $(j+1)$th column, the non-local slope is determined by a weighted sum of the local downstream slopes, i.e. $S_{NL} = \omega_1 S_{L_j} + \omega_2 S_{L_{j+1}} + \omega_3 S_{L_{j+2}} + \dots$.

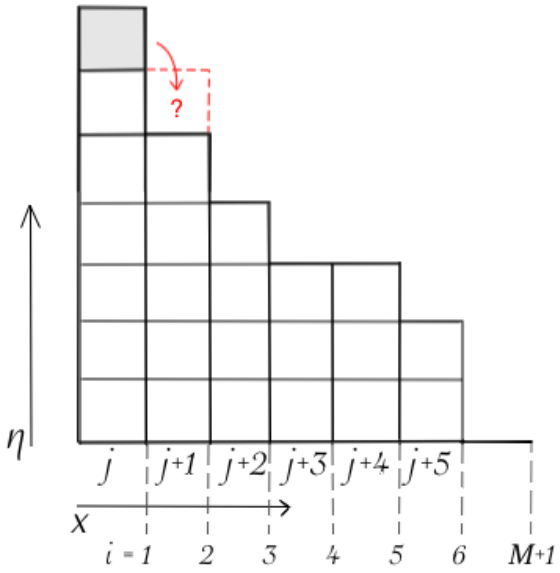

Figure 3.11: For the non-local rice pile model the stability of a column is determined not only by the difference in η between columns j and $j+1$ (S_L) but rather by a weighted sum of all downstream slopes where the weights decrease in increasing distance from column j. i represents the points between columns where local slopes are measured.

The local slope of each point j downstream of x contributes to the expression for $S_{NL}(x)$ with a weight ω_i that decreases with increasing distance from x

$$S_{NL}(x) = \sum_{i=1}^{M-1} \omega_i S_i \tag{3.6}$$

Where the length of the domain downstream of x is divided into $M-1$ sections of horizontal length Δx, and $M = \frac{1-x}{\Delta x} + 1$, and $i = 1$ corresponds tothe jth column. A possible set of weights to be used in Equation 3.6 are in terms of the Grünwald weights

$$\omega_i = \Delta x^{1-\beta} \sum_{k=1}^{i} g_k \tag{3.7}$$

where $0 < \beta \leq 1$ the Grünwald weights are (see page 23 in *Meerschaert and Sikorskii* [2012]):

$$g_1 = 1; \quad g_i = \frac{i-2-\beta}{i-1} g_{i-1}, \quad i \geq 2 \tag{3.8}$$

This is choice of weights is motivated by noting that in the limit that $\Delta x \to 0$ it can be shown that

$$S_{NL}(x) = \sum_{i=1}^{M-1} \omega_i S_i = \frac{1}{\Delta x^\beta} \sum_{i=1}^{M} g_i \eta_i \approx \frac{1}{\Gamma(1-\beta)} \int_x^1 (\xi - x)^{-\beta} S_L d\xi \equiv \frac{\partial^\beta \eta}{\partial (1-x)^\beta} \tag{3.9}$$

where $\Delta x = \frac{1-x}{M-1}$, $\eta_i = \eta(x + (i-1)\Delta x)$, i.e. this choice make the rice pile model compatible with our previous non-local fractional derivative treatment. The net result of this non-local model is a pile with an average profile of $\eta = (1-x)^\alpha$ and $\beta \approx \alpha$. Interestingly the avalanches in this system also appear in a power-law distribution as will be discussed further in Chapter 3.4.1.

When the results of these two models are compared to our experimental results (Figure 3.12) we can see that our choice of non-local model reproduces our experimentally observed profile while the local model does not. The local model produces an approximately linear profile with an average $\alpha = 0.98$ while the non-local model produces the same concave down profile observed in our experiments with an average $\alpha = 0.90$. This result verifies not only our conclusion that non-locality was observed in our experiments but also that the observed non-locality was downstream weighted.

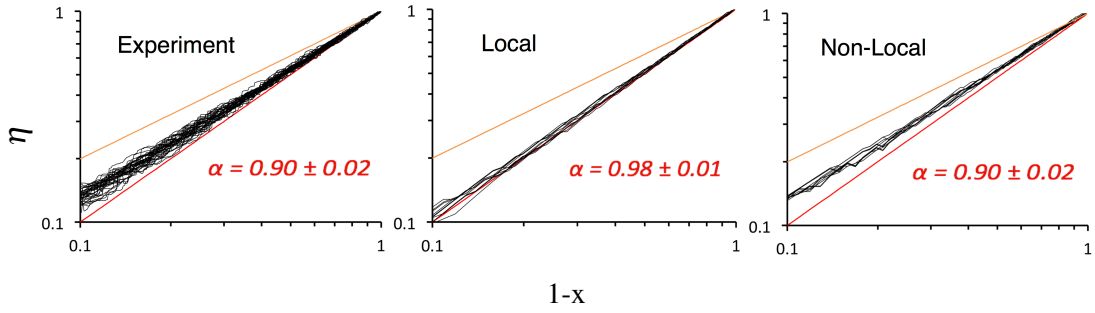

Figure 3.12: Rice pile profile data from numerical models. Sample profiles of the curvature are obtained using the previously presented rice pile model of *Christensen et al.* [1996] as the local model and the modified form of this model incorporating a non-local failure criterion. The numerical results reported here use an array of $M = 250$ cells and time steps $t = 2M^2 = 1.25x10^5$. The results obtained using the local model exhibit linear profiles, while the results obtained using the non-local form of the model exhibit the experimentally observed surface profiles with a power-law exponent of $\alpha = 0.90$. Non-linear least squares fitting indicates the results for both sets of data are well-fit by $\eta = (1-x)^{\alpha}$. Lines representing $\alpha = 1$ (linear) and $\alpha = 0.8$ are shown for reference.

3.4 Discussion

3.4.1 Power-law avalanche analysis

When the sizes of avalanches, (measures of the pile output from one input event), observed in granular piles are plotted against the frequency of occurrence a power-law pattern is evident for many granular piles [*Amaral and Lauritsen*, 1997, *Bak et al.*, 1987, *Frette et al.*, 1996, *Quintanilla et al.*, 2004]. This pattern demonstrates that in these systems there is an expected relative frequency of an avalanche of a given size inversely related to the size of an avalanche. A representative equation for such a power-law system in which the probability distribution of x is shaped by the experimentally determined exponent τ is

$$p(x) \sim x^{-\tau} \tag{3.10}$$

The power-law distribution, however, is not present for all granular piles [*Feder*, 1995].

For instance, *Bak et al.* [1987] predicted power-law distribution of avalanches in a sand pile and, while the description of a sand pile can be useful in picturing a process that would produce this pattern, *Nagel* [1992] shows clearly that the expected pattern is not seen with sand. One important characteristic is the anisotropy of the grains in the system [*Denisov et al.*, 2012, *Frette et al.*, 1996]. Although the aspect ratio of the rice grains was chosen specifically to ensure power-law behavior it is important to gather avalanche data to verify the expected patterns.

Our avalanche data is that of drop statistics. After removing known erroneous data from the set (e.g. large negative numbers during times when the blower was active) we plotted data collected during equilibrium. We plotted the avalanche size versus frequency. We did only one experiment for a length of time sufficient for power-law analysis, since large data sets are preferable to minimize fluctuations in this analysis [*Clauset et al.*, 2009]. The avalanche data from the scale was plotted on PDF plots (Figure 3.13 a) where patterns consistent with power-law distributions were observed. A linearized least squares fit to the experimental data yields a power-law exponent $\tau = -1.94$ which is consistent with results seen in literature [*Amaral and Lauritsen*, 1997, *Frette*, 1993, *Frette et al.*, 1996]. The power-law exponent cited in *Frette et al.* [1996] of $\tau = -2.02$ is reasonably close to our experimental value. This is an indication that the rice pile system studied here is consistent with other systems discussed in literature. It is interesting to note that the avalanche statistics for local and non-local models were also recorded (Figure 3.13 b) and power-law avalanche sizes were observed in both cases. This not only goes towards validating the model as we see this pattern with the model under both local and non-local conditions but it also goes towards showing that the presence of these power-law sized avalanches may not be a signal of non-locality.

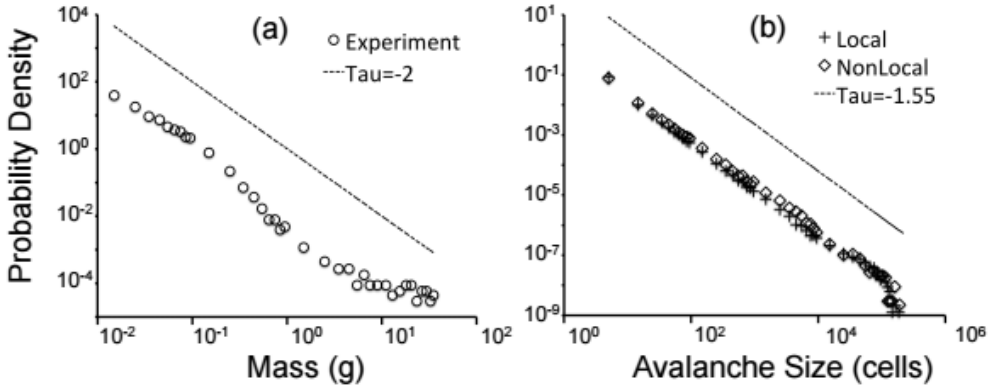

Figure 3.13: Avalanche size power-law distribution for experimental and modeled data. (a) The linearized least squares fit to the experimental data yields a power-law exponent $\tau = -1.94$, which is reasonably close with the $\tau = -2.02$ reported in the experiment of *Frette et al.* [1996]. (b) The local model yields a power-law exponent of $\tau = -1.57/pm0.02$, and the model with the non-local correction yields $\tau = -1.56 \pm 0.01$; both are consistent with values reported in literature [*Amaral and Lauritsen*, 1997, *Christensen et al.*, 1996]. The broken line serves as a guide to the eye and has a value of $\tau = -2.0$ for (a) and $\tau = -1.55$ for (b).

3.4.2 Further profile analysis

In conjunction with Anthony Longjas we analyzed surface profiles presented for the rice pile in *Frette et al.* [1996] and the sediment by-pass in *Postma et al.* [2008] for profile curvature, and a concave down profile was seen in both instances (Figure 3.14). The rice pile profiles in *Frette et al.* [1996] produced an α value of 0.86 ± 0.08 whereas the *Postma et al.* [2008] by-pass sediment profile produced an α value of 0.74. For each of these evaluations limited numbers of profiles were available but the results show clear consistency with our experiments. These results further strengthen the experimental results of profile curvature and the inclusion of non-local dynamics in the modeling of such systems.

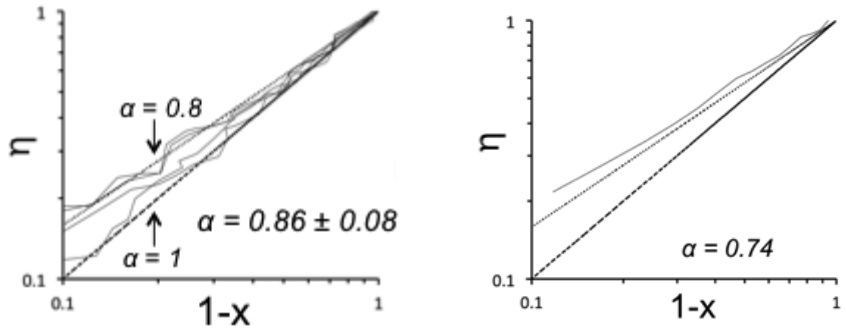

(i) (ii)

Figure 3.14: Long profile curvature results recovered from i) the rice pile presented in *Frette et al.* [1996] and ii) the by-pass sediment profile presented in *Postma et al.* [2008]. The recovered profiles were fitted with $\eta = (1-x)^{\alpha}$ resulting in $\alpha = 0.86 \pm 0.08$ and $\alpha = 0.74$, respectively. Lines representing $\alpha = 1$ (linear) and $\alpha = 0.8$ are shown for reference.

3.5 Rice Pile Profile Summary

The rice pile demonstration recognized a clear signal of non-local dynamics as was evidenced by a surface curvature, the shape of which further signals the direction of the non-locality to be downstream weighted.

- *Falcini et al.* [2013] predict a curvature in such a by-pass system if and only if non-locality is present.
- All experimental profiles present a concave down curvature, which demonstrates anomalous transport behavior caused by the presence of downstream non-local dynamics.
- This anomalous behavior is reproduced in a model through the use of downstream weighted non-local dynamics.
- Our model produces power-law sized avalanches using both local and non-local failure criteria, this result goes towards validating the model.

- The fact that both the local and non-local model reproduce power-law sized avalanches suggests, however, that there is no strong connection between power-law sized avalanches and non-locality.

Chapter 4

Evidence of Non-locality in the Active Layer

One of the goals of our work is not only to build experiments that exhibit strong signals of anomalous behavior and non-local transport but also to develop an explanation for the observed behaviors. In the infiltration experiments we were successful at linking our observation of anomalous diffusion to the level of heterogeneity in the system. A working hypothesis for the expected presence of non-local transport in the rice pile was the occurrence of power-law sized avalanches. The observation that both a local and non-local model were able to reproduce the same power-law statistics for observed avalanches, however, made us question if this feature was a direct signal of non-local transport dynamics. This lead us to look for other features in the dynamics of the rice pile that might have a more direct connection to non-local behavior.

Nichol et al. [2010] noted non-local behavior in a granular system where the dynamics in the creeping section were to some level controlled by the dynamics of the shear zone. The experimental design of *Nichol et al.* [2010] was a drum whose shear zone is at the bottom unlike our two dimensional rice pile. However, a rapidly flowing layer above a creeping layer was seen in a two dimensional granular pile by *Komatsu et al.* [2001]. Casual

observation of our rice pile appears to show a rapidly flowing layer on the surface with little or no movement beneath. *Jaeger et al.* [1996] noted that granular piles previously at rest whose angles are changed adjust with movement of only the surface grains where the grains deeper within the pile appear at rest rather than creeping. This leads us to explore whether our rice pile does contain a rapidly flowing layer (active layer) that reaches a distinct depth within the pile and whether the bulk of the rice pile is a zone of creeping or immobile grains.

The avalanching grains of the rice pile move with a non-uniform velocity profile wherein the grain velocity is greatest near the surface of the pile. The depth to which this movement extends defines an active layer. In grain flows with shear zones a zone of shear flow may be accompanied by a zone of creep [*Nichol et al.*, 2010] and *Komatsu et al.* [2001] claim that some degree of movement extends throughout the entire granular pile but it is not debated that the velocity profile is non-uniform where the top grains move more quickly than the grains below. The terminology surrounding the active layer is not used consistently in all of the literature; for instance *Jaeger and Nagel* [1992] referred to it as a zone of rapid shear flow. In this paper we will be using the term active layer to refer to the layer in which significant movement of grains, as determined by the process of image subtraction, is detected during the time frame of consideration.

While an active layer and a shear band are not identical the width of shear bands can be used as an analogy for the depth of the active layer. The width of shear bands in granular materials is not affected by any geometrical concerns of the system other than the grain dimensions themselves [*Muhlhaus and Vardoulakis*, 1987]. There are reports that the correlation between grain diameter and shear zone width are anywhere between a factor of 3 and a factor of 18. *Roscoe* [1970] observes in experiments with sand that shear zones are on the order of 10 grains thick. This value is also used in calculations by *Boutreux et al.* [1998]. *Aradian et al.* [1999] argue that a value of 3 is more appropriate for their calculations while *Muhlhaus and Vardoulakis* [1987] see experimental evidence of shear zones up

to 18 grains thick.

4.1 Search for the Active Layer and a Finite Thickness

To analyze the thickness of the active layer we performed image subtraction of two photographs representing various time intervals (Figure 4.1). Any area of the two photographs that are identical appears black on the final image. Areas showing rice deposited in previously empty space will show up bright (light grey to white) and clear as in Figure 4.1 i. Areas that contained rice in the first image but contained nothing in the second image will show as empty space (black). In Figure 4.1 ii, iii, & iv the mid to dark grey represents areas where rice was present in both of the images but has changed position. We defined the active layer in each subtracted image pair as the region that appeared white to dark grey, representing rice grains that had moved.

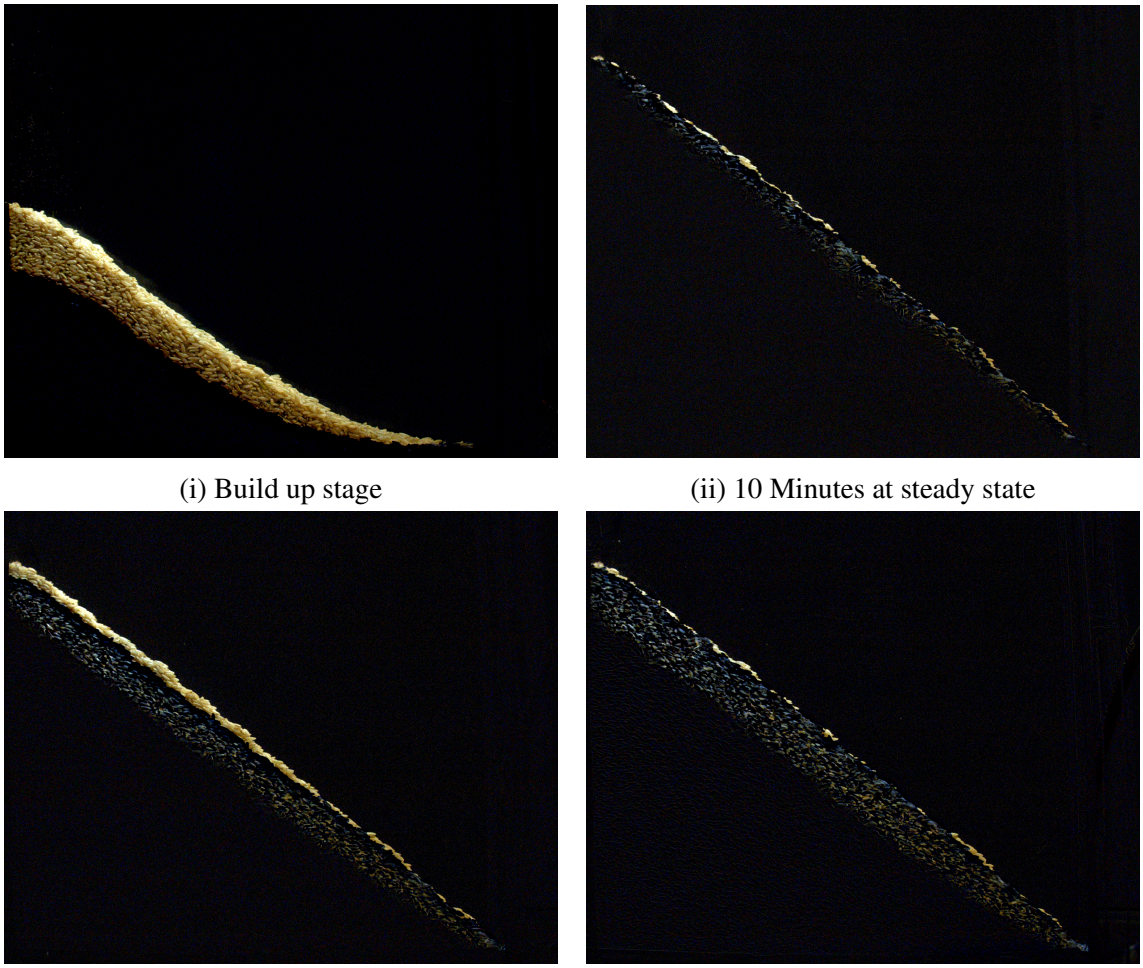

(i) Build up stage

(ii) 10 Minutes at steady state

(iii) 2 hours at steady state

(iv) 12 hours at steady state

Figure 4.1: Examples of image subtraction for a depositional environment, 10 minutes in a steady state environment, 2 hours in a steady state environment, and 12 hours in a steady state environment

We considered the width of the active layer to be represented by thickness of this grey region in the area. We measured this in five different locations on each image subtraction pair using standard image processing tools (image j). We averaged these results and then plotted the averages against the length of time between photos subtracted to investigate how the apparent width of the active layer changed with length of time between images (similar to the shutter speed in *Komatsu et al.* [2001]) (Figure 4.2). The apparent width of the active layer initially grows with this time interval, similar to *Komatsu et al.* [2001]. However,

unlike this previous work, in the rice piles, the width appears to approach a constant, (i.e. saturated), of approximately 2.44 cm as the length of time considered is increased. The range (showing lowest and highest recorded values) of average measurements (represented with black error bars) is very close to the width of a single grain of rice (represented with grey error bars).

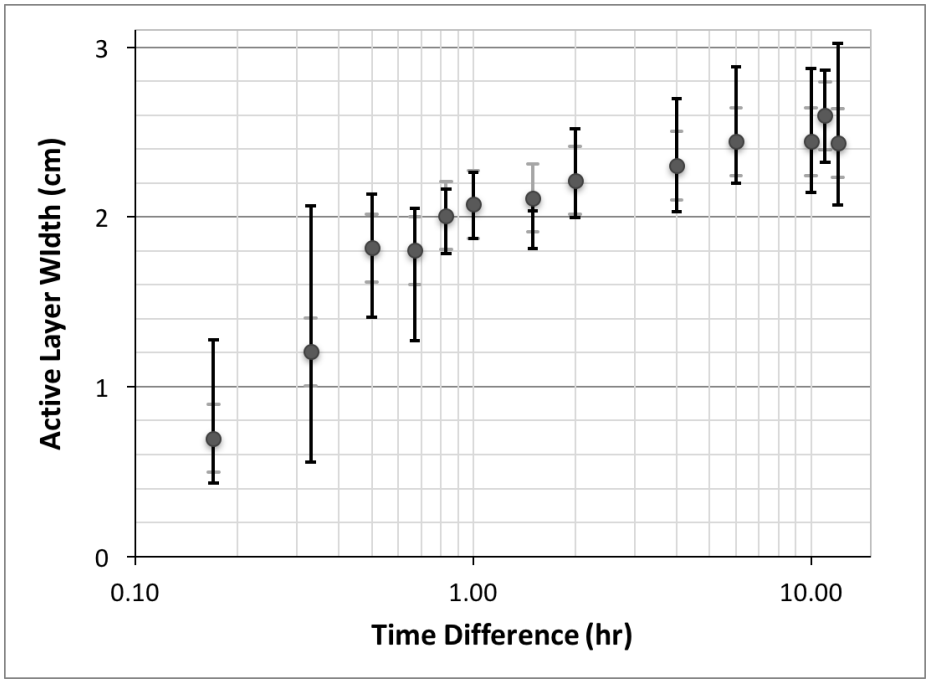

Figure 4.2: Width of active layer as determined through image subtraction plotted opposite the time difference between the subtracted images. Black error bars represent range in measurements, grey error bars represent the width of a grain of rice.

2.44 cm is only slightly greater than ten times the width (2.15 mm) of our rice grains. If we consider our shear zones analogous to shear bands as discussed at the beginning of this chapter, this is consistent with results from *Muhlhaus and Vardoulakis* [1987] who found that shear bands are typically approximately 8-10 grains thick. This is an indication that this system is consistent with comparable systems in literature. Since a grain of rice is not spherical it is interesting to note that this rule indicates that in a rice pile it is the width of the grain, rather than the length, that relates to the thickness of the active layer.

4.2 Evidence of Non-locality Involving the Bulk

When describing the active layer it is unclear how discontinuous the movement is from the rest of the pile. That is, to the naked eye there appears to be a static section of rice below the active layer, this section also appears immobile when using the image subtraction technique. However *Komatsu et al.* [2001] noted that in a system with spherical particles and steady surface flow the layer beneath the surface flow has a creep velocity that decays exponentially with depth beneath the free surface. Comparing their "creep zone" with our apparent fixed depth flowing layer motivated us to investigate this question in more detail in our grain piles. We did so by introducing a completely static wedge to the base of the pile to represent the apparently immobile rice grains in the system. We reason that if there is truly no creep in our pile beneath the flow, a sufficiently small wedge would have no effect. If there is a creep velocity of the grains within this wedge region we would expect that replacing these mobile grains with a completely immobile section would change the characteristics of the rice pile and/or statistics of the flow layer. To investigate this question of creep, for this thesis, we considered two characteristics of our rice pile, the active layer width and the average angle of repose.

Wedge Experiments			
Wedge Angle (θ)	Wedge Length (L_w)	Box Length (L)	Wedge Surface Texture
39°	17.5 cm	20.5	Rough
41°	17.5 cm	20.5	Rough
43°	17.5 cm	20.5	Rough
41°	27.2 cm	30.5	Smooth
41°	25.3 cm	30.5	Smooth
41°	29.0 cm	30.5	Rough
41°	28.8 cm	30.5	Rough
41°	28.1 cm	30.5	Rough
41°	27.6 cm	30.5	Rough
41°	27.2 cm	30.5	Rough
41°	26.6 cm	30.5	Rough
41°	25.9 cm	30.5	Rough
41°	25.3 cm	30.5	Rough
41°	24.5 cm	30.5	Rough
41°	23.1 cm	30.5	Rough
0°	0 cm	30.5	N/A

Table 4.1: Experiments conducted with a styrofoam wedge in the box to investigate active layer characteristics.

We performed the experiments in table 4.1 in the rice box monitoring outputs and instantaneous bed heights as described in Chapter 3 with two important changes : (1) for greater resolution we used a longer box than the one described in Chapter 3; (2) we inserted a styrofoam wedge that varied in size from one experiment to the next (Figure 4.3). We ran experiments with two different surfaces at the boundary between the wedge and the rice grains, smooth and rough. The smooth surface was the surface of the styrofoam sanded flat. The rough surface was developed by gluing rice grains (dropped onto the surface at random angles) to the contact surface. The experiments with the smooth wedge exhibited a flow-through environment with no rice remaining in the box whatsoever. The experiments with the roughened wedge surface exhibited a build up of rice in front of and on top of the wedge. This indicated that these experiments require a wedge contact surface that mimics the roughness of a static wedge of rice. The rough surface was used for all reported data.

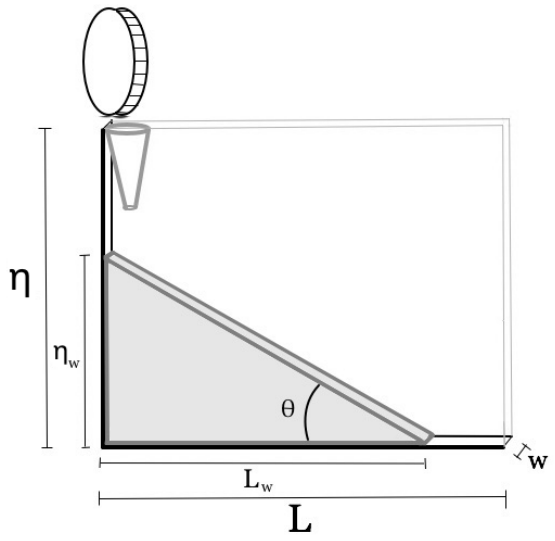

Figure 4.3: A styrofoam wedge was placed within the box simulating a static section of the rice pile.

We were interested in the steady state so we began each experiment with an empty box except for the styrofoam wedge (or completely empty). The addition of the wedge decreased the time it took to reach steady state (from the 14 hours for the experiments in Chapter 3) and varied inversely with the size of the wedge.

We conducted two sets of experiments. The first was to investigate whether or not, for a given wedge length $L_w < L$ there is a minimum θ below which the active layer would not be affected by the presence of the wedge. The second was to investigate whether or not, for a given wedge angle θ there is a minimum wedge length L_w below which the active layer would not be affected by the presence of the wedge.

For the first set of experiments we used a box length of $L(x) = 20.5$cm and a wedge length $L_w = 17.5$cm and three different wedge angles: 39, 41, and 43 degrees. The mobile grains on top of the wedge change their behavior with different values of θ (Figure 4.4). As is visible in Figure 4.4 the presence and characteristics of the static wedge can affect both the thickness of the active layer and the angle of the surface of the pile of rice. At 39°

the layer of rice above the wedge extends along the entire surface and appears to be slightly thicker at small x than at large x. At 41° the layer of rice above the wedge extends along the entire surface and appears similar in thickness from small x to large x. At 43° the layer of rice above the wedge does not extend all the way to small x, is thicker at small x than at large x, and even the thickest portion is thinner than either of the previous angle tests. The 41° wedge surface is closest to parallel to the surface of the rice and is not so large that is interferes with the development of an active layer. From this we concluded that 41° was below the minimum θ that would affect the active layer, also note that this value is similar to the average angle of the surface of the rice pile with no wedge (See Figure 4.5).

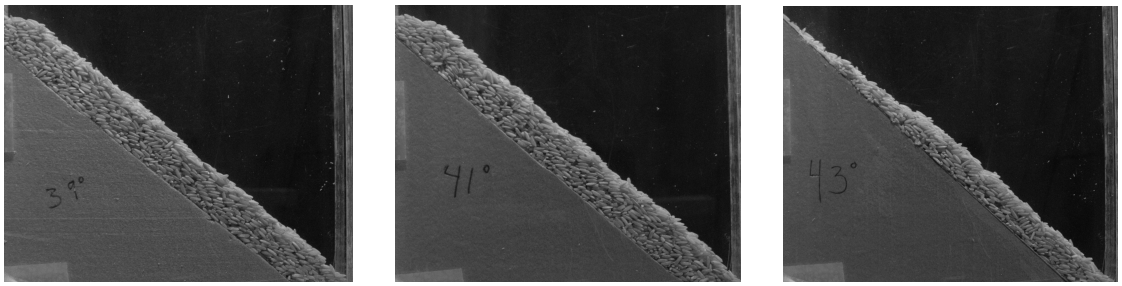

(i) (ii) (iii)

Figure 4.4: The angle of the wedge was varied until an angle was found where the active layer was clearly affected. Above are wedges with angles of $\theta = 39°$ (i), $\theta = 41°$ (ii), and $\theta = 43°$ (iii). When θ reaches 43° the mobile layer of grains no longer reaches the top of the wedge and the layer that is present is much thinner, even at the bottom of the wedge.

Based on these results, we performed the second set of these experiments using 41° wedges in a box where $L = 30.5$ to allow for more data points near the active layer transition. As one might expect, as the size of the wedge was decreased, the surface of the wedge moved further away from the visual approximation of the bottom of the active layer. We used two physical parameters to quantitatively evaluate the effect of the wedge on the flowing layer and how that effect varied with wedge size: (1) surface slope, and (2) active layer thickness.

As we have discussed, the surface of the rice pile contains a curvature rather than being a linear slope, so for this analysis we visually approximated an average slope to determine

how the average slope changed with wedge size (Figure 4.5). We recorded such slopes for 12 consecutive images from each wedge experiment, thus representing data from a two hour period. The average and spread of these slopes is presented in Figure 4.5. For the experiment with no wedge in the box with $L = 30.5$cm we recorded visually determined linear average slopes for two sets of 12 consecutive images. In other words two two hour periods of data are represented by the no wedge average and range.

These data indicate that while the wedge is large the surface angle of the pile is less than the surface angle of a pile with no wedge (and indeed often truncates on the wedge rather than extending to the top) but as the wedge size decreases the measured surface angles are very close to or within a normal range of values for a pile with no wedge. Surprisingly, for the smallest wedges measured the surface angle is lower than that without the wedge (Figure 4.5). We discuss this shortly.

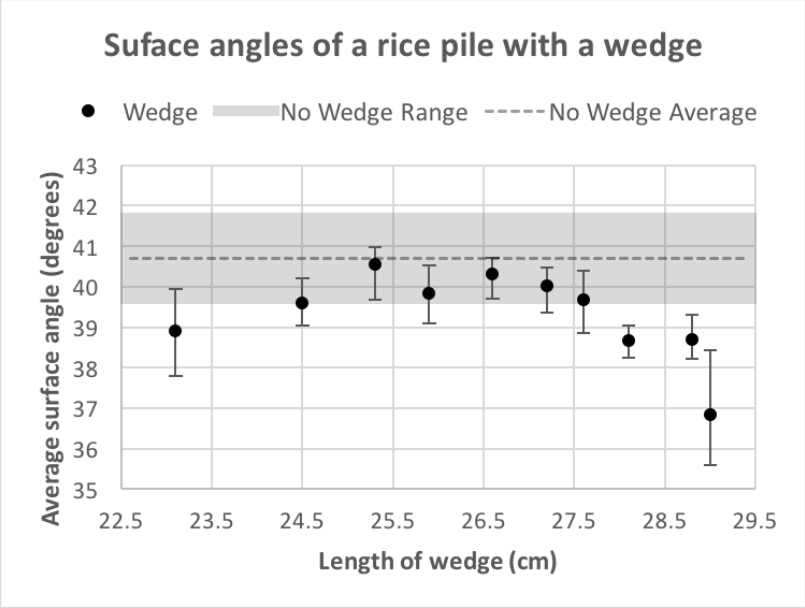

Figure 4.5: Approximate angle of rice surface with different sizes of styrofoam wedges below the flowing layer. Both the grey band, which represents the range of angles measured, and the dashed line, which represents the average surface angle measured, were measured in experiments without a wedge and are not associated with a Length value. All experiments presented here were preformed in a box with $L = 30.5$cm.

The width of the active layer was measured using the image subtraction technique de-

scribed earlier. The subtracted images were taken two hours apart. Each data point plotted here is calculated from the average of three two hour image subtraction image pairs, with black error bars representing the range of measured averages. In these data the disturbance from the presence of the wedge is, once again, observed with the three largest wedge sizes, after which the 2 hour active layer width falls within a normal range for a rice pile with no wedge. However, unlike the results from the measured surface angle, the thickness of the flowing layer is constant once the wedge is sufficiently small.

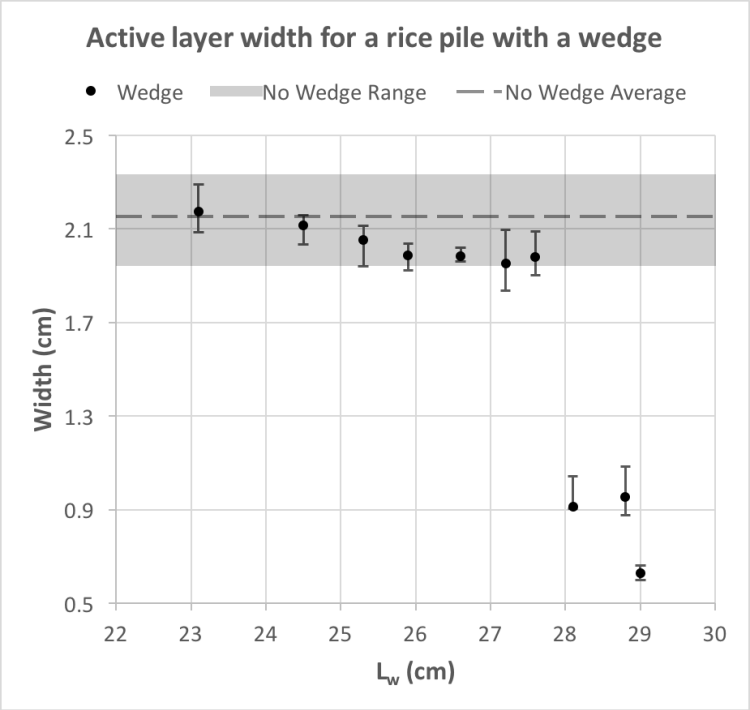

Figure 4.6: Approximate active layer width for rice piles with varying wedge sizes. Widths were calculated on image subtraction products with two hour time differences. Black error bars show the range of measured average values. Both the grey band, which represents the range of widths measured, and the dashed line, which represents the average active layer width measured, were measured in experiments without a wedge and are not associated with a Length value. All experiments analyzed here were performed in a box where $L =$ 30.5cm.

One might expect the wedge to have a clear effect if it is protruding into the region where without a wedge the active layer is present. Indeed, as illustrated in Figure 4.7 when we consider the results in Figures 4.6 &4.5, the presence of the wedge within this

active layer region decreases the thickness of the mobile layer and the angle of the surface compared to these details in experiments without a wedge. Once the wedge drops below what one might call a "buffer layer" below the measured bottom of the flowing layer with no wedge present, one might expect the presence of the wedge to have little or no effect. E.g., If we consider the active layer to be 2.15 cm thick (the average measurement for a 2 hour portion of the experiment) then it would extend along the x axis $x^* = \frac{2.15}{\sin 41^\circ}$ and $x^* = 3.28$ cm (Figure 4.7). Given that the full length of the box is 30.5 cm this puts the approximate transition point at 27.22 cm. If we consider the active layer to be 2.44 cm thick (the width the active layer appears to approach in Figure 4.2) then it would extend along the x axis $x^* = \frac{2.44}{\sin 41^\circ}$ and $x^* = 3.72$ cm (Figure 4.7). Given that the full length of the box is 30.5 cm this puts the approximate transition point at 26.78 cm. Both transitions are represented in Figure

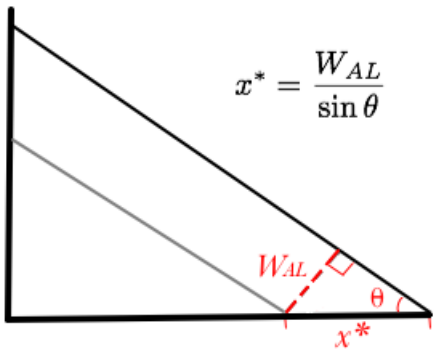

Figure 4.7: Schematic of a rice pile with an active layer shaded in grey. We can approximate how far along the x axis the active layer extends (x^*)with geometric arguments. In our experiments we measured both the width of the active layer (W_{AL}) and the average slope (θ). Dividing W_{AL} by $\sin\theta$ will give us x^*.

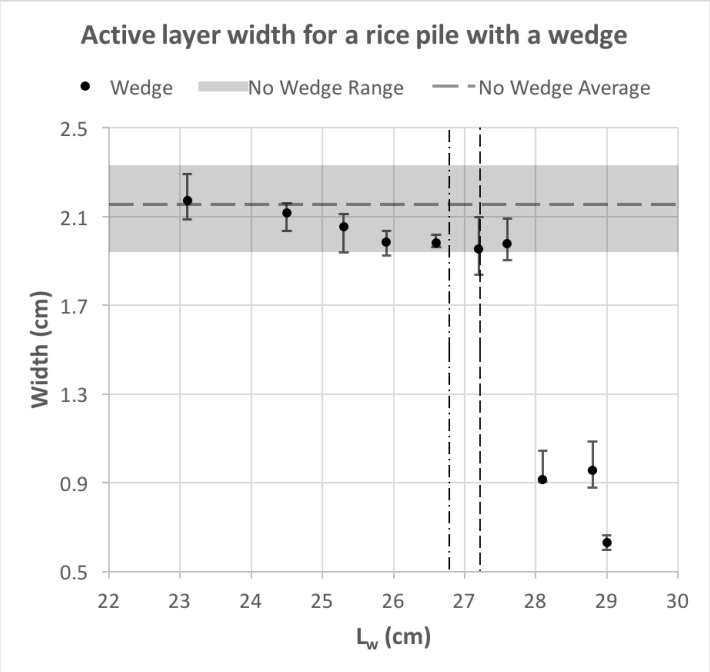

Figure 4.8: Lines representing possible active layer transitions are shown along with the active layer width data from Figure 4.6. The vertical dashed line is at $x = 27.22$cm which could represent the transition suggested by a 2.15 cm wide active layer. The vertical broken dashed line is at $x = 26.78$cm which could represent the transition suggestion by a 2.44 cm wide active layer.

In our experiments we found the flowing layer thickness and surface angle to be statistically similar to that without a wedge for the wedge length L_w in an intermediate range between 27.6 cm and 25.3 cm. This is surprising because our geometric arguments indicate that the first (and possibly second) wedge represented in this range ($L_w = 27.6$cm) extends beyond the transition and into the active layer. We also note that while the measurements for active layer width are within the range of what is measured with no wedge they all fall below the average until we reach a wedge size of $L = 24.5$cm which could indicate a buffer region between the bottom of the measured active layer and the bulk of 2.28-2.72 cm depending on where the transition is considered to occur.

Another surprising result is that for sufficiently small values of L_w, while the flowing layer thickness was the same as that from experiments without a wedge, the steady surface angle was smaller than the results without a wedge. A cursory inspection of this experiment

shows us that the large avalanches taking place result in a larger $\Delta\eta$ at $x = 0$ than is seen in experiments with no wedge. While we cannot draw a direct connection, perhaps these surprising results are somehow connected to the previously described non-locality in the rice pile. Non-locality in grain flows has been seen to alter the flow of grains far from the primary zone of movement, e.g. a non-local rheology where grains removed from the shear zone were affected by the shear zone was seen by *Nichol et al.* [2010]. It is possible that what we see here shows the converse of what was seen by *Nichol et al.* [2010] in that we may be seeing a change in the creep layer have a non-local effect on the grains in the active layer.

These data are preliminary, leaving much room for further expansion. Such possible studies include analysis of how such a wedge affects drop statistics, longer experiments to discern whether there is such a time where image subtraction will see movement throughout the pile, profile shape analyses, an investigation of the velocity profile within the active layer, experiments with smaller wedges, or smaller intervals between wedges. All of these studies could expand our understanding of the process and the role of the active layer.

4.3 Evidence of Non-locality in the Active Layer Summary

These active layer analyses demonstrated that while this rice pile has a discrete and measurable active layer where a majority the movement in the by-pass state is contained, the mobile properties of the bulk are important to the overall dynamics of the pile.

- Image subtraction shows a discrete active layer width approaching ~ 2.44 cm with increasing time between images.

- The inclusion of a static wedge most dramatically affected the observed width and angle when some portion of this wedge was within the previously measured active layer.

- Once the wedge was minimally within the active layer all active layer width measurements were consistent with no-wedge experiments but may show a buffer region where the active layer width stays below average but still within range.

- The smallest wedges produced surface angles lower than seen in no-wedge experiments.

- While not directly linked to the non-locality discussed in Chapter 3, the surprisingly low angle of a portion of our results may indicate some non-locality which we think should be investigated.

Chapter 5

Conclusion

In this work we discussed the related phenomena of anomalous diffusion and non-local transport. Anomalous diffusion refers to physical systems in which the spreading of a solute does not exhibit the classic square root of time behavior. Non-locality is the circumstance in which conditions removed (in time or space) from a given location affect the transport process at that location. It is very difficult to observe and experimentally isolate anomalous transport and non-locality since the signals it produces are commonly driven by multiple phenomena. The main objective here was to develop experiments to show a clear, clean signal of anomalous transport and non-locality.

The work we presented here looked at two systems, fluid infiltration into a thin cavity containing flow obstacles and the profile of a stable two dimensional rice pile. Both sets of experimental results confirmed the presence of non-locality or anomalous transport behavior. In each of these instances the presence of non-locality or anomalous transport behavior was tied to specific features which induce or control this behavior. In the case of the infiltration experiments into fractal obstacle patterns anomalous diffusion was confirmed by a transport time exponent $n < \frac{1}{2}$. This anomalous behavior was shown to be connected to the level of heterogeneity in the obstacle pattern. This is shown, first, by the observation that homogeneous patterns (empty cell or repeating obstacle pattern) confirmed normal

diffusion with time exponents $n = \frac{1}{2}$. Second, and more directly, when the obstacle is a fractal pattern we see a connection between the Hausdorff fractal dimension (H) and the observed time exponents (n) defined by a quadratic function. In the case of the rice pile experiment non-locality was indicated by the observation of a curvature of the long profile, $\eta = (1-x)^{\alpha}, \quad \alpha \neq 1$. The concave down shape of this curvature further indicates that the non-locality is downstream weighted. These observations were further validated by a numerical model that produces a linear surface when using local failure criteria and a surface whose curvature is consistent with our experimental results when using non-local failure criteria. This anomalous behavior might be controlled by the failure mechanisms which we show produce a discrete active layer for the total length of our experiments.

There are many possible directions for future work on these projects. The infiltration experiments could be improved by creating the cells in a manner that decreases or eliminates the possibility of warping. One possible extension to these infiltration experiments is to include additional patterns to increase the number of data points available to refine the connection between the Hausdorff fractal dimension (H) and the observed time exponents. Another possible extension is to alter the patterns to create fast paths rather than hold ups and thus investigate super-diffusion. It is suggested in [*Voller*, 2015] that placing cavities in the locations where obstacles were in our experiments is one way to produce super-diffusion in this system. Another suggestion to produce a super-diffusive environment [*Reis et al.*, In Preparation 2017] is to stagger the pattern of obstacles so that $y = 0$ and $y = 1$ lines run through the center of the large obstacle (what was previously $y = 0.5$) with a narrow area in the middle where there are no obstacles. Since each of these suggestions for producing super-diffusion contains a fractal pattern of obstacles (and thus a Hausdorff fractal dimension, H) the results from these experiments can be used to better understand the connection between the heterogeneity of the medium and observed time exponents.

The rice pile profile shape experiments could be improved by increasing the variation

of the boundary conditions. For example, one possible extension to the rice pile profile shape experiments is to run experiments for many different L values to see how this might affect the curvature of the surface. Another possible extension is to use grains with different shapes. *Denisov et al.* [2012] demonstrated that the shape of the grains affects the angle of repose and here we argue that we must approach the concept of angle of repose in a manner which includes the pile's surface curvature. We also argue that the level of profile curvature indicates the level of non-locality in the rice pile dynamics. Therefore by observing not only the average surface angle with relation to the x axis but also the profile curvature it may be possible to determine whether grain shape affects the level of non-locality in the dynamics of the grain pile.

We believe the insights presented in this thesis help to improve our understanding of both anomalous diffusion and non-local transport and improve our ability recognize and predict direct signals of both.

Bibliography

Alonso, J., and H. Herrmann (1996), Shape of the Tail of a Two-Dimensional Sandpile, *Physical Review Letters*, *76*(26), 4911–4914, doi:10.1103/PhysRevLett.76.4911.

Amaral, L. a. N., and K. B. Lauritsen (1997), Universality classes for rice-pile models, *Physical Review E*, *56*(1), 4, doi:10.1103/PhysRevE.56.231.

Anonymous (1963), *Physical Properties of Glycerin and its Solutions*, Glycerin Producers' Association, New York.

Aradian, a., E. Raphaël, and P. G. de Gennes (1999), Thick surface flows of granular materials: effect of the velocity profile on the avalanche amplitude., *Physical review. E, Statistical physics, plasmas, fluids, and related interdisciplinary topics*, *60*(2 Pt B), 2009–2019, doi:10.1103/PhysRevE.60.2009.

Bak, P., C. Tang, and K. Wiesenfeld (1987), Self-organized criticality: An explanation of the 1/f noise, *Physical Review Letters*, *59*(4), 381–384, doi:10.1103/PhysRevLett.59.381.

Batchelor, G. K. (1967), *An Introduction to Fluid Dynamics*, 615 pp., Cambridge University Press, Cambridge, UK.

Bear, J. (1988), *Dynamics of fluids in porous media*, 764 pp., Dover, New York.

Boutreux, T., E. Rapheël, and P.-G. de Gennes (1998), Surface flows of granular materials: A modified picture for thick avalanches, *Physical Review E*, *58*(4), 4692–4700, doi: 10.1103/PhysRevE.58.4692.

Caputo, M. (1967), Linear Models of Dissipation whose Q is almost Frequency Independent - II, *Annals of Geophysics*, *19*(4), 529–539.

Carpenter, T. A., E. S. Davies, C. Hall, L. D. Hall, W. D. Hoff, and M. A. Wilson (1993), Capillary water migration in rock: process and material properties examined by NMR imaging, *Materials and Structures*, *26*(5), 286–292, doi:10.1007/BF02472950.

Christensen, K., A. Corral, V. Frette, J. Feder, and T. Jø ssang (1996), Tracer Dispersion in a Self-Organized Critical System, *Physical Review Letters*, *77*(1), 107–110.

Clauset, A., C. R. Shalizi, and M. E. J. Newman (2009), Power-Law Distributions in Empirical Data, *SIAM Review*, *51*(4), 661–703.

Denisov, D. V., Y. Y. Villanueva, K. a. Lorincz, S. May, and R. J. Wijngaarden (2012), Relation between self-organized criticality and grain aspect ratio in granular piles, *Physical Review E - Statistical, Nonlinear, and Soft Matter Physics*, *85*(5), doi:10.1103/ PhysRevE.85.051309.

Drescher, A., and G. de Josselin de Jong (1972), Photoelastic verification of a mechanical model for the flow of a granular material, *Journal of the Mechanics and Physics of Solids*, *20*(5), 337–351, doi:10.1016/0022-5096(72)90029-4.

Einstein, a. (1905), Uber d4e von der rnolekuZarh%net4schem Theorie der WUrme geforderte Bewegumg vow in ruhenden P Z ikss4ykeitem, *Ann. d. Phys.*

El Abd, A. E. G., and J. J. Milczarek (2004), Neutron radiography study of water absorption in porous building materials: anomalous diffusion analysis, *Journal of Physics D-Applied Physics*, *37*(16), 2305–2313, doi:10.1088/0022-3727/37/16/013.

Falcini, F., E. Foufoula-Georgiou, V. Ganti, C. Paola, and V. R. Voller (2013), A combined nonlinear and nonlocal model for topographic evolution in channelized depositional systems, *Journal of Geophysical Research: Earth Surface*, *118*(3), 1617–1627, doi:10.1002/jgrf.20108.

Feder, J. (1995), THE EVIDENCE FOR SELF-ORGANIZED CRITICALITY IN SANDPILE DYNAMICS, *Fractals*, *03*(03), doi:10.1142/S0218348X95000357.

Filipovitch, N., K. Hill, A. Longjas, and V. Voller (2016), Infiltration experiments demonstrate an explicit connection between heterogeneity and anomalous diffusion behavior, *Water Resources Research*, *52*, 5167–5178, doi:10.1002/2016WR018667.Received.

Foufoula-Georgiou, E., V. Ganti, and W. E. Dietrich (2010), A nonlocal theory of sediment transport on hillslopes, *Journal of Geophysical Research*, *115*, 1–12, doi:10.1029/2009JF001280.

Frette, V. (1993), Sandpile models with dynamically varying critical slopes, *Physical Review Letters*, *70*(18), 2762–2765, doi:10.1103/PhysRevLett.70.2762.

Frette, V., K. Christensen, A. Malthe-Sø renssen, J. Feder, T. Jø ssang, and P. Meakin (1996), Avalanche dynamics in a pile of rice, *Nature*, *379*(6560), 49–52, doi:10.1038/379049a0.

Gabet, E. J., and M. K. Mendoza (2012), Particle transport over rough hillslope surfaces by dry ravel: Experiments and simulations with implications for nonlocal sediment flux, *Journal of Geophysical Research: Earth Surface*, *117*(1), 1–11, doi:10.1029/2011JF002229.

Gerolymatou, E., I. Vardoulakis, and R. Hilfer (2006), Modelling infiltration by means of a nonlinear fractional diffusion model, *Journal of Physics D: Applied Physics*, *39*, 4104–4110, doi:10.1088/0022-3727/39/18/022.

Guo, Q., H. Jiang, and L. Xi (2006), Hausdorff Dimension of Generalized Sierpinski Carpet, *International Journal of Nonlinear Science*, *2*(3), 153–158.

Jaeger, H. M., and S. R. Nagel (1992), Physics of the granular state., *Science (New York, N.Y.)*, *255*(5051), 1523–1531, doi:10.1126/science.255.5051.1523.

Jaeger, H. M., S. R. Nagel, and R. P. Behringer (1996), Granular solids, liquids, and gases, *Reviews of Modern Physics*, *68*(4), 1259–1273, doi:10.1103/RevModPhys.68.1259.

Jerolmack, D. J., and C. Paola (2010), Shredding of environmental signals by sediment transport, *Geophysical Research Letters*, *37*(19), n/a–n/a, doi:10.1029/2010GL044638, l19401.

Juanico, D. E., A. Longjas, R. Batac, and C. Monterola (2008), Avalanche statistics of driven granular slides in a miniature mound, *Geophysical Research Letters*, *35*(19), 1–4, doi:10.1029/2008GL035567.

Komatsu, T. S., S. Inagaki, N. Nakagawa, and S. Nasuno (2001), Creep motion in a granular pile exhibiting steady surface flow, *Physical Review Letters*, *86*(9), 1757–1760, doi:10.1103/PhysRevLett.86.1757.

Korabel, N., and E. Barkai (2011), Anomalous Infiltration, p. 21, doi:10.1088/1742-5468/2011/05/P05022.

Küntz, M., and P. Lavallée (2001), Experimental evidence and theoretical analysis of anomalous diffusion during water infiltration in porous building materials, *Journal of Physics D: Applied Physics*, *34*, 2547–2554.

Li, C., D. Qian, and Y. Chen (2011), On Reimann-Liouville and Caputo Derivatives, *Discrete Dynamics in Nature and Society*, *2011*(Article ID 562494), 15.

Martin, R. L., D. J. Jerolmack, and R. Schumer (2012), The physical basis for anomalous diffusion in bed load transport, *Journal of Geophysical Research: Earth Surface*, *117*(1), 1–18, doi:10.1029/2011JF002075.

Meerschaert, M. M., and A. Sikorskii (2012), *Stochastic models for fractional caluculus*, 291 pp., De Gruyter, Berlin, Boston.

Metzler, R., and J. Klafter (2004), The restaurant at the end of the random walk: recent developments in the description of anomalous transport by fractional dynamics, *Journal of Physics A: Mathematical and General*, *37*(31), R161–R208, doi:10.1088/0305-4470/37/31/R01.

Monbouquette, M. R. (2008), Obliteration of climate signals in an avalanching pile of rice and implications for interpreting stratigraphy, Ph.D. thesis, Carleton College.

Muhlhaus, H.-B., and I. Vardoulakis (1987), The thickness of shear bands in granular materials, *Géotechnique*, *38*(2), 331–331, doi:10.1680/geot.1988.38.2.331.

Nagel, S. R. (1992), Instabilities in a sandpile, *Reviews of Modern Physics*, *64*(1), 321–325, doi:10.1103/RevModPhys.64.321.

Nichol, K., A. Zanin, R. Bastien, E. Wandersman, and M. van Hecke (2010), Flow-Induced Agitations Create a Granular Fluid, *Physical Review Letters*, *104*(7), 48–51, doi:10.1103/PhysRevLett.104.078302.

Nikora, V. (2002), On bed particle diffusion in gravel bed flows under weak bed load transport, *Water Resources Research*, *38*(6), 1–9, doi:10.1029/2001WR000513.

Paola, C., and V. R. Voller (2005), A generalized Exner equation for sediment mass balance, *Journal of Geophysical Research: Earth Surface*, *110*(4), 1–8, doi:10.1029/2004JF000274.

Pel, L., K. Kopinga, G. Bertram, and G. Lang (1995), Water absorption in a fired-clay brick observed by NMR scanning, *Journal of Physics D: Applied Physics*, *28*(4), 675–680, doi:10.1088/0022-3727/28/4/009.

Pel, L., K. Kopinga, and H. Brocken (1996), Moisture transport in porous building materials, *Heron*, *41*(2), 95–105, doi:URN:NBN:NL:UI:25-431403-of.

Pel, L., K. Hazrati, K. Kopinga, and J. Marchand (1998), Water absorption in mortar determined by NMR, *Magnetic Resonance Imaging*, *16*(5), 525–528, doi:10.1016/S0730-725X(98)00061-7.

Philibert, J. (2005), One and a half century of diffusion: Fick, Einstein, before and beyond, *Diffusion Fundamentals*, *4*, 1–19.

Podlubny, I. (1999), *Fractional differential equations : an introduction to fractional derivatives, fractional differential equations, to methods of their solution and some of their applications*, 340 pp., Academic Press, San Diego.

Postma, G., M. G. Kleinhans, P. T. H. Meijer, and J. T. Eggenhuisen (2008), Sediment transport in analogue flume models compared with real-world sedimentary systems: A new look at scaling evolution of sedimentary systems in a flume, *Sedimentology*, *55*(6), 1541–1557, doi:10.1111/j.1365-3091.2008.00956.x.

Quintanilla, M. a. S., A. Castellanos, and J. M. Valverde (2004), Granular avalanches: Deterministic, correlated and decorrelated dynamics, *Europhysics Letters (EPL)*, *68*(6), 818–824, doi:10.1209/epl/i2004-10283-5.

Reis, F., D. Bolster, and V. Voller (In Preparation 2017), Moisture infiltration in a fractal obstacle field can exhibit both sub and super diffusion.

Roscoe, K. H. (1970), The Influence of Strains in Soil Mechanics, *Géotechnique*, *20*(2), 129–170, doi:10.1680/geot.1970.20.2.129.

Schumer, R., M. M. Meerschaert, and B. Baeumer (2009), Fractional advection-dispersion equations for modeling transport at the Earth surface, *Journal of Geophysical Research: Earth Surface*, *114*(4), 1–15, doi:10.1029/2008JF001246.

Taylor, S. C., W. D. Hoff, M. A. Wilson, and K. M. Green (1999), Anomalous water transport properties of Portland and blended cement-based materials, *Journal of Materials Science Letters*, *18*(23), 1925–1927, doi:10.1023/A:1006677014070.

Voller, V. R. (2015), A direct simulation demonstrating the role of spacial heterogeneity in determining anomalous diffusive transport, *Water Resources Research*, *51*(4), 2119–2127, doi:10.1002/2014WR016082.Received.

Voller, V. R., and C. Paola (2010), Can anomalous diffusion describe depositional fluvial profiles?, *Journal of Geophysical Research*, *115*, 1–11, doi:10.1029/2009JF001278.

Voller, V. R., V. Ganti, C. Paola, and E. Foufoula-Georgiou (2012), Does the flow of information in a landscape have direction?, *Geophysical Research Letters*, *39*(1), 1–5, doi:10.1029/2011GL050265.

Weeks, E. R., J. Urbach, and H. L. Swinney (1996), Anomalous diffusion in asymmetric random walks with a quasi-geostrophic flow example, *Physica D: Nonlinear Phenomena*, *97*(1-3), 291–310, doi:10.1016/0167-2789(96)00082-6.

Appendix A

Raw data for infiltration experiments

N	0		4		4		3	
m	0		0		0		2	
run	1		1		2		1	
	frame	%F	frame	%F	frame	%F	frame	%F
	34	2.382	47	0.789	35	2.208	35	1.717
	35	4.227	48	3.545	36	4.139	36	3.979
	36	5.77	49	5.297	37	5.251	37	5.693
	37	7.085	50	6.381	38	6.193	38	7.163
	38	8.249	51	7.278	39	6.938	39	8.25
	39	9.314	52	8.008	40	7.58	40	9.145
	40	10.327	53	8.625	41	8.151	41	9.995
	41	11.244	54	9.216	42	8.704	42	10.712
	42	12.092	55	9.738	43	9.196	43	11.413
	43	12.859	56	10.23	44	9.675	44	12.041
	44	13.632	57	10.697	45	10.129	45	12.62

45	14.407	58	11.131	46	10.536	46	13.177
46	15.041	59	11.552	47	10.945	47	13.709
47	15.799	60	11.977	48	11.354	48	14.246
48	16.39	61	12.375	49	11.721	49	14.703
49	17.053	62	12.772	50	12.11	50	15.191
50	17.678	63	13.15	51	12.475	51	15.648
51	18.26	64	13.525	52	12.846	52	16.085
52	18.824	65	13.898	53	13.218	53	16.513
53	19.406	66	14.251	54	13.587	54	16.956
54	19.948	67	14.619	55	13.937	55	17.357
55	20.494	68	14.978	56	14.285	56	17.764
56	21.007	69	15.328	57	14.635	57	18.172
57	21.515	70	15.671	58	14.975	58	18.563
58	22.016	71	16.024	59	15.316	59	18.945
59	22.508	72	16.388	60	15.653	60	19.328
60	22.989	73	16.735	61	15.994	61	19.702
61	23.463	74	17.063	62	16.33	62	20.073
62	23.922	75	17.394	63	16.671	63	20.446
63	24.373	76	17.71	64	17.002	64	20.812
64	24.819	77	18.042	65	17.341	65	21.181
65	25.253	78	18.381	66	17.674	66	21.527
66	25.677	79	18.709	67	18.014	67	21.888
67	26.091	80	19.041	68	18.339	68	22.246
68	26.516	81	19.385	69	18.681	69	22.605
69	26.932	82	19.716	70	19.037	70	22.965
70	27.34	83	20.041	71	19.358	71	23.311

71	27.736	84	20.369	72	19.682	72	23.664
72	28.132	85	20.658	73	19.993	73	24.009
73	28.519	86	20.954	74	20.33	74	24.342
74	28.91	87	21.26	75	20.661	75	24.652
75	29.288	88	21.55	76	20.997	76	24.978
76	29.666	89	21.85	77	21.305	77	25.315
77	30.028	90	22.144	78	21.611	78	25.631
78	30.4	91	22.453	79	21.931	79	25.935
79	30.777	92	22.745	80	22.229	80	26.247
80	31.125	93	23.029	81	22.527	81	26.561
81	31.471	94	23.305	82	22.805	82	26.878
82	31.834	95	23.582	83	23.103	83	27.161
83	32.178	96	23.842	84	23.385	84	27.436
84	32.514	97	24.117	85	23.661	85	27.702
85	32.859	98	24.364	86	23.955	86	27.966
86	33.19	99	24.613	87	24.205	87	28.24
87	33.527	100	24.857	88	24.451	88	28.497
88	33.848	101	25.11	89	24.717	89	28.756
89	34.181	102	25.35	90	24.955	90	29.001
90	34.499	103	25.591	91	25.183	91	29.26
91	34.813	104	25.82	92	25.424	92	29.51
92	35.135	105	26.057	93	25.648	93	29.752
93	35.445	106	26.28	94	25.876	94	30.007
94	35.762	107	26.531	95	26.107	95	30.247
95	36.069	108	26.754	96	26.326	96	30.49
96	36.365	109	26.952	97	26.539	97	30.726

97	36.686	110	27.162	98	26.755	98	30.96
98	36.981	111	27.361	99	26.968	99	31.198
99	37.272	112	27.559	100	27.181	100	31.427
100	37.559	113	27.756	101	27.389	101	31.658
101	37.863	114	27.956	102	27.599	102	31.884
102	38.16	115	28.159	103	27.802	103	32.121
103	38.438	116	28.349	104	28.004	104	32.347
104	38.73	117	28.528	105	28.197	105	32.566
105	39.014	118	28.717	106	28.389	106	32.8
106	39.289	119	28.899	107	28.58	107	33.014
107	39.564	120	29.092	108	28.763	108	33.229
108	39.844	121	29.278	109	28.95	109	33.454
109	40.127	122	29.455	110	29.133	110	33.67
110	40.4	123	29.639	111	29.314	111	33.876
111	40.674	124	29.822	112	29.485	112	34.085
112	40.943	125	29.996	113	29.668	113	34.276
113	41.207	126	30.178	114	29.85	114	34.474
114	41.473	127	30.354	115	30.023	115	34.674
115	41.723	128	30.526	116	30.201	116	34.863
116	41.998	129	30.698	117	30.372	117	35.039
117	42.249	130	30.871	118	30.545	118	35.22
118	42.52	131	31.05	119	30.72	119	35.402
119	42.775	132	31.222	120	30.894	120	35.58
120	43.038	133	31.397	121	31.066	121	35.753
121	43.296	134	31.581	122	31.182	122	35.937
122	43.54	135	31.75	123	31.353	123	36.12

123	43.798	136	31.914	124	31.518	124	36.285
124	44.039	137	32.088	125	31.689	125	36.456
125	44.289	138	32.255	126	31.858	126	36.619
126	44.538	139	32.432	127	32.028	127	36.786
127	44.779	140	32.598	128	32.199	128	36.949
128	45.028	141	32.779	129	32.375	129	37.111
129	45.267	142	32.941	130	32.547	130	37.27
130	45.513	143	33.119	131	32.713	131	37.429
131	45.744	144	33.29	132	32.864	132	37.591
132	45.987	145	33.456	133	33.04	133	37.745
133	46.223	146	33.625	134	33.208	134	37.906
134	46.467	147	33.795	135	33.38	135	38.063
135	46.699	148	33.91	136	33.553	136	38.213
136	46.937	149	34.08	137	33.704	137	38.353
137	47.167	150	34.252	138	33.88	138	38.512
138	47.408	151	34.416	139	34.05	139	38.66
139	47.634	152	34.586	140	34.221	140	38.806
140	47.868	153	34.762	141	34.377	141	38.908
141	48.093	154	34.967	142	34.543	142	39.061
142	48.323	155	35.083	143	34.714	143	39.199
143	48.547	156	35.247	144	34.871	144	39.346
144	48.763	157	35.419	145	35.04	145	39.492
145	48.991	158	35.578	146	35.198	146	39.634
146	49.212	159	35.746	147	35.374	147	39.778
147	49.441	160	35.921	148	35.544	148	39.914
148	49.664	161	36.137	149	35.694	149	40.05

149	49.883	162	36.302	150	35.864	150	40.191
150	50.107	163	36.464	151	36.024	151	40.376
151	50.326	164	36.628	152	36.196	152	40.466
152	50.539	165	36.795	153	36.361	153	40.605
153	50.755	166	36.975	154	36.531	154	40.741
154	50.959	167	37.13	155	36.7	155	40.875
155	51.184	168	37.305	156	36.863	156	41.018
156	51.393	169	37.477	157	37.033	157	41.153
157	51.611	170	37.668	158	37.196	158	41.288
158	51.82	171	37.842	159	37.373	159	41.426
159	52.032	172	38.024	160	37.542	160	41.56
160	52.245	173	38.199	161	37.72	161	41.695
161	52.461	174	38.35	162	37.893	162	41.837
162	52.671	175	38.501	163	38.064	163	41.967
163	52.87	176	38.655	164	38.229	164	42.093
164	53.075	177	38.804	165	38.402	165	42.224
165	53.269	178	38.952	166	38.546	166	42.353
166	53.476	179	39.129	167	38.708	167	42.487
167	53.682	180	39.287	168	38.877	168	42.612
168	53.888	181	39.449	169	39.049	169	42.741
169	54.099	182	39.613	170	39.224	170	42.878
170	54.288	183	39.78	171	39.401	171	43.006
171	54.49	184	39.946	172	39.576	172	43.136
172	54.694	185	40.114	173	39.753	173	43.262
173	54.897	186	40.271	174	39.919	174	43.398
174	55.104	187	40.435	175	40.089	175	43.526

175	55.297	188	40.597	176	40.25	176	43.664
176	55.492	189	40.752	177	40.418	177	43.789
177	55.683	190	40.916	178	40.567	178	43.921
178	55.881	191	41.092	179	40.727	179	44.059
179	56.08	192	41.253	180	40.899	180	44.187
180	56.271	193	41.426	181	41.069	181	44.318
181	56.465	194	41.564	182	41.211	182	44.444
182	56.657	195	41.691	183	41.355	183	44.578
183	56.858	196	41.853	184	41.52	184	44.706
184	57.049	197	42.02	185	41.672	185	44.833
185	57.241	198	42.177	186	41.838	186	44.961
186	57.431	199	42.316	187	42	187	45.092
187	57.612	200	42.467	188	42.157	188	45.217
188	57.807	201	42.605	189	42.313	189	45.345
189	57.998	202	42.756	190	42.463	190	45.482
190	58.183	203	42.899	191	42.623	191	45.615
191	58.367	204	43.043	192	42.772	192	45.754
192	58.551	205	43.209	193	42.925	193	45.884
193	58.746	206	43.344	194	43.088	194	46.011
194	58.934	207	43.486	195	43.216	195	46.138
195	59.112	208	43.628	196	43.381	196	46.262
196	59.288	209	43.767	197	43.532	197	46.394
197	59.471	210	43.909	198	43.68	198	46.53
198	59.656	211	44.045	199	43.823	199	46.657
199	59.838	212	44.179	200	43.97	200	46.78
200	60.014	213	44.311	201	44.103	201	46.901

201	60.196	214	44.445	202	44.248	202	47.028
202	60.389	215	44.58	203	44.38	203	47.147
203	60.561	216	44.712	204	44.514	204	47.287
204	60.732	217	44.799	205	44.653	205	47.408
205	60.913	218	44.937	206	44.784	206	47.535
206	61.098	219	45.061	207	44.927	207	47.667
207	61.286	220	45.193	208	45.053	208	47.789
208	61.45	221	45.32	209	45.18	209	47.914
209	61.624	222	45.445	210	45.308	210	48.044
210	61.751	223	45.577	211	45.437	211	48.168
211	61.917	224	45.696	212	45.571	212	48.29
212	62.102	225	45.827	213	45.697	213	48.418
213	62.278	226	45.937	214	45.824	214	48.544
214	62.451	227	46.063	215	45.95	215	48.662
215	62.628	228	46.197	216	46.079	216	48.788
216	62.802	229	46.323	217	46.208	217	48.91
217	62.973	230	46.444	218	46.325	218	49.034
218	63.144	231	46.573	219	46.451	219	49.153
219	63.322	232	46.692	220	46.58	220	49.275
220	63.497	233	46.818	221	46.698	221	49.41
221	63.67	234	46.933	222	46.825	222	49.523
222	63.835	235	47.056	223	46.94	223	49.65
223	64.01	236	47.176	224	47.061	224	49.764
224	64.178	237	47.297	225	47.181	225	49.887
225	64.353	238	47.421	226	47.298	226	50.005
226	64.512	239	47.534	227	47.421	227	50.131

227	64.69	240	47.654	228	47.531	228	50.251
228	64.86	241	47.772	229	47.659	229	50.362
229	65.026	242	47.889	230	47.773	230	50.487
230	65.197	243	48.007	231	47.886	231	50.604
231	65.355	244	48.122	232	47.999	232	50.724
232	65.525	245	48.23	233	48.118	233	50.843
233	65.695	246	48.344	234	48.233	234	50.964
234	65.854	247	48.455	235	48.348	235	51.079
235	66.026	248	48.57	236	48.46	236	51.195
236	66.192	249	48.683	237	48.571	237	51.316
237	66.357	250	48.796	238	48.688	238	51.441
238	66.52	251	48.906	239	48.804	239	51.543
239	66.678	252	49.021	240	48.923	240	51.671
240	66.845	253	49.125	241	49.033	241	51.788
241	67.014	254	49.238	242	49.141	242	51.893
242	67.169	255	49.35	243	49.261	243	52.02
243	67.335	256	49.459	244	49.37	244	52.138
244	67.495	257	49.574	245	49.481	245	52.25
245	67.658	258	49.682	246	49.593	246	52.365
246	67.818	259	49.781	247	49.711	247	52.49
247	67.977	260	49.895	248	49.812	248	52.604
248	68.137	261	49.999	249	49.932	249	52.721
249	68.299	262	50.114	250	50.042	250	52.83
250	68.46	263	50.214	251	50.155	251	52.947
251	68.614	264	50.328	252	50.256	252	53.072
252	68.776	265	50.442	253	50.367	253	53.188

253	68.935	266	50.547	254	50.477	254	53.303
254	69.091	267	50.661	255	50.592	255	53.417
255	69.255	268	50.772	256	50.692	256	53.536
256	69.412	269	50.874	257	50.809	257	53.657
257	69.566	270	50.981	258	50.922	258	53.775
258	69.721	271	51.091	259	51.03	259	53.893
259	69.885	272	51.201	260	51.141	260	54.021
260	70.039	273	51.306	261	51.246	261	54.145
261	70.192	274	51.414	262	51.359	262	54.254
262	70.351	275	51.528	263	51.473	263	54.379
263	70.505	276	51.63	264	51.587	264	54.479
264	70.659	277	51.734	265	51.692	265	54.6
265	70.811	278	51.848	266	51.797	266	54.72
266	70.968	279	51.937	267	51.901	267	54.821
267	71.126	280	52.05	268	52.012	268	54.919
268	71.277	281	52.158	269	52.121	269	55.012
269	71.428	282	52.265	270	52.234	270	55.114
270	71.579	283	52.373	271	52.335	271	55.224
271	71.732	284	52.467	272	52.451	272	55.329
272	71.887	285	52.576	273	52.549	273	55.437
273	72.035	286	52.683	274	52.659	274	55.537
274	72.182	287	52.772	275	52.771	275	55.642
275	72.336	288	52.876	276	52.878	276	55.747
276	72.485	289	52.983	277	52.987	277	55.859
277	72.636	290	53.086	278	53.104	278	55.971
278	72.793	291	53.193	279	53.212	279	56.079

279	72.938	292	53.288	280	53.316	280	56.183
280	73.087	293	53.389	281	53.426	281	56.289
281	73.237	294	53.484	282	53.525	282	56.397
282	73.383	295	53.603	283	53.639	283	56.502
283	73.533	296	53.699	284	53.744	284	56.61
284	73.677	297	53.809	285	53.854	285	56.713
285	73.827	298	53.918	286	53.969	286	56.816
286	73.972	299	54.007	287	54.069	287	56.919
287	74.118	300	54.118	288	54.186	288	57.022
288	74.266	301	54.22	289	54.297	289	57.126
289	74.411	302	54.329	290	54.401	290	57.229
290	74.558	303	54.422	291	54.511	291	57.34
291	74.71	304	54.521	292	54.613	292	57.448
292	74.85	305	54.644	293	54.726	293	57.548
293	74.994	306	54.744	294	54.834	294	57.653
294	75.135	307	54.853	295	54.941	295	57.761
295	75.284	308	54.955	296	55.05	296	57.859
296	75.433	309	55.062	297	55.165	297	57.97
297	75.566	310	55.166	298	55.265	298	58.063
298	75.718	311	55.263	299	55.377	299	58.171
299	75.854	312	55.369	300	55.49	300	58.27
300	75.993	313	55.472	301	55.591	301	58.376
301	76.14	314	55.569	302	55.7	302	58.483
302	76.276	315	55.687	303	55.816	303	58.586
303	76.419	316	55.784	304	55.911	304	58.687
304	76.562	317	55.894	305	56.032	305	58.79

305	76.701	318	55.985	306	56.144	306	58.885
306	76.839	319	56.098	307	56.251	307	58.986
307	76.983	320	56.198	308	56.364	308	59.09
308	77.121	321	56.31	309	56.483	309	59.189
309	77.264	322	56.418	310	56.6	310	59.294
310	77.402	323	56.512	311	56.722	311	59.396
311	77.537	324	56.63	312	56.832	312	59.502
312	77.68	325	56.738	313	56.951	313	59.598
313	77.822	326	56.84	314	57.044	314	59.703
314	77.955	327	56.955	315	57.148	315	59.798
315	78.097	328	57.063	316	57.262	316	59.896
316	78.233	329	57.185	317	57.338	317	60.001
317	78.371	330	57.281	318	57.444	318	60.096
318	78.512	331	57.384	319	57.556	319	60.195
319	78.649	332	57.494	320	57.677	320	60.298
320	78.786	333	57.599	321	57.779	321	60.395
321	78.922	334	57.69	322	57.898	322	60.492
322	79.05	335	57.774	323	58.007	323	60.591
323	79.191	336	57.866	324	58.125	324	60.696
324	79.322	337	57.964	325	58.237	325	60.79
325	79.462	338	58.071	326	58.339	326	60.898
326	79.602	339	58.188	327	58.451	327	60.988
327	79.726	340	58.293	328	58.574	328	61.1
328	79.873	341	58.395	329	58.696	329	61.19
329	80.005	342	58.499	330	58.805	330	61.294
330	80.137	343	58.599	331	58.924	331	61.396

331	80.274	344	58.715	332	59.049	332	61.497
332	80.397	345	58.813	333	59.156	333	61.591
333	80.539	346	58.931	334	59.265	334	61.703
334	80.662	347	59.029	335	59.388	335	61.789
335	80.799	348	59.148	336	59.5	336	61.9
336	80.929	349	59.261	337	59.602	337	61.987
337	81.061	350	59.368	338	59.718	338	62.082
338	81.198	351	59.474	339	59.82	339	62.178
339	81.328	352	59.588	340	59.928	340	62.282
340	81.458	353	59.699	341	60.006	341	62.375
341	81.586	354	59.814	342	60.108	342	62.477
342	81.726	355	59.924	343	60.222	343	62.58
343	81.843	356	60.032	344	60.325	344	62.678
344	81.981	357	60.136	345	60.443	345	62.778
345	82.106	358	60.245	346	60.546	346	62.882
346	82.242	359	60.358	347	60.652	347	62.974
347	82.361	360	60.471	348	60.757	348	63.072
348	82.502	361	60.583	349	60.864	349	63.167
349	82.626	362	60.673	350	60.976	350	63.272
350	82.758	363	60.756	351	61.072	351	63.366
351	82.884	364	60.883	352	61.178	352	63.461
352	83.011	365	60.976	353	61.288	353	63.557
353	83.145	366	61.086	354	61.396	354	63.657
354	83.273	367	61.192	355	61.494	355	63.76
355	83.395	368	61.294	356	61.603	356	63.86
356	83.529	369	61.398	357	61.712	357	63.956

357	83.659	370	61.499	358	61.805	358	64.054
358	83.781	371	61.603	359	61.912	359	64.153
359	83.912	372	61.698	360	62.016	360	64.259
360	84.038	373	61.795	361	62.119	361	64.339
361	84.165	374	61.899	362	62.229	362	64.445
362	84.295	375	62	363	62.326	363	64.532
363	84.419	376	62.09	364	62.42	364	64.624
364	84.548	377	62.19	365	62.522	365	64.723
365	84.667	378	62.287	366	62.609	366	64.815
366	84.792	379	62.357	367	62.718	367	64.917
367	84.922	380	62.458	368	62.807	368	65.012
368	85.04	381	62.548	369	62.899	369	65.112
369	85.167	382	62.647	370	62.991	370	65.211
370	85.285	383	62.733	371	63.087	371	65.309
371	85.408	384	62.831	372	63.176	372	65.411
372	85.537	385	62.912	373	63.268	373	65.501
373	85.662	386	63	374	63.362	374	65.586
374	85.78	387	63.097	375	63.454	375	65.687
375	85.904	388	63.186	376	63.542	376	65.782
376	86.027	389	63.277	377	63.639	377	65.867
377	86.16	390	63.361	378	63.739	378	65.966
378	86.278	391	63.447	379	63.828	379	66.054
379	86.399	392	63.526	380	63.92	380	66.146
380	86.519	393	63.624	381	64.005	381	66.24
381	86.646	394	63.711	382	64.091	382	66.329
382	86.763	395	63.803	383	64.193	383	66.425

383	86.888	396	63.892	384	64.272	384	66.522
384	87.005	397	63.971	385	64.366	385	66.612
385	87.136	398	64.056	386	64.456	386	66.717
386	87.248	399	64.158	387	64.545	387	66.806
387	87.373	400	64.242	388	64.635	388	66.901
388	87.485	401	64.338	389	64.722	389	66.992
389	87.615	402	64.425	390	64.818	390	67.087
390	87.725	403	64.513	391	64.904	391	67.197
391	87.849	404	64.602	392	64.996	392	67.288
392	87.966	405	64.683	393	65.085	393	67.39
393	88.09	406	64.784	394	65.172	394	67.488
394	88.201	407	64.861	395	65.264	395	67.582
395	88.322	408	64.941	396	65.36	396	67.676
396	88.442	409	65.038	397	65.439	397	67.77
397	88.558	410	65.108	398	65.533	398	67.87
398	88.67	411	65.209	399	65.623	399	67.962
399	88.795	412	65.299	400	65.711	400	68.06
400	88.905	413	65.372	401	65.794	401	68.169
401	89.033	414	65.443	402	65.878	402	68.268
402	89.138	415	65.554	403	65.964	403	68.363
403	89.26	416	65.626	404	66.053	404	68.453
404	89.372	417	65.714	405	66.146	405	68.539
405	89.489	418	65.798	406	66.232	406	68.634
406	89.603	419	65.867	407	66.312	407	68.732
407	89.713	420	65.961	408	66.393	408	68.821
408	89.837	421	66.044	409	66.48	409	68.917

409	89.948	422	66.125	410	66.567	410	68.999
410	90.063	423	66.204	411	66.645	411	69.091
411	90.171	424	66.281	412	66.73	412	69.183
412	90.294	425	66.351	413	66.812	413	69.278
413	90.402	426	66.428	414	66.896	414	69.379
414	90.518	427	66.514	415	66.977	415	69.475
415	90.627	428	66.592	416	67.07	416	69.569
416	90.742	429	66.669	417	67.142	417	69.657
417	90.856	430	66.75	418	67.223	418	69.756
418	90.965	431	66.835	419	67.315	419	69.848
419	91.082	432	66.905	420	67.395	420	69.938
420	91.192	433	66.986	421	67.478	421	70.03
421	91.306	434	67.069	422	67.563	422	70.129
422	91.419	435	67.157	423	67.644	423	70.227
423	91.534	436	67.235	424	67.734	424	70.363
424	91.64	437	67.328	425	67.821	425	70.459
425	91.755	438	67.401	426	67.908	426	70.575
426	91.874	439	67.485	427	67.992	427	70.676
427	91.972	440	67.561	428	68.091	428	70.774
428	92.093	441	67.63	429	68.193	429	70.874
429	92.195	442	67.719	430	68.288	430	70.966
430	92.31	443	67.793			431	71.162
431	92.413	444	67.873			432	71.265
432	92.53	445	67.969			433	71.369
433	92.632	446	68.032			434	71.474
434	92.747	447	68.117				

435	92.855	448	68.192		
436	92.97	449	68.279		
437	93.074	450	68.354		
438	93.183	451	68.432		
439	93.295	452	68.516		
440	93.402	453	68.6		
441	93.511	454	68.68		
442	93.624	455	68.765		
443	93.731	456	68.85		
444	93.845	457	68.942		
445	93.944	458	69.024		
446	94.069	459	69.114		
447	94.164	460	69.2		
448	94.282	461	69.275		
449	94.387	462	69.398		
450	94.493				
451	94.605				
452	94.709				
453	94.821				
454	94.92				
455	95.04				
456	95.148				
457	95.257				
458	95.371				
459	95.489				
460	95.606				

	461	95.738						
	462	95.868						
N	5		4		4		4	
m	2		1		2		2	
run	1		1		1		2	
	frame	%F	frame	%F	frame	%F	frame	%F
	39	0.592	34	1.485	36	2.234	33	2.12
	40	2.047	35	3.526	37	4.035	34	3.751
	41	2.86	36	5.178	38	5.176	35	4.79
	42	3.498	37	6.601	39	6.086	36	5.676
	43	4.055	38	7.854	40	6.814	37	6.388
	44	4.541	39	8.992	41	7.468	38	7.019
	45	4.987	40	9.998	42	8.052	39	7.558
	46	5.399	41	10.94	43	8.593	40	8.067
	47	5.778	42	11.813	44	9.098	41	8.542
	48	6.132	43	12.647	45	9.565	42	8.973
	49	6.494	44	13.42	46	10.008	43	9.393
	50	6.851	45	14.156	47	10.446	44	9.773
	51	7.182	46	14.873	48	10.863	45	10.136
	52	7.466	47	15.575	49	11.266	46	10.5
	53	7.751	48	16.221	50	11.632	47	10.84
	54	8.031	49	16.889	51	11.989	48	11.199
	55	8.314	50	17.483	52	12.36	49	11.529
	56	8.589	51	18.068	53	12.718	50	11.861
	57	8.863	52	18.704	54	13.036	51	12.205
	58	9.136	53	19.257	55	13.342	52	12.53

59	9.418	54	19.786	56	13.67	53	12.815
60	9.663	55	20.333	57	13.979	54	13.089
61	9.861	56	20.883	58	14.296	55	13.368
62	10.047	57	21.426	59	14.607	56	13.645
63	10.21	58	21.965	60	14.924	57	13.934
64	10.369	59	22.31	61	15.194	58	14.207
65	10.528	60	22.565	62	15.427	59	14.475
66	10.688	61	22.879	63	15.655	60	14.756
67	10.838	62	23.22	64	15.882	61	15.016
68	11	63	23.526	65	16.1	62	15.286
69	11.162	64	23.82	66	16.32	63	15.577
70	11.334	65	24.107	67	16.539	64	15.855
71	11.47	66	24.391	68	16.757	65	16.072
72	11.601	67	24.671	69	16.983	66	16.253
73	11.752	68	24.941	70	17.199	67	16.474
74	11.875	69	25.206	71	17.41	68	16.669
75	11.987	70	25.467	72	17.619	69	16.858
76	12.095	71	25.716	73	17.833	70	17.05
77	12.179	72	25.972	74	18.041	71	17.25
78	12.281	73	26.214	75	18.246	72	17.461
79	12.373	74	26.449	76	18.429	73	17.659
80	12.459	75	26.681	77	18.616	74	17.849
81	12.551	76	26.913	78	18.798	75	18.034
82	12.633	77	27.141	79	18.984	76	18.196
83	12.718	78	27.366	80	19.162	77	18.359
84	12.801	79	27.587	81	19.339	78	18.526

85	12.876	80	27.806	82	19.514	79	18.688
86	12.951	81	28.014	83	19.679	80	18.849
87	13.033	82	28.232	84	19.839	81	19.015
88	13.105	83	28.446	85	19.985	82	19.171
89	13.181	84	28.645	86	20.131	83	19.335
90	13.253	85	28.854	87	20.272	84	19.483
91	13.321	86	29.053	88	20.411	85	19.614
92	13.397	87	29.257	89	20.544	86	19.755
93	13.464	88	29.456	90	20.675	87	19.893
94	13.543	89	29.641	91	20.807	88	20.021
95	13.607	90	29.83	92	20.926	89	20.145
96	13.672	91	30.021	93	21.044	90	20.277
97	13.751	92	30.206	94	21.164	91	20.398
98	13.812	93	30.387	95	21.277	92	20.523
99	13.88	94	30.568	96	21.391	93	20.639
100	13.95	95	30.75	97	21.5	94	20.753
101	14.012	96	30.927	98	21.612	95	20.863
102	14.078	97	31.105	99	21.713	96	20.975
103	14.158	98	31.277	100	21.819	97	21.075
104	14.221	99	31.452	101	21.924	98	21.187
105	14.284	100	31.629	102	22.023	99	21.289
106	14.361	101	31.798	103	22.13	100	21.393
107	14.422	102	31.965	104	22.231	101	21.491
108	14.493	103	32.135	105	22.336	102	21.592
109	14.554	104	32.298	106	22.431	103	21.687
110	14.63	105	32.459	107	22.525	104	21.779

111	14.702	106	32.628	108	22.621	105	21.874
112	14.766	107	32.789	109	22.719	106	21.964
113	14.839	108	32.952	110	22.816	107	22.057
114	14.911	109	33.113	111	22.907	108	22.149
115	14.975	110	33.267	112	23.007	109	22.239
116	15.046	111	33.433	113	23.098	110	22.323
117	15.117	112	33.583	114	23.191	111	22.417
118	15.182	113	33.738	115	23.283	112	22.504
119	15.252	114	33.906	116	23.374	113	22.593
120	15.318	115	34.053	117	23.46	114	22.68
121	15.397	116	34.195	118	23.558	115	22.765
122	15.462	117	34.353	119	23.647	116	22.856
123	15.534	118	34.501	120	23.736	117	22.939
124	15.609	119	34.651	121	23.82	118	23.022
125	15.674	120	34.793	122	23.915	119	23.112
126	15.742	121	34.944	123	24.006	120	23.189
127	15.806	122	35.087	124	24.098	121	23.28
128	15.876	123	35.227	125	24.194	122	23.368
129	15.937	124	35.384	126	24.285	123	23.449
130	16.009	125	35.518	127	24.374	124	23.535
131	16.082	126	35.666	128	24.463	125	23.62
132	16.158	127	35.811	129	24.556	126	23.704
133	16.219	128	35.949	130	24.647	127	23.789
134	16.298	129	36.087	131	24.739	128	23.871
135	16.373	130	36.221	132	24.827	129	23.951
136	16.421	131	36.357	133	24.92	130	24.042

137	16.484	132	36.504	134	25.009	131	24.121
138	16.542	133	36.638	135	25.073	132	24.208
139	16.59	134	36.77	136	25.16	133	24.29
140	16.652	135	36.863	137	25.256	134	24.373
141	16.722	136	36.996	138	25.343	135	24.464
142	16.783	137	37.125	139	25.433	136	24.533
143	16.842	138	37.258	140	25.525	137	24.623
144	16.895	139	37.387	141	25.613	138	24.704
145	16.94	140	37.522	142	25.71	139	24.783
146	16.991	141	37.651	143	25.801	140	24.873
147	17.046	142	37.78	144	25.886	141	24.956
148	17.072	143	37.911	145	25.974	142	25.034
149	17.13	144	38.037	146	26.069	143	25.123
150	17.177	145	38.169	147	26.156	144	25.201
151	17.221	146	38.296	148	26.249	145	25.291
152	17.272	147	38.424	149	26.331	146	25.364
153	17.321	148	38.548	150	26.43	147	25.454
154	17.369	149	38.679	151	26.514	148	25.536
155	17.412	150	38.802	152	26.606	149	25.617
156	17.46	151	38.928	153	26.702	150	25.69
157	17.506	152	39.048	154	26.786	151	25.771
158	17.572	153	39.176	155	26.884	152	25.855
159	17.603	154	39.294	156	26.984	153	25.935
160	17.644	155	39.416	157	27.087	154	26.016
161	17.7	156	39.539	158	27.177	155	26.107
162	17.743	157	39.661	159	27.279	156	26.186

163	17.785	158	39.78	160	27.355	157	26.266
164	17.832	159	39.907	161	27.431	158	26.342
165	17.877	160	40.023	162	27.507	159	26.425
166	17.915	161	40.147	163	27.6	160	26.503
167	17.963	162	40.264	164	27.681	161	26.585
168	18.002	163	40.383	165	27.78	162	26.67
169	18.059	164	40.503	166	27.86	163	26.758
170	18.089	165	40.617	167	27.942	164	26.846
171	18.13	166	40.738	168	28.03	165	26.93
172	18.171	167	40.85	169	28.117	166	27.015
173	18.21	168	40.969	170	28.205	167	27.096
174	18.258	169	41.081	171	28.289	168	27.173
175	18.295	170	41.194	172	28.371	169	27.256
176	18.334	171	41.313	173	28.462	170	27.338
177	18.377	172	41.432	174	28.544	171	27.407
178	18.412	173	41.546	175	28.626	172	27.491
179	18.457	174	41.657	176	28.709	173	27.562
180	18.509	175	41.769	177	28.792	174	27.639
181	18.546	176	41.886	178	28.875	175	27.709
182	18.584	177	41.997	179	28.957	176	27.778
183	18.623	178	42.114	180	29.032	177	27.845
184	18.669	179	42.228	181	29.103	178	27.917
185	18.704	180	42.332	182	29.178	179	27.998
186	18.758	181	42.446	183	29.247	180	28.067
187	18.797	182	42.544	184	29.321	181	28.14
188	18.837	183	42.657	185	29.392	182	28.22

189	18.879	184	42.762	186	29.462	183	28.291
190	18.926	185	42.877	187	29.537	184	28.37
191	18.967	186	42.976	188	29.607	185	28.445
192	19.009	187	43.092	189	29.675	186	28.52
193	19.059	188	43.19	190	29.736	187	28.594
194	19.105	189	43.299	191	29.805	188	28.663
195	19.15	190	43.403	192	29.881	189	28.744
196	19.197	191	43.518	193	29.944	190	28.805
197	19.235	192	43.621	194	30.011	191	28.872
198	19.282	193	43.729	195	30.073	192	28.934
199	19.329	194	43.844	196	30.138	193	29.003
200	19.365	195	43.948	197	30.206	194	29.069
201	19.415	196	44.056	198	30.269	195	29.144
202	19.457	197	44.151	199	30.336	196	29.211
203	19.508	198	44.261	200	30.399	197	29.281
204	19.551	199	44.358	201	30.464	198	29.339
205	19.598	200	44.459	202	30.523	199	29.398
206	19.64	201	44.566	203	30.584	200	29.462
207	19.682	202	44.667	204	30.646	201	29.521
208	19.732	203	44.775	205	30.704	202	29.587
209	19.777	204	44.876	206	30.766	203	29.647
210	19.824	205	44.984	207	30.828	204	29.712
211	19.875	206	45.074	208	30.888	205	29.776
212	19.912	207	45.183	209	30.948	206	29.814
213	19.963	208	45.281	210	31.007	207	29.876
214	20.003	209	45.385	211	31.065	208	29.939

215	20.05	210	45.488	212	31.129	209	29.996
216	20.089	211	45.583	213	31.185	210	30.061
217	20.14	212	45.69	214	31.242	211	30.116
218	20.18	213	45.782	215	31.303	212	30.176
219	20.224	214	45.881	216	31.36	213	30.235
220	20.272	215	45.981	217	31.417	214	30.291
221	20.315	216	46.08	218	31.482	215	30.348
222	20.364	217	46.183	219	31.531	216	30.407
223	20.41	218	46.277	220	31.585	217	30.461
224	20.452	219	46.381	221	31.642	218	30.521
225	20.501	220	46.478	222	31.695	219	30.579
226	20.551	221	46.609	223	31.755	220	30.636
227	20.595	222	46.668	224	31.812	221	30.689
228	20.642	223	46.765	225	31.868	222	30.741
229	20.691	224	46.868	226	31.92	223	30.804
230	20.736	225	46.963	227	31.984	224	30.858
231	20.787	226	47.06	228	32.038	225	30.912
232	20.84	227	47.157	229	32.107	226	30.967
233	20.887	228	47.255	230	32.148	227	31.023
234	20.933	229	47.352	231	32.208	228	31.077
235	20.973	230	47.443	232	32.261	229	31.122
236	21.026	231	47.548	233	32.321	230	31.183
237	21.067	232	47.665	234	32.376	231	31.227
238	21.115	233	47.741	235	32.428	232	31.29
239	21.166	234	47.826	236	32.484	233	31.34
240	21.205	235	47.919	237	32.536	234	31.395

241	21.246	236	48.016	238	32.595	235	31.44
242	21.292	237	48.109	239	32.648	236	31.493
243	21.331	238	48.204	240	32.705	237	31.551
244	21.378	239	48.291	241	32.761	238	31.6
245	21.422	240	48.381	242	32.816	239	31.652
246	21.462	241	48.476	243	32.865	240	31.704
247	21.508	242	48.567	244	32.926	241	31.753
248	21.559	243	48.664	245	32.981	242	31.801
249	21.602	244	48.754	246	33.033	243	31.857
250	21.658	245	48.845	247	33.09	244	31.907
251	21.704	246	48.93	248	33.149	245	31.961
252	21.743	247	49.026	249	33.199	246	32.009
253	21.783	248	49.126	250	33.256	247	32.059
254	21.821	249	49.209	251	33.31	248	32.109
255	21.851	250	49.295	252	33.368	249	32.162
256	21.892	251	49.381	253	33.425	250	32.214
257	21.936	252	49.474	254	33.476	251	32.261
258	21.982	253	49.566	255	33.537	252	32.313
259	22.023	254	49.653	256	33.589	253	32.359
260	22.06	255	49.747	257	33.652	254	32.412
261	22.092	256	49.827	258	33.698	255	32.464
262	22.113	257	49.916	259	33.759	256	32.518
263	22.149	258	50.006	260	33.809	257	32.567
264	22.183	259	50.099	261	33.866	258	32.621
265	22.214	260	50.193	262	33.915	259	32.667
266	22.248	261	50.27	263	33.978	260	32.718

267	22.27	262	50.36	264	34.027	261	32.767
268	22.31	263	50.452	265	34.085	262	32.823
269	22.343	264	50.538	266	34.139	263	32.871
270	22.38	265	50.62	267	34.197	264	32.922
271	22.41	266	50.706	268	34.255	265	32.969
272	22.446	267	50.802	269	34.315	266	33.018
273	22.476	268	50.885	270	34.365	267	33.068
274	22.515	269	50.967	271	34.419	268	33.118
275	22.545	270	51.06	272	34.478	269	33.163
276	22.574	271	51.148	273	34.535	270	33.222
277	22.61	272	51.224	274	34.59	271	33.27
278	22.645	273	51.317	275	34.653	272	33.32
279	22.68	274	51.406	276	34.702	273	33.365
280	22.709	275	51.494	277	34.758	274	33.419
281	22.745	276	51.586	278	34.819	275	33.468
282	22.772	277	51.665	279	34.878	276	33.52
283	22.804	278	51.755	280	34.928	277	33.566
284	22.836	279	51.842	281	34.982	278	33.619
285	22.871	280	51.927	282	35.041	279	33.669
286	22.903	281	52.009	283	35.09	280	33.722
287	22.936	282	52.104	284	35.148	281	33.77
288	22.967	283	52.189	285	35.202	282	33.825
289	22.994	284	52.274	286	35.255	283	33.866
290	23.027	285	52.36	287	35.318	284	33.925
291	23.062	286	52.448	288	35.369	285	33.969
292	23.087	287	52.527	289	35.437	286	34.028

293	23.12	288	52.619	290	35.485	287	34.078
294	23.15	289	52.701	291	35.545	288	34.125
295	23.186	290	52.787	292	35.602	289	34.18
296	23.213	291	52.874	293	35.656	290	34.217
297	23.239	292	52.961	294	35.715	291	34.279
298	23.27	293	53.043	295	35.772	292	34.328
299	23.305	294	53.126	296	35.83	293	34.377
300	23.34	295	53.212	297	35.88	294	34.423
301	23.365	296	53.295	298	35.941	295	34.481
302	23.396	297	53.377	299	35.995	296	34.529
303	23.429	298	53.462	300	36.045	297	34.583
304	23.455	299	53.549	301	36.114	298	34.634
305	23.488	300	53.629	302	36.176	299	34.68
306	23.514	301	53.712	303	36.229	300	34.729
307	23.549	302	53.795	304	36.293	301	34.778
308	23.574	303	53.865	305	36.353	302	34.835
309	23.607	304	53.962	306	36.411	303	34.882
310	23.634	305	54.03	307	36.486	304	34.931
311	23.669	306	54.12	308	36.55	305	34.979
312	23.696	307	54.21	309	36.607	306	35.026
313	23.716	308	54.286	310	36.659	307	35.082
314	23.749	309	54.373	311	36.718	308	35.127
315	23.785	310	54.45	312	36.766	309	35.18
316	23.809	311	54.53	313	36.8	310	35.236
317	23.842	312	54.612	314	36.857	311	35.279
318	23.871	313	54.691	315	36.918	312	35.33

319	23.907	314	54.783	316	36.97	313	35.387
320	23.933	315	54.857	317	37.026	314	35.438
321	23.964	316	54.951	318	37.083	315	35.486
322	23.993	317	55.016	319	37.145	316	35.544
323	24.025	318	55.112	320	37.197	317	35.591
324	24.056	319	55.186	321	37.256	318	35.646
325	24.086	320	55.271	322	37.309	319	35.697
326	24.116	321	55.355	323	37.367	320	35.74
327	24.152	322	55.433	324	37.42	321	35.785
328	24.177	323	55.512	325	37.483	322	35.847
329	24.21	324	55.595	326	37.535	323	35.896
330	24.248	325	55.677	327	37.585	324	35.939
331	24.276	326	55.758	328	37.645	325	35.996
332	24.307	327	55.837	329	37.703	326	36.056
333	24.34	328	55.927	330	37.756	327	36.111
334	24.372	329	56	331	37.81	328	36.161
335	24.405	330	56.085	332	37.87	329	36.22
336	24.433	331	56.163	333	37.924	330	36.275
337	24.462	332	56.248	334	37.978	331	36.313
338	24.498	333	56.326	335	38.039	332	36.369
339	24.531	334	56.41	336	38.085	333	36.413
340	24.557	335	56.489	337	38.138	334	36.454
341	24.595	336	56.572	338	38.206	335	36.495
342	24.628	337	56.654	339	38.249	336	36.555
343	24.657	338	56.73	340	38.312	337	36.588
344	24.704	339	56.814	341	38.364	338	36.634

345	24.72	340	56.891	342	38.42	339	36.686
346	24.764	341	56.971	343	38.478	340	36.737
347	24.789	342	57.057	344	38.541	341	36.79
348	24.82	343	57.132	345	38.59	342	36.84
349	24.854	344	57.212	346	38.639	343	36.895
350	24.887	345	57.293	347	38.687	344	36.953
351	24.917	346	57.378	348	38.733	345	36.998
352	24.951	347	57.453	349	38.78	346	37.054
353	24.986	348	57.534	350	38.83	347	37.1
354	25.016	349	57.609	351	38.882	348	37.147
355	25.054	350	57.687	352	38.93	349	37.187
356	25.089	351	57.767	353	38.984	350	37.24
357	25.117	352	57.844	354	39.032	351	37.278
358	25.157	353	57.929	355	39.081	352	37.319
359	25.184	354	58.006	356	39.133	353	37.37
360	25.22	355	58.089	357	39.178	354	37.422
361	25.263	356	58.169	358	39.222	355	37.466
362	25.293	357	58.241	359	39.279	356	37.521
363	25.327	358	58.318	360	39.323	357	37.564
364	25.357	359	58.394	361	39.375	358	37.614
365	25.389	360	58.474	362	39.417	359	37.669
366	25.425	361	58.55	363	39.465	360	37.717
367	25.456	362	58.628	364	39.513	361	37.764
368	25.493	363	58.712	365	39.556	362	37.807
369	25.523	364	58.788	366	39.608	363	37.867
370	25.552	365	58.872	367	39.655	364	37.909

371	25.587	366	58.945	368	39.703	365	37.953
372	25.628	367	59.023	369	39.748	366	38.011
373	25.656	368	59.104	370	39.8	367	38.054
374	25.695	369	59.178	371	39.85	368	38.098
375	25.727	370	59.255	372	39.893	369	38.145
376	25.766	371	59.331	373	39.938	370	38.192
377	25.796	372	59.419	374	39.988	371	38.249
378	25.826	373	59.49	375	40.036	372	38.286
379	25.861	374	59.564	376	40.08	373	38.338
380	25.906	375	59.644	377	40.13	374	38.382
381	25.937	376	59.725	378	40.174	375	38.423
382	25.973	377	59.801	379	40.221	376	38.466
383	26.008	378	59.884	380	40.271	377	38.507
384	26.048	379	59.956	381	40.313	378	38.557
385	26.076	380	60.032	382	40.367	379	38.6
386	26.107	381	60.112	383	40.41	380	38.644
387	26.141	382	60.19	384	40.454	381	38.693
388	26.173	383	60.266	385	40.509	382	38.741
389	26.205	384	60.343	386	40.557	383	38.792
390	26.234	385	60.417	387	40.606	384	38.837
391	26.267	386	60.498	388	40.653	385	38.882
392	26.3	387	60.567	389	40.701	386	38.945
393	26.336	388	60.653	390	40.753	387	38.988
394	26.355	389	60.719	391	40.799	388	39.023
395	26.391	390	60.808	392	40.844	389	39.06
396	26.424	391	60.883	393	40.884	390	39.099

397	26.457	392	60.964	394	40.94	391	39.139
398	26.484	393	61.037	395	40.984	392	39.184
399	26.514	394	61.117	396	41.037	393	39.226
400	26.551	395	61.197	397	41.084	394	39.265
401	26.578	396	61.263	398	41.13	395	39.313
402	26.61	397	61.347	399	41.17	396	39.357
403	26.641	398	61.422	400	41.218	397	39.4
404	26.673	399	61.494	401	41.254	398	39.443
405	26.713	400	61.581	402	41.307	399	39.49
406	26.737	401	61.651	403	41.359	400	39.534
407	26.769	402	61.736	404	41.4	401	39.579
408	26.805	403	61.812	405	41.445	402	39.619
409	26.845	404	61.889	406	41.499	403	39.665
410	26.886	405	61.971	407	41.537	404	39.724
411	26.914	406	62.041	408	41.59	405	39.755
412	26.94	407	62.127	409	41.632	406	39.799
413	26.974	408	62.271	410	41.681	407	39.84
414	27.005	409	62.354	411	41.728	408	39.886
415	27.033	410	62.427	412	41.776	409	39.92
416	27.06	411	62.501	413	41.812	410	39.974
417	27.086	412	62.589	414	41.863	411	40.008
418	27.108	413	62.663	415	41.906	412	40.048
419	27.124	414	62.76	416	41.951	413	40.104
420	27.154	415	62.846	417	42.002	414	40.137
421	27.182			418	42.043	415	40.191
422	27.205			419	42.093	416	40.225

423	27.233		420	42.136	417	40.264
424	27.262		421	42.182	418	40.312
425	27.285		422	42.228	419	40.351
426	27.31		423	42.274	420	40.391
427	27.339		424	42.317	421	40.438
428	27.373		425	42.364	422	40.48
429	27.39		426	42.415	423	40.525
430	27.413		427	42.456	424	40.571
431	27.436		428	42.507	425	40.609
432	27.474		429	42.549	426	40.65
433	27.502		430	42.594	427	40.7
434	27.536		431	42.637	428	40.742
435	27.565		432	42.684	429	40.786
436	27.588		433	42.72	430	40.826
437	27.625		434	42.769	431	40.869
438	27.647		435	42.82	432	40.909
439	27.677		436	42.86	433	40.962
440	27.707		437	42.91	434	41.003
441	27.735		438	42.944	435	41.043
442	27.76		439	42.997	436	41.09
443	27.794		440	43.041	437	41.134
444	27.824		441	43.082	438	41.171
445	27.853		442	43.127	439	41.214
446	27.879		443	43.178	440	41.259
447	27.911		444	43.216	441	41.299
448	27.942		445	43.271	442	41.342

449	27.972		446	43.311	443	41.381
450	28.003		447	43.349	444	41.428
451	28.03		448	43.404	445	41.461
452	28.065		449	43.445	446	41.51
453	28.092		450	43.486	447	41.553
454	28.113		451	43.534	448	41.587
455	28.144		452	43.573	449	41.629
456	28.173		453	43.619	450	41.674
457	28.191		454	43.667	451	41.711
458	28.232		455	43.712	452	41.753
459	28.255		456	43.762	453	41.799
460	28.284		457	43.807	454	41.836
461	28.315		458	43.85	455	41.886
462	28.339		459	43.894	456	41.921
463	28.369		460	43.937	457	41.967
464	28.401		461	43.98	458	42.004
465	28.432		462	44.027	459	42.043
466	28.457		463	44.071	460	42.081
467	28.48		464	44.118	461	42.124
468	28.51		465	44.163	462	42.166
469	28.538		466	44.205	463	42.207
470	28.569		467	44.245	464	42.245
471	28.595		468	44.295	465	42.289
472	28.621		469	44.333	466	42.327
473	28.643		470	44.381	467	42.374
474	28.675		471	44.428	468	42.405

475	28.705		472	44.473	469	42.449
476	28.73		473	44.511	470	42.496
477	28.759		474	44.553	471	42.535
478	28.793		475	44.601	472	42.573
479	28.821		476	44.64	473	42.619
480	28.84		477	44.69	474	42.659
481	28.866		478	44.731	475	42.692
482	28.899		479	44.773	476	42.738
483	28.929		480	44.825	477	42.782
484	28.939		481	44.872	478	42.823
485	28.971		482	44.914	479	42.861
486	28.994		483	44.942	480	42.903
487	29.023		484	44.986	481	42.947
488	29.047		485	45.026	482	42.985
489	29.069		486	45.074	483	43.023
490	29.098		487	45.113	484	43.05
491	29.123		488	45.16	485	43.095
492	29.15		489	45.214	486	43.128
493	29.187		490	45.25	487	43.171
494	29.205		491	45.293	488	43.214
495	29.235		492	45.339	489	43.25
496	29.265		493	45.379	490	43.291
497	29.291		494	45.423	491	43.345
498	29.318		495	45.466	492	43.386
499	29.345		496	45.508	493	43.431
500	29.376		497	45.552	494	43.464

501	29.4		498	45.595	495	43.51
502	29.426		499	45.636	496	43.548
503	29.454		500	45.687	497	43.587
504	29.478		501	45.723	498	43.624
505	29.507		502	45.774	499	43.668
506	29.528		503	45.822	500	43.707
507	29.558		504	45.865	501	43.745
508	29.594		505	45.907	502	43.785
509	29.615		506	45.954	503	43.827
510	29.642		507	46.003	504	43.865
511	29.671		508	46.044	505	43.905
512	29.694		509	46.093	506	43.948
513	29.723		510	46.131	507	43.979
514	29.753		511	46.186	508	44.018
515	29.776		512	46.225	509	44.062
516	29.811		513	46.278	510	44.096
517	29.834		514	46.33	511	44.149
518	29.858		515	46.381	512	44.187
519	29.886		516	46.435	513	44.223
520	29.915		517	46.483	514	44.27
521	29.946		518	46.537	515	44.304
522	29.975		519	46.598	516	44.346
523	30		520	46.649	517	44.387
524	30.021		521	46.704	518	44.427
525	30.05		522	46.744	519	44.467
526	30.078		523	46.787	520	44.509

527	30.104		524	46.842	521	44.545
528	30.133		525	46.894	522	44.588
529	30.16		526	46.936	523	44.625
530	30.182		527	46.981	524	44.662
531	30.205		528	47.026	525	44.706
532	30.235		529	47.067	526	44.744
533	30.262		530	47.111	527	44.783
534	30.295				528	44.825
535	30.322				529	44.865
536	30.349				530	44.904
537	30.366				531	44.949
538	30.403				532	44.986
539	30.422				533	45.027
540	30.458				534	45.065
541	30.487				535	45.101
542	30.51				536	45.146
543	30.535				537	45.182
544	30.564				538	45.222
545	30.595				539	45.262
546	30.613				540	45.3
547	30.642				541	45.341
548	30.669				542	45.384
549	30.698				543	45.418
550	30.72				544	45.476
551	30.758				545	45.515
552	30.785				546	45.555

553	30.809
554	30.84
555	30.862
556	30.903
557	30.929
558	30.987
559	31.016
560	31.05

547	45.597
548	45.632
549	45.677
550	45.719
551	45.753
552	45.792
553	45.83
554	45.86
555	45.899
556	45.934
557	45.978
558	46.013
559	46.061
560	46.101
561	46.139
562	46.172
563	46.217
564	46.26
565	46.296
566	46.341
567	46.387
568	46.424
569	46.474
570	46.502
571	46.55
572	46.595

					573	46.63
					574	46.675
					575	46.713
N	4		4			
m	3		3			
run	1		2			
	frame	%F	frame	%F		
	37	1.257	35	0.644		
	38	3.018	36	1.804		
	39	3.316	37	2.627		
	40	3.659	38	3.046		
	41	3.916	39	3.413		
	42	4.121	40	3.762		
	43	4.323	41	4.003		
	44	4.517	42	4.247		
	45	4.734	43	4.469		
	46	4.941	44	4.72		
	47	5.151	45	4.939		
	48	5.326	46	5.139		
	49	5.469	47	5.311		
	50	5.629	48	5.493		
	51	5.801	49	5.662		
	52	5.947	50	5.846		
	53	6.071	51	5.996		
	54	6.192	52	6.146		
	55	6.282	53	6.27		

56	6.385	54	6.408		
57	6.511	55	6.54		
58	6.632	56	6.688		
59	6.767	57	6.826		
60	6.884	58	6.965		
61	7.009	59	7.087		
62	7.12	60	7.228		
63	7.246	61	7.344		
64	7.37	62	7.449		
65	7.469	63	7.545		
66	7.58	64	7.651		
67	7.668	65	7.76		
68	7.762	66	7.884		
69	7.853	67	8.014		
70	7.944	68	8.132		
71	8.042	69	8.257		
72	8.148	70	8.392		
73	8.25	71	8.515		
74	8.362	72	8.634		
75	8.492	73	8.764		
76	8.6	74	8.874		
77	8.705	75	8.967		
78	8.794	76	9.076		
79	8.894	77	9.184		
80	8.986	78	9.291		
81	9.064	79	9.403		

82	9.151	80	9.477		
83	9.236	81	9.571		
84	9.328	82	9.671		
85	9.417	83	9.763		
86	9.508	84	9.871		
87	9.601	85	9.964		
88	9.691	86	10.058		
89	9.789	87	10.131		
90	9.869	88	10.208		
91	9.958	89	10.291		
92	10.036	90	10.388		
93	10.133	91	10.477		
94	10.221	92	10.571		
95	10.295	93	10.671		
96	10.369	94	10.762		
97	10.426	95	10.836		
98	10.491	96	10.93		
99	10.561	97	11.018		
100	10.634	98	11.112		
101	10.715	99	11.212		
102	10.791	100	11.3		
103	10.868	101	11.387		
104	10.951	102	11.441		
105	11.026	103	11.503		
106	11.105	104	11.571		
107	11.184	105	11.639		

108	11.265	106	11.698		
109	11.35	107	11.756		
110	11.448	108	11.831		
111	11.527	109	11.9		
112	11.601	110	11.979		
113	11.677	111	12.052		
114	11.748	112	12.132		
115	11.803	113	12.214		
116	11.87	114	12.283		
117	11.928	115	12.356		
118	11.989	116	12.431		
119	12.053	117	12.516		
120	12.106	118	12.594		
121	12.163	119	12.678		
122	12.231	120	12.778		
123	12.295	121	12.84		
124	12.369	122	12.918		
125	12.439	123	12.985		
126	12.521	124	13.039		
127	12.58	125	13.124		
128	12.645	126	13.183		
129	12.703	127	13.242		
130	12.761	128	13.295		
131	12.808	129	13.346		
132	12.877	130	13.403		
133	12.958	131	13.432		

134	13.007	132	13.496		
135	13.077	133	13.547		
136	13.175	134	13.622		
137	13.244	135	13.661		
138	13.291	136	13.717		
139	13.324	137	13.767		
140	13.358	138	13.82		
141	13.409	139	13.879		
142	13.462	140	13.905		
143	13.519	141	13.955		
144	13.591	142	14.007		
145	13.659	143	14.065		
146	13.709	144	14.113		
147	13.752	145	14.16		
148	13.797	146	14.199		
149	13.832	147	14.24		
150	13.873	148	14.28		
151	13.933	149	14.333		
152	13.983	150	14.38		
153	14.044	151	14.43		
154	14.089	152	14.482		
155	14.124	153	14.537		
156	14.166	154	14.581		
157	14.217	155	14.618		
158	14.268	156	14.665		
159	14.329	157	14.708		

160	14.386	158	14.748		
161	14.447	159	14.8		
162	14.498	160	14.85		
163	14.542	161	14.902		
164	14.579	162	14.941		
165	14.612	163	14.984		
166	14.659	164	15.016		
167	14.695	165	15.047		
168	14.741	166	15.086		
169	14.777	167	15.126		
170	14.825	168	15.145		
171	14.879	169	15.174		
172	14.921	170	15.206		
173	14.958	171	15.232		
174	15	172	15.269		
175	15.041	173	15.295		
176	15.082	174	15.326		
177	15.128	175	15.357		
178	15.166	176	15.39		
179	15.219	177	15.428		
180	15.258	178	15.474		
181	15.298	179	15.495		
182	15.335	180	15.549		
183	15.379	181	15.589		
184	15.415	182	15.631		
185	15.449	183	15.668		

186	15.49	184	15.694		
187	15.515	185	15.718		
188	15.545	186	15.737		
189	15.578	187	15.755		
190	15.609	188	15.78		
191	15.626	189	15.816		
192	15.654	190	15.836		
193	15.683	191	15.87		
194	15.714	192	15.895		
195	15.742	193	15.93		
196	15.773	194	15.954		
197	15.788	195	15.987		
198	15.822	196	16.019		
199	15.85	197	16.045		
200	15.883	198	16.067		
201	15.918	199	16.103		
202	15.95	200	16.133		
203	15.975	201	16.162		
204	16.004	202	16.195		
205	16.038	203	16.221		
206	16.07	204	16.237		
207	16.109	205	16.256		
208	16.129	206	16.284		
209	16.158	207	16.307		
210	16.2	208	16.333		
211	16.239	209	16.357		

212	16.267	210	16.382		
213	16.294	211	16.405		
214	16.33	212	16.426		
215	16.362	213	16.457		
216	16.392	214	16.486		
217	16.419	215	16.509		
218	16.457	216	16.541		
219	16.476	217	16.577		
220	16.495	218	16.613		
221	16.525	219	16.645		
222	16.55	220	16.68		
223	16.573	221	16.717		
224	16.592	222	16.748		
225	16.622	223	16.778		
226	16.65	224	16.804		
227	16.679	225	16.835		
228	16.699	226	16.857		
229	16.725	227	16.882		
230	16.746	228	16.908		
231	16.773	229	16.915		
232	16.799	230	16.95		
233	16.823	231	16.977		
234	16.851	232	17.003		
235	16.88	233	17.026		
236	16.907	234	17.055		
237	16.938	235	17.074		

238	16.965	236	17.098		
239	16.99	237	17.136		
240	17.026	238	17.168		
241	17.06	239	17.189		
242	17.087	240	17.227		
243	17.115	241	17.244		
244	17.136	242	17.267		
245	17.155	243	17.291		
246	17.172	244	17.315		
247	17.198	245	17.344		
248	17.217	246	17.374		
249	17.248	247	17.391		
250	17.273	248	17.421		
251	17.301	249	17.443		
252	17.325	250	17.465		
253	17.343	251	17.488		
254	17.364	252	17.513		
255	17.385	253	17.539		
256	17.41	254	17.564		
257	17.437	255	17.598		
258	17.463	256	17.611		
259	17.485	257	17.641		
260	17.515	258	17.668		
261	17.528	259	17.694		
262	17.558	260	17.718		
263	17.576	261	17.742		

264	17.598	262	17.769		
265	17.622	263	17.792		
266	17.646	264	17.817		
267	17.674	265	17.845		
268	17.696	266	17.877		
269	17.721	267	17.896		
270	17.752	268	17.929		
271	17.781	269	17.953		
272	17.805	270	17.981		
273	17.835	271	18.01		
274	17.863	272	18.048		
275	17.89	273	18.07		
276	17.914	274	18.102		
277	17.943	275	18.132		
278	17.977	276	18.16		
279	17.999	277	18.196		
280	18.034	278	18.228		
281	18.062	279	18.255		
282	18.099	280	18.293		
283	18.12	281	18.315		
284	18.151	282	18.346		
285	18.18	283	18.376		
286	18.202	284	18.403		
287	18.235	285	18.427		
288	18.266	286	18.442		
289	18.293	287	18.46		

290	18.327	288	18.486		
291	18.354	289	18.505		
292	18.379	290	18.539		
293	18.408	291	18.571		
294	18.43	292	18.604		
295	18.444	293	18.629		
296	18.468	294	18.66		
297	18.502	295	18.681		
298	18.528	296	18.723		
299	18.561	297	18.75		
300	18.583	298	18.788		
301	18.607	299	18.815		
302	18.633	300	18.852		
303	18.669	301	18.878		
304	18.703	302	18.904		
305	18.731	303	18.942		
306	18.759	304	18.974		
307	18.783	305	18.997		
308	18.812	306	19.032		
309	18.843	307	19.053		
310	18.866	308	19.077		
311	18.893	309	19.122		
312	18.923	310	19.142		
313	18.943	311	19.172		
314	18.963	312	19.207		
315	18.988	313	19.236		

316	19.011	314	19.258		
317	19.027	315	19.281		
318	19.044	316	19.308		
319	19.056	317	19.333		
320	19.085	318	19.352		
321	19.106	319	19.365		
322	19.136	320	19.384		
323	19.161	321	19.406		
324	19.188	322	19.429		
325	19.223	323	19.451		
326	19.239	324	19.473		
327	19.27	325	19.504		
328	19.293	326	19.528		
329	19.32	327	19.548		
330	19.349	328	19.577		
331	19.365	329	19.606		
332	19.4	330	19.633		
333	19.42	331	19.656		
334	19.447	332	19.68		
335	19.472	333	19.712		
336	19.501	334	19.74		
337	19.53	335	19.768		
338	19.551	336	19.796		
339	19.574	337	19.823		
340	19.594	338	19.855		
341	19.613	339	19.876		

342	19.647	340	19.9		
343	19.669	341	19.919		
344	19.696	342	19.947		
345	19.723	343	19.97		
346	19.746	344	20.003		
347	19.776	345	20.031		
348	19.802	346	20.053		
349	19.823	347	20.073		
350	19.851	348	20.095		
351	19.867	349	20.13		
352	19.896	350	20.14		
353	19.919	351	20.163		
354	19.939	352	20.192		
355	19.968	353	20.21		
356	19.992	354	20.239		
357	20.016	355	20.262		
358	20.035	356	20.286		
359	20.06	357	20.318		
360	20.076	358	20.343		
361	20.095	359	20.381		
362	20.127	360	20.404		
363	20.156	361	20.425		
364	20.174	362	20.459		
365	20.199	363	20.489		
366	20.227	364	20.507		
367	20.261	365	20.541		

368	20.291	366	20.568		
369	20.325	367	20.597		
370	20.356	368	20.62		
371	20.377	369	20.644		
372	20.412	370	20.668		
373	20.433	371	20.698		
374	20.452	372	20.723		
375	20.482	373	20.744		
376	20.499	374	20.769		
377	20.524	375	20.792		
378	20.552	376	20.821		
379	20.584	377	20.846		
380	20.608	378	20.881		
381	20.633	379	20.905		
382	20.657	380	20.925		
383	20.681	381	20.952		
384	20.695	382	20.979		
385	20.724	383	21.002		
386	20.75	384	21.02		
387	20.776	385	21.046		
388	20.798	386	21.064		
389	20.829	387	21.085		
390	20.852	388	21.093		
391	20.873	389	21.115		
392	20.885	390	21.14		
393	20.905	391	21.155		

394	20.92	392	21.183		
395	20.948	393	21.205		
396	20.971	394	21.222		
397	20.989	395	21.243		
398	21.02	396	21.257		
399	21.044	397	21.299		
400	21.069	398	21.317		
401	21.094	399	21.335		
402	21.111	400	21.345		
403	21.131	401	21.366		
404	21.151	402	21.388		
405	21.171	403	21.41		
406	21.195	404	21.421		
407	21.216	405	21.461		
408	21.24	406	21.493		
409	21.268	407	21.501		
410	21.29	408	21.525		
411	21.313	409	21.541		
412	21.334	410	21.562		
413	21.359	411	21.582		
414	21.372	412	21.605		
415	21.398	413	21.624		
416	21.42	414	21.646		
417	21.452	415	21.668		
418	21.482	416	21.684		
419	21.503	417	21.712		

420	21.526	418	21.72		
421	21.544	419	21.742		
422	21.566	420	21.761		
423	21.584	421	21.779		
424	21.602	422	21.808		
425	21.625	423	21.829		
426	21.649	424	21.857		
427	21.666	425	21.876		
428	21.696	426	21.903		
429	21.714	427	21.924		
430	21.734	428	21.946		
431	21.758	429	21.969		
432	21.782	430	21.992		
433	21.8	431	22.019		
434	21.823	432	22.044		
435	21.843	433	22.075		
436	21.857	434	22.099		
437	21.885	435	22.116		
438	21.904	436	22.147		
439	21.925	437	22.178		
440	21.937	438	22.193		
441	21.957	439	22.218		
442	21.98	440	22.236		
443	22	441	22.262		
444	22.014	442	22.282		
445	22.028	443	22.316		

446	22.047	444	22.339		
447	22.065	445	22.356		
448	22.078	446	22.37		
449	22.09	447	22.39		
450	22.126	448	22.406		
451	22.142	449	22.425		
452	22.16	450	22.454		
453	22.176	451	22.469		
454	22.2	452	22.483		
455	22.217	453	22.503		
456	22.238	454	22.527		
457	22.259	455	22.538		
458	22.277	456	22.556		
459	22.287	457	22.578		
460	22.304	458	22.597		
461	22.32	459	22.605		
462	22.34	460	22.619		
463	22.356	461	22.632		
464	22.375	462	22.643		
465	22.392	463	22.671		
466	22.405	464	22.68		
467	22.418	465	22.705		
468	22.433	466	22.728		
469	22.452	467	22.736		
470	22.462	468	22.751		
471	22.487	469	22.764		

472	22.498	470	22.779		
473	22.52	471	22.799		
474	22.536	472	22.814		
475	22.551	473	22.831		
476	22.582	474	22.847		
477	22.594	475	22.864		
478	22.617	476	22.872		
479	22.637	477	22.888		
480	22.659	478	22.91		
481	22.668	479	22.918		
482	22.687	480	22.929		
483	22.697	481	22.95		
484	22.717	482	22.961		
485	22.733	483	22.984		
486	22.754	484	22.999		
487	22.773	485	23.022		
488	22.788	486	23.034		
489	22.805	487	23.053		
490	22.828	488	23.067		
491	22.845	489	23.088		
492	22.864	490	23.108		
493	22.883	491	23.128		
494	22.904	492	23.153		
495	22.914	493	23.171		
496	22.933	494	23.19		
497	22.951	495	23.211		

498	22.971	496	23.22		
499	22.982	497	23.246		
500	23.01	498	23.267		
501	23.027	499	23.292		
502	23.043	500	23.307		
503	23.06	501	23.327		
504	23.074	502	23.366		
505	23.091	503	23.388		
506	23.108	504	23.406		
507	23.123	505	23.417		
508	23.142	506	23.432		
509	23.159	507	23.45		
510	23.173	508	23.473		
511	23.19	509	23.482		
512	23.2	510	23.497		
513	23.214	511	23.515		
514	23.228	512	23.545		
515	23.243	513	23.562		
516	23.256	514	23.576		
517	23.268	515	23.588		
518	23.284	516	23.605		
519	23.296	517	23.625		
520	23.315	518	23.626		
521	23.333	519	23.651		
522	23.347	520	23.664		
523	23.365	521	23.676		

524	23.387	522	23.7		
525	23.405	523	23.727		
526	23.425	524	23.73		
527	23.437	525	23.746		
528	23.454	526	23.766		
529	23.475	527	23.781		
530	23.489	528	23.795		
531	23.504	529	23.807		
532	23.518	530	23.824		
533	23.545	531	23.842		
534	23.562	532	23.872		
535	23.578	533	23.887		
536	23.593	534	23.907		
537	23.608	535	23.926		
538	23.618	536	23.937		
539	23.64	537	23.962		
540	23.657	538	23.972		
541	23.671	539	23.988		
542	23.684	540	24.002		
543	23.698	541	24.028		
544	23.714	542	24.04		
545	23.723	543	24.056		
546	23.741	544	24.07		
547	23.753	545	24.089		
548	23.767	546	24.1		
549	23.776	547	24.115		

550	23.791	548	24.127		
551	23.814	549	24.137		
552	23.825	550	24.15		
553	23.841	551	24.179		
554	23.861	552	24.194		
555	23.876	553	24.209		
556	23.893	554	24.218		
557	23.907	555	24.23		
558	23.92	556	24.241		
559	23.935	557	24.256		
560	23.959	558	24.276		
561	23.974	559	24.287		
562	23.985	560	24.295		
563	24.002	561	24.33		
564	24.02	562	24.334		
565	24.036	563	24.343		
566	24.059	564	24.362		
567	24.082	565	24.378		
568	24.096	566	24.389		
569	24.11	567	24.4		
570	24.135	568	24.419		
571	24.149	569	24.432		
572	24.164	570	24.444		
573	24.183	571	24.477		
574	24.19	572	24.498		
575	24.213	573	24.505		

576	24.231	574	24.525		
577	24.244	575	24.539		
578	24.26	576	24.551		
579	24.275	577	24.564		
580	24.288	578	24.586		
581	24.305	579	24.603		
582	24.321	580	24.607		
583	24.341	581	24.63		
584	24.357	582	24.651		
585	24.372	583	24.66		
586	24.382	584	24.675		
587	24.4	585	24.697		
588	24.41	586	24.707		
589	24.424	587	24.732		
590	24.444	588	24.746		
591	24.458	589	24.766		
592	24.473	590	24.791		
593	24.492	591	24.808		
594	24.51	592	24.827		
595	24.521	593	24.847		
596	24.538	594	24.863		
597	24.552	595	24.88		
598	24.573	596	24.883		
599	24.586	597	24.906		
600	24.599	598	24.913		
601	24.617	599	24.929		

602	24.628	600	24.961		
603	24.647	601	24.984		
604	24.659	602	25.006		
605	24.678	603	25.02		
606	24.688	604	25.039		
607	24.707	605	25.061		
608	24.715	606	25.079		
609	24.734	607	25.108		
610	24.744	608	25.124		
611	24.757	609	25.142		
612	24.772	610	25.146		
613	24.784	611	25.177		
614	24.796	612	25.187		
615	24.818	613	25.211		
616	24.833	614	25.22		
617	24.842	615	25.24		
618	24.857	616	25.254		
619	24.864	617	25.271		
620	24.872	618	25.282		
621	24.891	619	25.299		
622	24.909	620	25.307		
623	24.928	621	25.337		
624	24.943	622	25.35		
625	24.957	623	25.364		
626	24.969	624	25.38		
627	24.988	625	25.395		

628	25.002	626	25.41		
629	25.019	627	25.435		
630	25.035	628	25.446		
631	25.049	629	25.466		
632	25.063	630	25.467		
633	25.081	631	25.482		
634	25.097	632	25.49		
635	25.116	633	25.51		
636	25.127	634	25.53		
637	25.138	635	25.541		
638	25.154	636	25.559		
639	25.172	637	25.573		
640	25.196	638	25.587		
641	25.205	639	25.594		
642	25.224	640	25.613		
643	25.235	641	25.622		
644	25.254	642	25.64		
645	25.27	643	25.636		
646	25.29	644	25.645		
647	25.298	645	25.679		
648	25.315	646	25.691		
649	25.328	647	25.694		
650	25.348	648	25.704		
651	25.36	649	25.721		
652	25.379	650	25.735		
653	25.391	651	25.748		

654	25.416	652	25.769		
655	25.437	653	25.767		
656	25.458	654	25.786		
657	25.476	655	25.796		
658	25.483	656	25.81		
659	25.495	657	25.815		
660	25.513	658	25.831		
661	25.531	659	25.85		
662	25.543	660	25.858		
663	25.556	661	25.869		
664	25.572	662	25.89		
665	25.596	663	25.894		
666	25.613	664	25.9		
667	25.629	665	25.919		
668	25.648	666	25.925		
669	25.661	667	25.945		
670	25.684	668	25.965		
671	25.695	669	25.973		
672	25.71	670	25.983		
673	25.721	671	26.002		
674	25.726	672	26.019		
675	25.741	673	26.033		
676	25.757	674	26.05		
677	25.778	675	26.052		
678	25.795	676	26.067		
679	25.81	677	26.069		

680	25.821	678	26.077		
681	25.842	679	26.099		
682	25.857	680	26.112		
683	25.872	681	26.12		
684	25.886	682	26.136		
685	25.9	683	26.147		
686	25.924	684	26.148		
687	25.942	685	26.168		
688	25.954	686	26.183		
689	25.976	687	26.198		
690	25.989	688	26.207		
691	26.005	689	26.215		
692	26.017	690	26.226		
693	26.033	691	26.232		
694	26.05	692	26.243		
695	26.059	693	26.265		
696	26.081	694	26.273		
697	26.092	695	26.283		
698	26.113	696	26.28		
699	26.129	697	26.289		
700	26.142	698	26.294		
701	26.16	699	26.309		
702	26.169	700	26.324		
703	26.184	701	26.344		
704	26.202	702	26.359		
705	26.219	703	26.377		

706	26.235	704	26.392		
707	26.258	705	26.405		
708	26.269	706	26.422		
709	26.287	707	26.439		
710	26.303	708	26.457		
711	26.32	709	26.48		
712	26.343	710	26.496		
713	26.358	711	26.511		
714	26.374	712	26.523		
715	26.399	713	26.545		
716	26.411	714	26.558		
717	26.431	715	26.578		
718	26.45	716	26.593		
719	26.463	717	26.608		
720	26.48	718	26.626		
721	26.494	719	26.644		
722	26.507	720	26.665		
723	26.525	721	26.687		
724	26.546	722	26.697		
725	26.56	723	26.711		
726	26.564	724	26.732		
727	26.582	725	26.742		
728	26.595	726	26.757		
729	26.618	727	26.77		
730	26.627	728	26.783		
731	26.648	729	26.803		

732	26.662	730	26.814		
733	26.681	731	26.833		
734	26.695	732	26.854		
735	26.712	733	26.861		
736	26.724	734	26.879		
737	26.744	735	26.891		
738	26.756	736	26.908		
739	26.767	737	26.926		
740	26.787	738	26.949		
741	26.802	739	26.962		
742	26.816	740	26.974		
743	26.824	741	26.988		
744	26.84	742	27.005		
745	26.856	743	27.018		
746	26.868	744	27.039		
747	26.887	745	27.049		
748	26.9	746	27.064		
749	26.92	747	27.082		
750	26.935	748	27.09		
751	26.954	749	27.109		
752	26.969	750	27.119		
753	26.984	751	27.132		
754	26.999	752	27.15		
755	27.014	753	27.166		
756	27.027	754	27.183		
757	27.044	755	27.192		

758	27.081	756	27.201		
759	27.097	757	27.22		
760	27.106	758	27.232		
761	27.128	759	27.244		
762	27.141	760	27.268		
763	27.157	761	27.274		
764	27.167	762	27.282		
765	27.188	763	27.303		
766	27.202	764	27.312		
767	27.22	765	27.329		
768	27.219	766	27.344		
769	27.257	767	27.361		
770	27.268	768	27.378		
771	27.277	769	27.391		
772	27.297	770	27.402		
773	27.317	771	27.416		
774	27.331	772	27.427		
775	27.338	773	27.447		
776	27.351	774	27.465		
777	27.353	775	27.479		
778	27.372	776	27.491		
779	27.397	777	27.516		
780	27.406	778	27.529		
781	27.425	779	27.541		
782	27.446	780	27.551		
783	27.462	781	27.574		

784	27.466	782	27.593		
785	27.492	783	27.607		
786	27.499	784	27.619		
787	27.514	785	27.639		
788	27.521	786	27.659		
789	27.538	787	27.677		
790	27.562	788	27.696		
791	27.567	789	27.71		
792	27.576	790	27.73		
793	27.586	791	27.738		
794	27.606	792	27.754		
795	27.616	793	27.783		
796	27.631	794	27.795		
797	27.656	795	27.808		
798	27.677	796	27.829		
799	27.682	797	27.833		
800	27.701	798	27.856		
801	27.726	799	27.867		
802	27.747	800	27.889		
803	27.754	801	27.907		
804	27.764	802	27.921		
805	27.77	803	27.935		
806	27.79	804	27.961		
807	27.801	805	27.974		
808	27.802	806	27.984		
809	27.815	807	28.006		

810	27.832	808	28.019		
811	27.854	809	28.033		
812	27.864	810	28.041		
813	27.877	811	28.064		
814	27.894	812	28.068		
815	27.902	813	28.082		
816	27.909	814	28.098		
817	27.916	815	28.112		
818	27.928	816	28.133		
819	27.94	817	28.154		
820	27.955	818	28.181		
821	27.965	819	28.19		
822	27.977	820	28.201		
823	27.99	821	28.212		
824	27.998	822	28.233		
825	28.019	823	28.247		
826	28.027	824	28.266		
827	28.047	825	28.279		
828	28.052	826	28.28		
829	28.061	827	28.297		
830	28.077	828	28.305		
831	28.098	829	28.308		
832	28.109	830	28.322		
833	28.119	831	28.343		
834	28.129	832	28.352		
835	28.142	833	28.361		

836	28.154	834	28.38		
837	28.169	835	28.391		
838	28.187	836	28.393		
839	28.189	837	28.411		
840	28.213	838	28.433		
841	28.228	839	28.443		
842	28.242	840	28.458		
843	28.252	841	28.46		
844	28.269	842	28.47		
845	28.283	843	28.483		
846	28.298	844	28.491		
847	28.306	845	28.513		
848	28.325	846	28.524		
849	28.335	847	28.538		
850	28.347	848	28.557		
851	28.356	849	28.556		
852	28.38	850	28.58		
853	28.389	851	28.594		
854	28.4	852	28.619		
855	28.416	853	28.622		
856	28.431	854	28.632		
857	28.45	855	28.644		
858	28.463	856	28.661		
859	28.472	857	28.677		
860	28.486	858	28.697		
861	28.501	859	28.702		

862	28.516	860	28.721		
863	28.53	861	28.73		
864	28.546	862	28.754		
865	28.555	863	28.76		
866	28.569	864	28.777		
867	28.585	865	28.795		
868	28.605	866	28.808		
869	28.62	867	28.819		
870	28.637	868	28.826		
871	28.652	869	28.846		
872	28.664	870	28.855		
873	28.702	871	28.863		
874	28.713	872	28.879		
875	28.735	873	28.899		
876	28.744	874	28.903		
877	28.757	875	28.918		
878	28.778	876	28.934		
879	28.798	877	28.94		
880	28.809	878	28.951		
881	28.827	879	28.968		
882	28.845	880	28.986		
883	28.856	881	29		
884	28.87	882	29.004		
885	28.885	883	29.018		
886	28.898	884	29.041		
887	28.915	885	29.054		

888	28.929	886	29.067		
889	28.939	887	29.082		
890	28.953	888	29.099		
891	28.972	889	29.112		
892	28.983	890	29.124		
893	29.004	891	29.142		
894	29.015	892	29.152		
895	29.035	893	29.177		
896	29.049	894	29.186		
897	29.062	895	29.19		
898	29.08	896	29.208		
899	29.095	897	29.219		
900	29.106	898	29.234		
901	29.122	899	29.242		
902	29.138	900	29.258		
903	29.147	901	29.276		
904	29.167	902	29.296		
905	29.187	903	29.298		
906	29.195	904	29.318		
907	29.209	905	29.343		
908	29.224	906	29.354		
909	29.232	907	29.356		
910	29.245	908	29.376		
911	29.253	909	29.402		
912	29.268	910	29.403		
913	29.275	911	29.43		

914	29.298	912	29.445		
915	29.304	913	29.456		
916	29.31	914	29.474		
917	29.329	915	29.493		
918	29.336	916	29.511		
919	29.349	917	29.526		
920	29.37	918	29.542		
921	29.371	919	29.554		
922	29.383	920	29.565		
923	29.393	921	29.579		
924	29.395	922	29.601		
925	29.421	923	29.619		
926	29.431	924	29.636		
927	29.444	925	29.641		
928	29.455	926	29.659		
929	29.47	927	29.682		
930	29.479	928	29.696		
931	29.487	929	29.707		
932	29.495	930	29.721		
933	29.516	931	29.732		
934	29.533	932	29.753		
935	29.553	933	29.772		
936	29.561	934	29.783		
937	29.567	935	29.807		
938	29.574	936	29.825		
939	29.589	937	29.837		

940	29.601	938	29.854		
941	29.618	939	29.868		
942	29.626	940	29.885		
943	29.638	941	29.901		
944	29.656	942	29.901		
945	29.656	943	29.907		
946	29.68	944	29.918		
947	29.695	945	29.939		
948	29.706	946	29.959		
949	29.72	947	29.965		
950	29.734	948	29.986		
951	29.742	949	29.999		
952	29.757	950	30.022		
953	29.765	951	30.029		
954	29.781	952	30.043		
955	29.782	953	30.07		
956	29.804	954	30.074		
957	29.817	955	30.106		
958	29.826	956	30.126		
959	29.839	957	30.124		
960	29.85	958	30.136		
961	29.867	959	30.149		
962	29.875	960	30.153		
963	29.888	961	30.195		
964	29.899	962	30.202		
965	29.92	963	30.217		

966	29.941	964	30.238		
967	29.952	965	30.245		
968	29.968	966	30.25		
969	29.973	967	30.266		
970	29.986	968	30.284		
971	30.006	969	30.282		
972	30.013	970	30.3		
973	30.027	971	30.308		
974	30.046	972	30.322		
975	30.057	973	30.344		
976	30.06	974	30.357		
977	30.083	975	30.375		
978	30.096	976	30.389		
979	30.105	977	30.395		
980	30.113	978	30.402		
981	30.129	979	30.425		
982	30.141	980	30.438		
983	30.155	981	30.453		
984	30.157	982	30.456		
985	30.164	983	30.492		
986	30.171	984	30.502		
987	30.188	985	30.515		
988	30.198	986	30.527		
989	30.215	987	30.542		
990	30.224	988	30.552		
991	30.241	989	30.563		

992	30.25	990	30.572		
993	30.259	991	30.596		
994	30.276	992	30.614		
995	30.291	993	30.624		
996	30.306	994	30.641		
997	30.321	995	30.651		
998	30.327	996	30.666		
999	30.343	997	30.681		
1000	30.36	998	30.71		
1001	30.38	999	30.722		
1002	30.391	1000	30.776		
1003	30.403	1001	30.793		
1004	30.42	1002	30.802		
1005	30.429	1003	30.823		
1006	30.447	1004	30.831		
1007	30.461	1005	30.85		
1008	30.481	1006	30.866		
1009	30.497	1007	30.869		
1010	30.512	1008	30.879		
1011	30.52	1009	30.907		
1012	30.54	1010	30.918		
1013	30.555	1011	30.932		
1014	30.56	1012	30.943		
1015	30.582	1013	30.965		
1016	30.603	1014	30.976		
1017	30.613	1015	31.001		

1018	30.629	1016	31.007		
1019	30.642	1017	31.035		
1020	30.653	1018	31.049		
1021	30.668	1019	31.051		
1022	30.68	1020	31.068		
1023	30.685	1021	31.059		
1024	30.697	1022	31.094		
1025	30.714	1023	31.088		
1026	30.723	1024	31.113		
1027	30.734	1025	31.141		
1028	30.756	1026	31.127		
1029	30.769	1027	31.154		
1030	30.78	1028	31.137		
1031	30.794	1029	31.163		
1032	30.81	1030	31.176		
1033	30.819	1031	31.184		
1034	30.828	1032	31.183		
1035	30.837	1033	31.226		
1036	30.85	1034	31.236		
1037	30.863	1035	31.239		
1038	30.882	1036	31.27		
1039	30.899	1037	31.25		
1040	30.905	1038	31.287		
1041	30.917	1039	31.302		
1042	30.92	1040	31.303		
1043	30.942	1041	31.32		

1044	30.955	1042	31.342		
1045	30.969	1043	31.351		
1046	30.976	1044	31.361		
1047	30.99	1045	31.375		
1048	31.003	1046	31.377		
1049	31.018	1047	31.403		
1050	31.023	1048	31.412		
1051	31.036	1049	31.423		
1052	31.048	1050	31.446		
1053	31.054	1051	31.468		
1054	31.07	1052	31.48		
1055	31.09	1053	31.485		
1056	31.102	1054	31.499		
1057	31.118	1055	31.501		
1058	31.113	1056	31.526		
1059	31.132	1057	31.551		
1060	31.152	1058	31.596		
1061	31.163	1059	31.632		
1062	31.177	1060	31.636		
1063	31.192	1061	31.637		
1064	31.204	1062	31.669		
1065	31.214	1063	31.683		
1066	31.228	1064	31.7		
1067	31.239	1065	31.708		
1068	31.249	1066	31.72		
1069	31.264	1067	31.725		

1070	31.269	1068	31.744		
1071	31.275	1069	31.767		
1072	31.285	1070	31.762		
1073	31.296	1071	31.773		
1074	31.311	1072	31.81		
1075	31.317	1073	31.816		
1076	31.337	1074	31.834		
1077	31.354	1075	31.854		
1078	31.367	1076	31.861		
1079	31.37	1077	31.884		
1080	31.395	1078	31.897		
1081	31.402	1079	31.905		
1082	31.418	1080	31.915		
1083	31.418	1081	31.931		
1084	31.434	1082	31.948		
1085	31.457	1083	31.96		
1086	31.461	1084	31.967		
1087	31.472	1085	31.983		
1088	31.487	1086	31.999		
1089	31.499	1087	32.011		
1090	31.508	1088	32.026		
1091	31.524	1089	32.031		
1092	31.534	1090	32.04		
1093	31.55	1091	32.057		
1094	31.56	1092	32.07		
1095	31.576	1093	32.091		

1096	31.585	1094	32.09		
1097	31.6	1095	32.107		
1098	31.607	1096	32.116		
1099	31.624	1097	32.145		
1100	31.635	1098	32.158		
1101	31.65	1099	32.159		
1102	31.687	1100	32.17		
1103	31.695	1101	32.201		
1104	31.713	1102	32.206		
1105	31.727	1103	32.225		
1106	31.737	1104	32.227		
1107	31.75	1105	32.242		
1108	31.76	1106	32.253		
1109	31.78	1107	32.262		
1110	31.791	1108	32.271		
1111	31.798	1109	32.279		
1112	31.81	1110	32.298		
1113	31.827	1111	32.308		
1114	31.84	1112	32.303		
1115	31.848	1113	32.329		
1116	31.858	1114	32.354		
1117	31.879	1115	32.345		
1118	31.891	1116	32.365		
		1117	32.371		
		1118	32.386		
		1119	32.399		

	1120 32.41		
	1121 32.424		
	1122 32.43		
	1123 32.448		
	1124 32.454		
	1125 32.473		
	1126 32.476		
	1127 32.5		
	1128 32.506		
	1129 32.522		
	1130 32.525		
	1131 32.546		
	1132 32.56		
	1133 32.569		
	1134 32.59		
	1135 32.614		
	1136 32.619		
	1137 32.64		
	1138 32.661		
	1139 32.664		
	1140 32.681		
	1141 32.691		
	1142 32.702		
	1143 32.732		
	1144 32.758		
	1145 32.758		

	1146 32.774		
	1147 32.784		
	1148 32.796		
	1149 32.815		
	1150 32.812		
	1151 32.838		
	1152 32.843		
	1153 32.863		
	1154 32.877		
	1155 32.885		
	1156 32.89		
	1157 32.908		
	1158 32.923		
	1159 32.945		
	1160 32.95		
	1161 32.959		
	1162 32.986		
	1163 33.007		
	1164 33.012		
	1165 33.031		
	1166 33.035		
	1167 33.05		
	1168 33.064		
	1169 33.087		
	1170 33.103		
	1171 33.125		

	1172 33.13		
	1173 33.137		
	1174 33.154		
	1175 33.161		
	1176 33.186		
	1177 33.196		
	1178 33.225		
	1179 33.211		
	1180 33.235		
	1181 33.266		
	1182 33.283		
	1183 33.287		
	1184 33.307		
	1185 33.309		
	1186 33.324		
	1187 33.342		
	1188 33.346		
	1189 33.381		
	1190 33.378		
	1191 33.402		
	1192 33.41		
	1193 33.42		
	1194 33.444		
	1195 33.446		
	1196 33.464		
	1197 33.47		

	1198 33.509		
	1199 33.52		
	1200 33.541		
	1201 33.539		
	1202 33.552		
	1203 33.579		
	1204 33.584		
	1205 33.599		
	1206 33.595		
	1207 33.631		
	1208 33.652		
	1209 33.655		
	1210 33.668		
	1211 33.678		
	1212 33.694		
	1213 33.711		
	1214 33.712		
	1215 33.74		
	1216 33.741		
	1217 33.746		
	1218 33.77		
	1219 33.752		
	1220 33.79		
	1221 33.796		
	1222 33.817		
	1223 33.817		

	1224 33.833 1225 33.841 1226 33.851 1227 33.852 1228 33.89 1229 33.906 1230 33.912		